Feshbach resonances in Bose-Einstein condensates

Please check the document version of this publication:

• A submitted manuscript is the version of the article upon submission and before peer-review. There can be important differences between the submitted version and the official published version of record. People interested in the research are advised to contact the author for the final version of the publication, or visit the DOI to the publisher's website.
• The final author version and the galley proof are versions of the publication after peer review.
• The final published version features the final layout of the paper including the volume, issue and page numbers.

Link to publication

Feshbach Resonances in
Bose-Einstein Condensates

PROEFSCHRIFT

ter verkrijging van de graad van doctor aan de
Technische Universiteit Eindhoven, op gezag van
de Rector Magnificus, prof.dr. M. Rem, voor een
commissie aangewezen door het College voor
Promoties in het openbaar te verdedigen
op dinsdag 29 juni 1999 om 16.00 uur

door

Johannes Mathijs Vogels

geboren te Mariahout

Johnny Vogels
Group for Theoretical and Experimental Atomic Physics and Quantum Electronics
Physics Department
Eindhoven University of Technology
Box 513
5600 MB Eindhoven
The Netherlands

Contents

1. Introduction

Quantum degeneracy is the generic name for a set of phenomena that play a role in a system of particles when their deBroglie wavelength is of the order of or larger than the mean interparticle spacing:

$$\lambda_{dB} \gtrsim n^{-1/3}. \tag{1}$$

For a given density this regime is reached for low enough temperatures. Quantum degeneracy can be found in a variety of systems. Perhaps the most familiar example can be found in atoms. There the dynamics of electrons is strongly restricted by the Pauli exclusion principle, which in turn makes matter stable against collapse. Another example is nuclear matter where the picture of independent particle motion (the nuclear shell model) owes its validity to the fact that changes of particle state in collisions are highly suppressed due to the unavailability of already occupied states as final states [1]. An extreme form of (quantum degenerate) nuclear matter can be found in neutron stars [2].

The previous examples deal with fermions, where due to the quantum degeneracy the particles effectively repel each other. This is in strong contrast with the case of bosons. Instead of obeying an exclusion principle for particles to be in the same state, bosons move preferably to states which are already occupied, which expresses itself in the form of boson stimulation factors. Photons, massless bosons, can thus be emitted in a stimulated way to fill a mode of a cavity in large numbers, giving rise to lasers and masers [3]. Massive bosons can become Bose-Einstein condensed. In this way helium-4 undergoes a transition to a superfluid state below the λ point at 2.17 K. Superconductivity is another such phenomenon, caused by Bose-Einstein condensation of Cooper pairs of electrons, behaving as charged bosons.

1.1   Bose-Einstein condensation (BEC) in dilute ultracold atomic gases

From a theoretical point of view the massive boson systems have the disadvantage that the bosons have complicated interactions in the liquid or solid state, making it very hard to understand the BEC phenomenon on the basis of first principles. The observation of BEC in dilute atomic gases of rubidium [4, 5], sodium [6], lithium [7], and hydrogen [8] has opened up an exciting new field of research. To produce a condensate of alkali atoms, a temperature typically below 500 nK is reached at densities of around 10^{13} atoms per cubic centimeter. For hydrogen 40 μK turned out to be sufficient at 10^{14} atoms/cm^3. These experiments have provided the first realizations of a Bose condensate in its nearly ideal form, that does allow for treatments from first principles. This is not to say that interactions are unimportant in these systems. A striking example is the spin domain structure recently observed in a spinor condensate [9], an amazing and counterintuitive phenomenon for an extremely dilute system.

One of the reasons that a treatment of the new condensates from first principles is possible is that, at sufficiently low density, two-body interaction processes in such
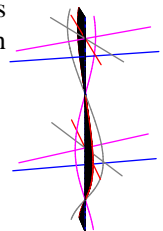
a gas are dominant. Such processes are in addition greatly simplified due to the low temperatures. The deBroglie wavelength of the atoms is much larger than the interaction range, causing just the spherically symmetric s wave, with orbital angular momentum $l = 0$, to contribute. For s-wave scattering near zero energy the radial wavefunction $u(r)$ tends to a sine form at long range:

$$u \sim sin(kr + \delta_0) \approx \sin k(r - a), \tag{2}$$

where δ_0 is the $l = 0$ phase shift and

$$a = -lim_{k \to 0}(\delta_0(k)/k) \tag{3}$$

is the scattering length [10]. This is illustrated in Fig. 1, which shows the wavefunction for the triplet scattering of two ^{7}Li and of two ^{23}Na ground state atoms. The wavefunction undergoes a large number of radial oscillations due to the strong short range part of the potential. However, at long range the wavefunction tends to a constant times $r - a$, which is just the low-energy limit of Eq. (2). The effect of the potential is simply to shift the sine function over a fixed distance a. For positive a it is the same as the shift for a hard wall at $r = a$ and the interaction is effectively repulsive. When the scattering length is negative the atoms effectively attract each other. It is illustrative to consider the behavior of a when one gradually increases the depth of the potential well. The number of bound states contained in the well then increases. At the depth where a new bound state is added, a goes from large negative values through $-\infty$ and comes back again at $+\infty$. Subsequently it decreases again to large negative values until a new bound state enters the potential well. The wave functions presented in Fig. 1 are actual examples for triplet scattering with positive a (^{23}Na) and negative a (^{7}Li).

1.2   Role of interactions in BEC

Both for the formation of a condensate and for its properties, the scattering length a is of crucial importance. In fact, in current setups the stimulated processes which cause the atoms to go into the macroscopically occupied state, are elastic two-body collisions with the low-energy cross section

$$\sigma = 8\pi a^2. \tag{4}$$

This implies that a has to be large enough in absolute magnitude to lead to a formation rate dominating the decay rates due to competing processes.

Next, most of the properties of a condensate depend strongly on a. In the mean-field approximation the time-independent and time-dependent behavior of the condensate wavefunction $\phi(\mathbf{x}, t)$ is described by the Gross-Pitaevskii equation [11]:

$$i\hbar\dot{\phi} = \left(-\frac{\hbar^2}{2m}\nabla^2 + V_{trap}(\mathbf{x}) + \frac{4\pi\hbar^2 a}{m}|\phi|^2\right)\phi, \tag{5}$$

with V_{trap} the trap potential. This is a nonlinear Schrödinger equation containing a condensate self-energy term

$$U = \frac{4\pi\hbar^2 a}{m}|\phi|^2 \tag{6}$$

proportional to a. The self-energy plays an important role in determining many properties of a condensate, including its size, shape, and excitation spectrum [11]. In par-
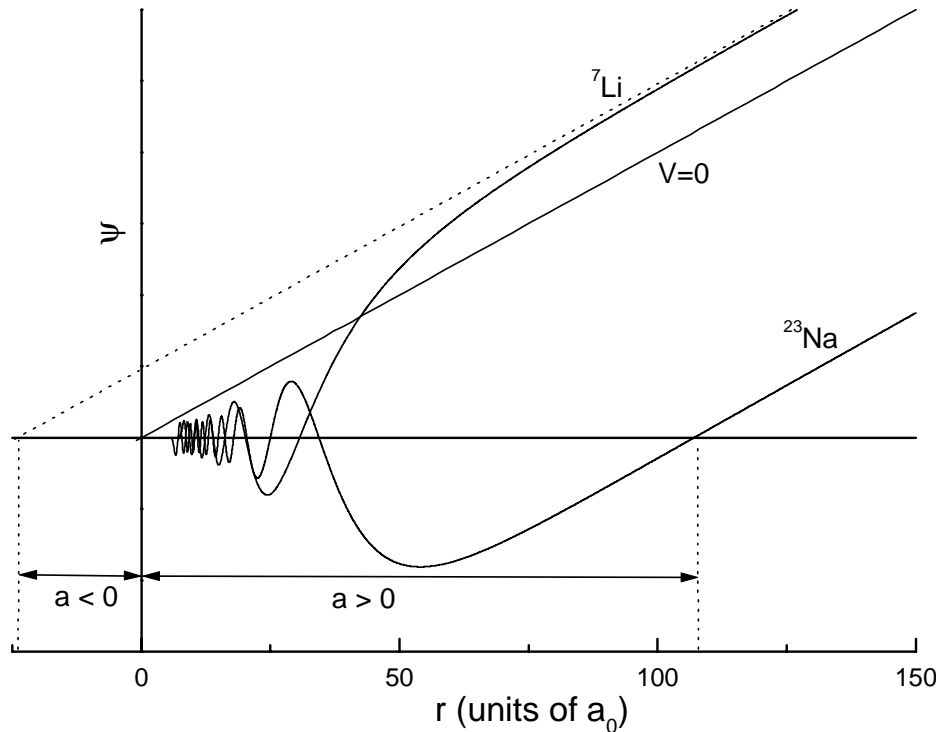
Figure 1: Zero-energy scattering wavefunctions for the ^7Li and ^{23}Na triplet interaction and the interaction-less (V=0) situation (straight line). The scattering length can be found by extrapolating the solution at large distances to the r-axis.

ticular, the sign of a is crucial. As pointed out above, for positive a the interactions are effectively repulsive and tend to stabilize the BEC. For negative a the interactions are effectively attractive, and BEC will not be stable unless stabilization is provided by the trapping potential [12]. Energetically the most favorable solution then is to have all atoms close together. In this situation three- and many-body collisions are certain to produce molecules, with the gas being fully on its way towards the real ground state, a solid. At zero scattering length the atoms effectively do not interact and the solution of the Gross-Pitaevskii equation equals the single-atom ground state in the trap potential. The self-energy is one of the 'coherent' collisional effects, which are proportional to a rather than to its square. Other effects of this type are the refraction of matter waves [13] and atomic clock frequency shifts [14].

1.3   Spin states and collisions

Although low-energy elastic two-body collisions are characterized by a single number relevant for BEC, the collision physics itself is sometimes quite rich. Ground state alkali atoms have a (valence) electron spin **s** and a nuclear spin **i** and the atoms in a condensate
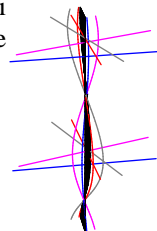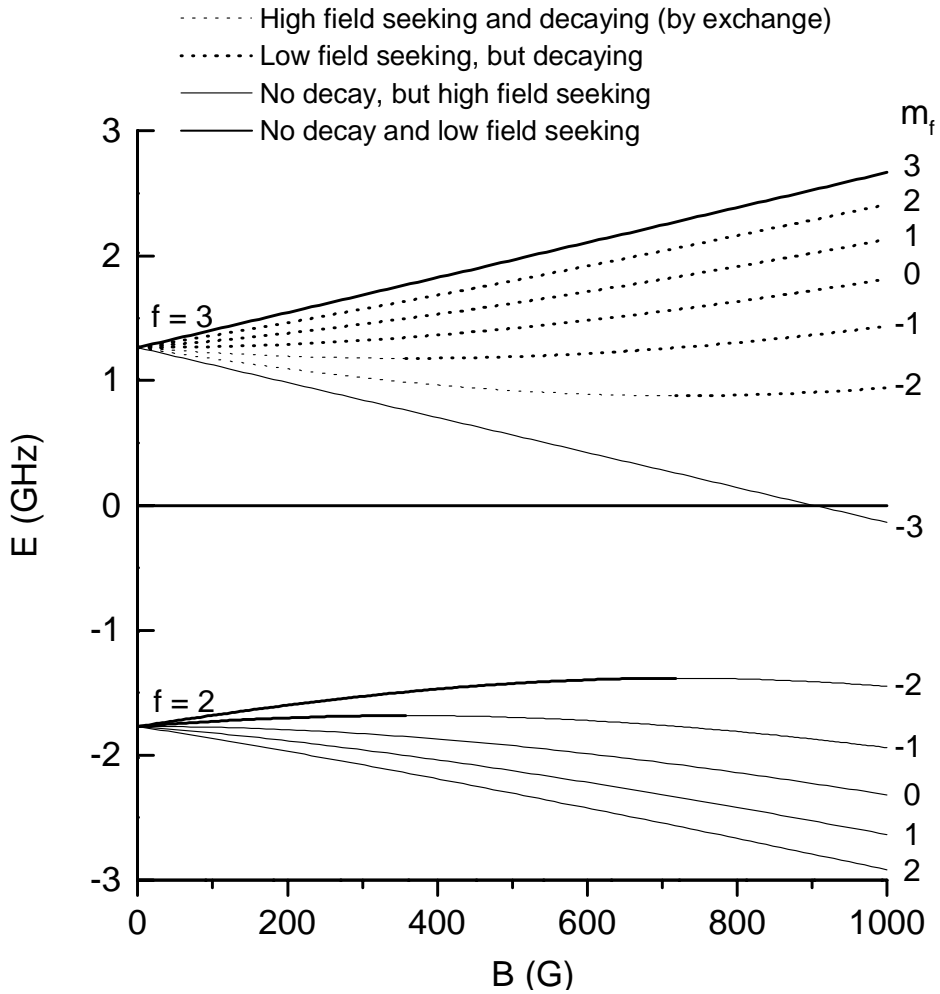
Figure 2: Hyperfine diagram of an ^{85}Rb atom, which has a nuclear spin $i = \frac{5}{2}$. States which are high field seeking are indicated by thin lines. States which are decaying in collisions due to the exchange interaction are dotted. Only three states can thus be used to produce a condensate in a magnetic trap, of which only the two $f = i - \frac{1}{2}$ states possibly have Feshbach resonances. In fact, the $f = 2$, $m_f = -2$ state has three resonances.

can be in one of several hyperfine states. We use lower case symbols for single atom spins s, i, $f = s + i$, and capital symbols for the corresponding two-atom spins. Fig. 2 shows the example of the ^{85}Rb ground state hyperfine diagram for a single atom.

The most common type of trap presently used for stable confinement of a condensate is a magnetic trap. For a hyperfine state to be kept in such a trap it has to be 'low-field seeking', since a static magnetic field maximum cannot be realized in free space. This leaves the $f = i + \frac{1}{2}$, $m_f > -f$ and the $f = i - \frac{1}{2}$, $m_f < 0$ states as possible candidates, as shown in the figure where also the field ranges in which they are low field seeking are indicated.

There is, however, another requirement on a hyperfine state to be appropriate for trapping. This requirement relates to what may happen when two atoms collide. In such a collision the exchange interaction, proportional to the difference between the interatomic interactions in the $S = 1$ (triplet) and the $S = 0$ (singlet) spin states, can induce transitions between different two-atom hyperfine spin states. In this way one of the atoms or both can go to an untrapped hyperfine state. Whether this will occur is determined by selection rules and by the availability of energetically accessible final states. Without external field the total spin $\mathbf{F}$ is conserved, leading to the selection rules $\Delta F = 0$, $\Delta m_F = 0$. In the magnetic field of a magnetic trap only the component F_z along the local magnetic field survives as a rigorously conserved quantity with the associated selection rule $\Delta m_F = 0$.

One state that can thus be used is the 'doubly spin-polarized' state with $f = i + s = i + \frac{1}{2}$, and $m_f = +f$, where the two-atom system is in the simple quantum state $F = 2i + 1$, $m_F = 2i + 1$. Since there is no other two-atom spin state with this value of m_F, the system is stable against decay via the exchange interaction. Since the electron spins are parallel, the collision proceeds purely along the doubly polarized, pure triplet potential. In Fig. 2 the doubly polarized single atom state has $f = m_f = +3$. The possibility of decay via the exchange interaction virtually prohibits using the $f = i + \frac{1}{2}$, $|m_f| < f$ states in a condensate (but not absolutely [15]).

A second single-atom state suitable for magnetic trapping of a condensate is the state with $f = i - \frac{1}{2}$, and $m_f = -f$. In this case we have a two-atom m_F value equal to $-2i + 1$ and there are no other energetically accessible states with that value of m_F. Also the other $f = i - \frac{1}{2}$ states turn out to fulfill this requirement. In Fig. 2 the single-atom states relevant for BEC in a magnetic trap are indicated.

Optical traps have the advantage that the above requirement with respect to the low-field seeking property does not play a role. As a consequence, both doubly polarized states $f = i + \frac{1}{2}$, $m_f = \pm f$ and all states $f = i - \frac{1}{2}$ can then be used [16].

An attractive feature of the choice $f = i - \frac{1}{2}$ is that it may be possible to realize a situation where the scattering length can be magnetically tuned to arbitrary positive, negative and zero values, in a single experiment. This is possible in case of a Feshbach resonance at zero collision energy [17].

1.4   Feshbach resonances

Feshbach resonances [10] were first introduced as a concept in the nuclear physics literature at the end of the fifties. It is of importance to distinguish this concept from that of a shape resonance, also referred to as potential resonance. As the name suggests, the
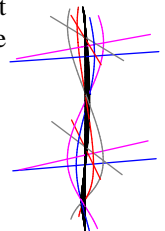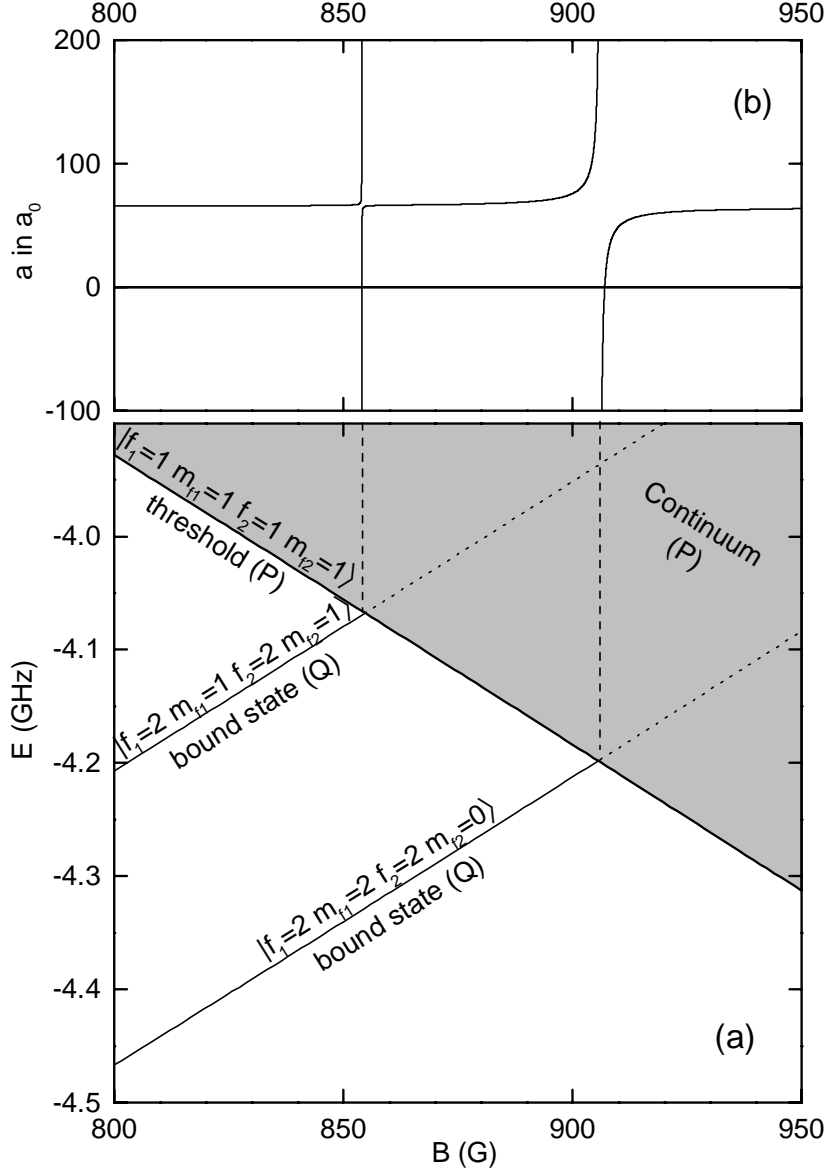
Figure 3: a) Field dependent threshold energy and two field dependent bound states for a pair of ^{23}Na atoms with $m_F = +2$. The $T = 0$ collision takes place at the $|f_1 = 1, m_{f1} = 1, f_2 = 1, m_{f2} = 1\rangle$ threshold, which consists of high field seekers; This was no problem since the experiment happened in an optical trap. The rising bound states have the approximate spin structures $|f_1 = 2, m_{f1} = 1, f_2 = 2, m_{f2} = 1\rangle$ and $|f_1 = 2, m_{f1} = 2, f_2 = 2, m_{f2} = 0\rangle$ respectively. b) Scattering length at threshold of atoms colliding at $|f_1 = 1, m_{f1} = 1, f_2 = 1, m_{f2} = 1\rangle$ threshold. For the 907 G resonance the atoms have a negative scattering length when the externally applied field is within a range of 1 G

latter occur in potential scattering, i.e. only the external, spatial, dynamics of the scattering partners in their interaction potential is involved. In practice they arise for partial waves $l > 0$ when a quasibound state occurs inside the centrifugal barrier.

For Feshbach resonances the interplay between the external and internal dynamics of the scattering partners is essential, i.e. they occur in multichannel scattering. In this case the quasibound state has an internal structure orthogonal to that of the combined scattering partners in the initial state. Such quasibound states can arise also for $l = 0$. We will not go into their detailed mathematical description [10], briefly summarized by Moerdijk et al. [18]. Rather, we will describe the basic aspects.

One starts by splitting the Hilbert space of the total system describing both the external and internal dynamics into two orthogonal subspaces. One subspace, denoted by P, contains all possible states in which the internal dynamics corresponds to the scattering channels that are open at the total energy E considered. The orthogonal complement Q is associated with all closed channels. Whereas for a shape resonance the quasibound state turns into a rigorously bound state in the approximation where the centrifugal potential is changed into an impenetrable barrier, the Feshbach quasibound state becomes a bound eigenstate in the isolated Q space in the approximation where the coupling to the P space is left out. In both cases, relaxing the approximation results in the discrete bound state acquiring a finite width. This width occurs via the well-known Breit-Wigner denominator in the diagonal and non-diagonal scattering amplitudes in P space for the various channels open at energy E.

As an example, the situation of a Feshbach resonance occurring in the scattering of two ground state Na atoms is illustrated in Fig. 3. This figure shows the field-dependent threshold energy where the $E = 0$ collision takes place for two $f, m_f = 1, +1$ atoms, and the field-dependent energies of two bound states with $m_F = +2$, which according to theoretical calculations turn out to have the approximate spin structures $|f_1 = 2, m_{f1} = 1, f_2 = 2, m_{f2} = 1\rangle$ and $|f_1 = 2, m_{f1} = 0, f_2 = 2, m_{f2} = 2\rangle$. The P space consists of states in which the atoms are in the collision spin state. The Q space contains in particular the two bound states shown. Above threshold Feshbach resonances occur when E is approximately equal to a value on the dotted extrapolation of one of the bound states.

Expressions for the elastic scattering amplitude in the single open spin channel available in these circumstances can be derived by considering solutions of the Schrödinger equation for any $E > 0$ in the separate isolated P and Q spaces and subsequently introducing the PQ coupling [10, 18]. For the cold collisions studied in this thesis we are interested in the elastic scattering amplitude $S_{l=0} = \exp(2i\delta_{l=0})$ for E close to threshold. Specializing the general expression to that limit we have $\delta_{l=0} \approx -ka$ where $a(B)$ displays a dispersive feature:

$$a(B) = a_\infty \left(1 + \frac{\Delta B}{B - B_0} \right). \tag{7}$$

At the resonance field strength B_0, defined by the crossing of a bound state with the threshold in Fig. 3, the scattering length a is infinite. The field width ΔB is proportional to the strength of the PQ coupling squared and inversely proportional to the difference in effective magnetic moments of the free two-atom system and of the bound state considered, i.e. inversely proportional to the difference in slope of the crossing lines in Fig. 3 (see Ref. [18]). It specifies the range in field for which the scattering length has a
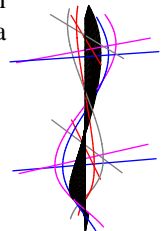
different sign. Off-resonance the scattering length is not affected by the PQ coupling, so that it is determined by the interatomic potential diagonal in the open spin channel.

In the applications we have in mind the distinction between the P and Q subspaces corresponds directly with a selection of pairs of hyperfine states for the two atoms. The PQ coupling then comes only from the part of the interatomic interaction that is non-diagonal in the hyperfine states. Apart from the much weaker magnetic dipole interaction, this is the exchange interaction mentioned in the previous subsection.

1.5   Observation of Feshbach resonances

Feshbach resonances enable an experimenter to change the scattering length in a condensate in a single experiment in sign and magnitude by just changing the field in the trap. So on the wish-list are resonances which arise in collisions between atoms in magnetically trappable states. Since the field range where $f = i - \frac{1}{2}$, $m_f < 0$ states can be trapped is limited (See fig. 2), they do not occur for all alkali species. In fact, since light pairs of atoms do not feature many bound states, it is a coincidence when such a resonance occurs. The first three Feshbach resonances in a field range accessible for magnetic trapping were predicted in ^{85}Rb by Vogels et al. [19]. One of these has been observed in the meantime by two groups [20, 21]. To our knowledge, BEC has not been reached for this isotope due to cooling problems and three body decay.

Experimentally, the first resonances, including the dispersive shape of the scattering length, have been observed by Ketterle's group at MIT [16] in ^{23}Na in a BEC in an optical trap. Predictions for Feshbach resonances in ^{7}Li and ^{23}Na observable in optical traps were made by Moerdijk et al. [18]. The accuracy of these predictions was much improved by Van Abeelen et al. [22, 23]. Unexpectedly, extremely strong loss processes occurred experimentally when the resonances in ^{23}Na were approached in an attempt to increase the observed range of a values, so negative values could not be reached [24]. A nice alternative might be ^{39}K, which seems to feature [25] a very broad resonance covering almost the entire field range available for magnetic trapping.

1.6   How to predict Feshbach resonances

An important goal of this thesis work is the prediction of Feshbach resonances and their properties. For atomic hydrogen and to a lesser extent lithium one can use ab-initio interaction potentials to reliably predict collision processes in general and Feshbach resonances in particular. For heavier atoms these potentials can be expected to be increasingly inaccurate, but more importantly they are required to be much more accurate. The number of bound states in these potentials increases up to more than 135 in the case of the $S = 0$ ($\mathbf{S} = \mathbf{s}_1 + \mathbf{s}_2$ is the total two-atom electron spin) Cs - Cs potential [26], and to determine a scattering length the precise energy position of the last bound state is particularly important.

Hence, to reliably predict Feshbach resonances, one has to rely on experiments, measuring the properties and behavior of pairs of atoms. A reliable way is to determine the energy position of bound two-atom states, which occur as closely as possible to the collision threshold, preferably the ones causing the resonances. The various collision

parameters can then be extracted.

Types of measurements and their role which have contributed to the knowledge of collision parameters for collisions of cold atoms are

- Measurements of the field position and field width of Feshbach resonances, enabling accurate prediction of others [27, 20, 21]. The width of a Feshbach resonance is directly related to the difference between the singlet and triplet scattering length. The position gives very accurate and reliable information about the shape of the potentials and the scattering lengths.
- Measurements of lifetimes of shape resonances, i.e. quasi-bound states behind a centrifugal barrier [28, 29, 30]. This information is crucial for finding the scattering length and the long range shape of the potential.
- Measurements of collisional frequency-shifts in atomic clocks [31, 32, 33]. Frequency shifts are related to the fact that different states experience different mean field energies due to differences in cross sections.
- Observations of coexisting condensates in different hyperfine states [34, 15]. Such condensates would normally decay in collision processes. Due to the fact that the singlet and triplet scattering lengths are approximately equal in ^{87}Rb, this decay is suppressed. This also enabled the use of the $f = i + \frac{1}{2}, m_f = i - \frac{1}{2}$ states in [15].
- Observations of the decay of condensates by inelastic processes [35]
- Measurements of cross-dimensional thermalization, allowing for the determination of elastic cross sections of cold atoms, including their energy dependence (example: Ref. [36])
- Measurements of photoassociation spectra (line positions and line shapes) [37, 38]. The latest attempt to understand potassium collisions [25] is another beautiful example of this method.

1.7 Organization of chapters

The goal of the investigations presented in this thesis is to obtain a better understanding of cold collisions and to obtain new or more accurate information on interactions controlling cold collisions. In turn, this information is crucial for applications such as BEC and atomic clocks.

In Chapter 2 we start with a description of a simple picture for weakly bound and colliding pairs of atoms. It enables one to understand a large variety of phenomena encountered in the field of cold atoms, ranging from interactions between condensates to the characteristics of Feshbach resonances and bound states. Three two-atom parameters turn out to be critical: the triplet ($S = 1$) scattering length a_T, the singlet ($S = 0$) scattering length a_S and the C_6 dispersion parameter, determining the long range interaction.

Chapter 3 deals with a two-color photoassociation experiment on a trapped ^{85}Rb gas sample and its analysis, yielding information on the most weakly bound ^{85}Rb + ^{85}Rb states, as well as on the corresponding cold collisions.

In Chapter 4 a general method is presented to determine interaction parameters from a two-atom bound state spectrum. It is based on a coupled form of an inverse perturbation approach, including the use of accumulated phases.
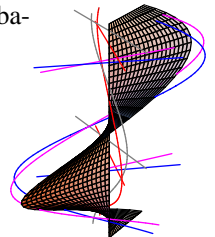
The results of Chapters 3 and 4 culminate in Chapter 5, which describes the prediction of Feshbach resonances in ^{85}Rb and ^{87}Rb.

Finally, in Chapter 6 we treat a rigorous method to calculate the stationary collision state of a three-body collision between three ultracold double polarized ground state alkali atoms. The method is based on the Faddeev formalism. The circumstances of the collision correspond to Bose-Einstein condensed and other ultracold gases. The method combines a pair-correlated expansion in hyperspherical harmonics in 6D with the accumulated phase for the pair interactions. It allows us to calculate the complex 6D elastic scattering length and the three-particle recombination rate. The work described in this chapter has been realized with roughly equal contributions from Frank van Abeelen and myself.

References

[1] L.C. Gomes, J.D. Walecka, and V. Weisskopf, Ann. Phys. **3**, 241 (1958).

[2] D. Pines and M. Ali Alpar, Nature **316**, 27 (1985)

[3] D. Kleppner, H.M. Goldenberg, and N.F. Ramsey, Phys. Rev. **126**, 603 (1962).

[4] M.H.Anderson, J.R. Ensher, M.R. Matthews, C.E. Wieman, and E.A. Cornell, Science **269**, 198 (1995).

[5] C.J. Myatt, E.A. Burt, R.W. Ghrist, E.A. Cornell, and C.E. Wieman, Phys. Rev. Lett. **78**, 586 (1997).

[6] K.B. Davis, M.-O. Mewes, M.R. Andrews, N.J. van Druten, D.S. Durfee, D.M. Kurn, and W. Ketterle, Phys. Rev. Lett. **75**, 3969 (1995); M.-O Mewes, M.R. Andrews, N.J. van Druten, D.M. Kurn, D.S. Durfee, and W. Ketterle, Phys. Rev. Lett. **77**, 416 (1996).

[7] C.C. Bradley, C.A. Sacket, J.J. Tollett, and R.G. Hulet, Phys. Rev. Lett. **75**, 1687 (1995); C.C. Bradley, C.A. Sacket, and R.G. Hulet, Phys. Rev. Lett. **78**, 985 (1997).

[8] D.G. Fried, T.C. Killian, L. Willmann, D.Landhuis, S.C. Moss, D. Kleppner, and T.J. Greytak, Phys. Rev. Lett. **81**, 3811 (1998).

[9] J. Stenger, S. Inouye, D.M. Stamper-Kurn, H.-J. Miesner, and W. Ketterle **396**, 345 (1998).

[10] C.J. Joachain, *Quantum Collision Theory* (North-Holland, New York, 1972).

[11] F. Dalfovo, Rev. Mod. Phys. **71** (1991) (April issue).

[12] Yu. Kagan, E.L. Surkov, and G.V. Shlyapnikov, Phys. Rev. Lett. **79**, 2604 (1997).

[13] J. Vigué, Phys. Rev. A **52**, 3973 (1995).

[14] B.J. Verhaar, in *Atomic Physics* **14**, edited by C.E. Wieman, D.J. Wineland, and S.J. Smith (AIP, New York, 1995), pp. 351-368.

[15] D.S. Hall, M.R. Matthews, C.E. Wieman, and E.A. Cornell, Phys. Rev. Lett. **81**, 1543 (1998).

[16] S. Inouye, M.R. Andrews, J. Stenger, H.-J. Miesner, D.M. Stamper-Kurn, and

W. Ketterle, Nature **392**, 154 (1998).

[17] E. Tiesinga, A.J. Moerdijk, B.J. Verhaar, and H.T.C. Stoof, Phys. Rev. A **46**, R1167 (1992); E. Tiesinga, B.J. Verhaar, and H.T.C. Stoof, *ibid.* **47**, 4114 (1993);

[18] A.J. Moerdijk, B.J. Verhaar, and A. Axelsson, Phys. Rev. A **51**, 4852 ((1995).

[19] J.M. Vogels, C.C. Tsai, R.S. Freeland, S.J.J.M.F. Kokkelmans, B.J. Verhaar, and D.J. Heinzen, Phys. Rev. A **56**, R1067 (1997) (Chapter 3).

[20] P. Courteille, R.S. Freeland, D.J. Heinzen, F.A. van Abeelen, and B.J. Verhaar, Phys. Rev. Lett. **81**, 69 (1998).

[21] J.L. Roberts, N.R. Claussen, J.P. Burke, Jr., C.H. Greene, E.A. Cornell, and C.E. Wieman, Phys. Rev. Lett. **81**, 5109 (1998).

[22] F. van Abeelen and B.J. Verhaar, Phys. Rev. A **55**, 4377 (1997).

[23] F. van Abeelen and B.J. Verhaar, Phys. Rev. A **59**, 578 (1999).

[24] J. Stenger, S. Inouye, M.R. Andrews, H.-J. Miesner, D.M. Stamper-Kurn, and W. Ketterle, Phys. Rev. Lett. **82**, 2422 (1999).

[25] J. P. Burke, Jr., Chris H. Greene, and John L. Bohn, H. Wang, P. L. Gould, and W.C. Stwalley, *Determination of ^{39}K Scattering Lengths Using Photoassociation Spectroscopy of the 0_g^- state*; J.L. Bohn, J.P. Burke, C.H. Greene, H. Wang, P.L. Gonki, and W.C. Stwalley (unpublished), *Collisional properties of ultracold potassium: consequences for degenerate Bose and Fermi gases* (unpublished); H.Wang, W.C. Stwalley, A.N. Nikolov, E.E. Eyler, PlL. Gould, J.P. Burke, J.L. Bohn, C.H. Greene, E. Tiesinga, C.J. Williams, P.S. Julienne, *Double-Resonance Photoassociative Spectroscopy of Ultracold ^{39}K Atoms near the Lowest Asymptote* (unpublished).

[26] W. Weickenmeier, U. Diemer, M. Wahl, M. Raab, W. Demtröder, and W. Müller, J. Chem. Phys. **82**, 5354 (1985).

[27] S. Inouye, M.R. Andrews, J. Stenger, H.-J. Miesner, D.M. Stamper-Kurn, and W. Ketterle, Nature (London) **392**, 151 (1998).

[28] H.M.J.M. Boesten, C.C. Tsai, B.J. Verhaar, and D.J. Heinzen, Phys. Rev. Lett. **77**, 5194 (1996).

[29] H.M.J.M. Boesten, C.C. Tsai, J.R. Gardner, D.J. Heinzen, and B.J. Verhaar, Phys. Rev. A **55**, 636 (1997).

[30] H.M.J.M. Boesten, C.C. Tsai, D.J. Heinzen, A.J. Moonen, and B.J. Verhaar, J. Phys. B **32**, 287 (1999).

[31] K. Gibble and S. Chu, Phys. Rev. Lett. **70**, 1771 (1993).

[32] B.J. Verhaar, K. Gibble, and S. Chu, Phys. Rev. A **48**, R3429 (1993).

[33] S.J.J.M.F. Kokkelmans, B.J. Verhaar, and K. Gibble, Phys. Rev. Lett. **81**, 951 (1998).

[34] C.J. Myatt, E.A. Burt, R.W. Ghrist, E.A. Cornell, and C.E. Wieman, Phys. Rev. Lett. **78**, 586 (1997).

[35] W. Ketterle and N.J. van Druten, Adv. At. Mol. Opt. Phys. **37**, 181 (1996).

[36] C.R. Monroe, E.A. Cornell, C.A. Sacket, C.J. Myatt, and C.E. Wieman, Phys. Rev. Lett. **70**, 414 (1993).
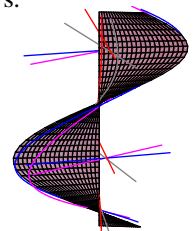
[37] J.R. Gardner, R.A. Cline, J.D. Miller, D.J. Heinzen, H.M.J.M. Boesten, and B.J. Verhaar, Phys. Rev. Lett. **74**, 3764 (1995).

[38] E. Tiesinga, C.J. Williams, P.S. Julienne, K.M. Jones, P.D. Lett, and W.D. Phillips, J. Res. Natl. Stand. Technol. **101**, 505 (1996).

2. Diabatic models for weakly-bound states and cold collisions of ground-state alkali atoms

J.M. Vogels, B.J. Verhaar, and R.H. Blok

Eindhoven University of Technology, Box 513, 5600MB Eindhoven, The Netherlands

Abstract

We apply a simplified description to weakly-bound states and cold-collision continuum states of pairs of ground-state alkali atoms, which complements the usual more elaborate coupled-channels treatment. It is based on a diabatic treatment of the transition region between the exchange-dominated interatomic distance range at small r and the hyperfine-dominated range at large r. The models contain the Degenerate Internal States approximation for H atoms as a special case.

Ultracold collisions of alkali atoms play a key role in applications of laser cooling, such as Bose-Einstein condensation and atomic clocks. For that reason a number of groups are collecting information on interactions between cold alkali atoms, like scattering lengths and dispersion coefficients, from a suitable set of collision processes and weakly-bound states of pairs of ground-state atoms. The analysis of such experiments is commonly based on the coupled-channels method [1, 2], i.e. numerically solving a set of coupled differential equations for the amplitudes of the various spin modes as they vary with interatomic distance r. Such calculations have the advantage of being rigorous. They are elaborate and time-consuming, however, so that the development of a simplified description would be very helpful as a complement to the coupled-channels method.

During the collision the atoms experience besides the hyperfine interaction V_{hf}, which is also encountered in separate atoms, an interaction $V(r)$. It depends on the total electron spin S and is equal to $V_S(r)$ for a singlet ($S = 0$) state and equal to $V_T(r)$ for a triplet ($S = 1$) state:

$$V = P_S V_S + P_T V_T, \tag{1}$$

with P_S and P_T projection operators on the singlet and triplet subspaces of Hilbert space. A relatively innocent part of V is the average $\frac{1}{2}(V_S + V_T)$ of the singlet and triplet potentials. An aspect that does complicate the dynamics of colliding cold alkali atoms is the incompatibility of the spin coupling schemes associated with two other parts of the Hamiltonian. One is the remaining, exchange part of V, corresponding to
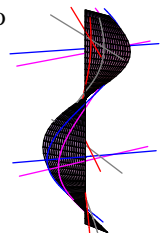
the difference of the singlet and triplet potentials:

$$V_{exch} = \frac{1}{2}(P_S - P_T)(V_S - V_T). \tag{2}$$

In classical terms it gives rise to the precession of the electronic spins $\mathbf{s}_1$ and $\mathbf{s}_2$ of the two atoms about their vector sum $\mathbf{S}$. Another part is the sum

$$V_{hf} = \frac{a_{hf}}{\hbar^2}(\mathbf{s}_1 \cdot \mathbf{i}_1 + \mathbf{s}_2 \cdot \mathbf{i}_2) \tag{3}$$

of the two single-atom hyperfine (hf) interactions. Classically, it gives rise to the independent single-atom precessions of $\mathbf{s}_k$ and $\mathbf{i}_k$ about their sum vector $\mathbf{f}_k$ ($k = 1, 2$). The simultaneous occurrence of the exchange and hf precessions in the same r interval, is the classical counterpart of the incompatible spin coupling schemes in the quantum collision problem. Although in many applications an external magnetic field is present, for the sake of simplicity we leave it aside for a moment, since it is irrelevant for most of our discussion.

In previous work a simplified description was shown to be very useful for cold H atoms: the Degenerate-Internal-States (DIS) approximation [2], which neglects the energy splittings due to V_{hf}. Leaving it out reduces the collision to separate much simpler $S = 0$ and $S = 1$ potential scattering problems. The combination of single-atom hf states in the incident channel is considered as a superposition of singlet and triplet states, that are reflected from their respective potentials. The reflected waves in turn can be written as a superposition of outgoing hf states, thus determining the S-matrix in a basis of hf channels [3].

The first attempt to apply this picture to alkali atoms [4] showed convincingly that the DIS is not a suitable approximation for these systems. The picture to be presented here extends it to a more generally applicable approach. We first point out that the exact collision problem is simple in a range of small interatomic distances $r < r_0$, where the exchange interaction V_{exch} dominates over V_{hf} so that the problem reduces to potential scattering in a set of channels with pure $S = 0$ or 1, associated with the exchange spin-coupling scheme. It is easy to include in this range the part $V_{hf}^+ = \frac{1}{2}a_{hf}/\hbar^2 \mathbf{S} \cdot \mathbf{I}$ of V_{hf} that is diagonal in S, with $\mathbf{I}$ the total two-atom nuclear spin. It turns out that V_{hf}^+ can have a significant influence on the oscillations of the individual triplet radial wavefunctions, in contrast to the remaining part $V_{hf}^- = \frac{1}{2}a_{hf}/\hbar^2(\mathbf{s}_1 - \mathbf{s}_2) \cdot (\mathbf{i}_2 - \mathbf{i}_2)$, which is negligible since it couples the more widely spaced singlet and triplet potentials. The collision problem is also simple in a range of large r values, $r > r_1$, where V_{hf} dominates over V_{exch}. Here, the problem reduces again to potential scattering, this turn in a set of hf channels associated with eigenstates of V_{hf}, i.e. with the hf spin-coupling scheme. In the intermediate range $r_0 < r < r_1$, V_{exch} is comparable to V_{hf} so that a more complicated coupled-channels problem results that can be formulated in either of the two bases. The simplest version of our new description results from the assumption that the atoms traverse an intermediate distance range so rapidly that any relatively slow spin precession due to V_{exch} and V_{hf} can be neglected. Neglecting V_{exch} and V_{hf} in this range, the Hamiltonian becomes a scalar in spin space and all local wave numbers in the $S = 0, 1$ and hf channels are equal. We thus end up in a situation where the most complicated part of the collision problem reduces to the most simple part: an interval where nothing happens with the spin degrees of freedom.

Actually, the above assumption can be relaxed somewhat without sacrificing the
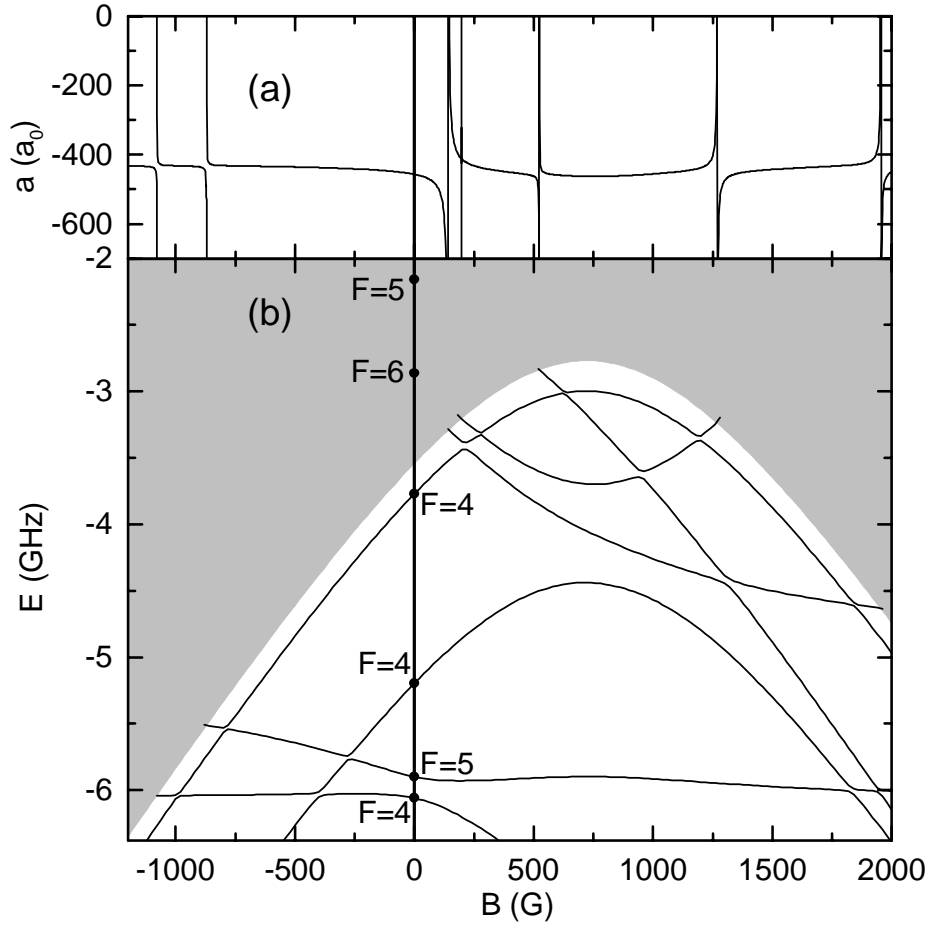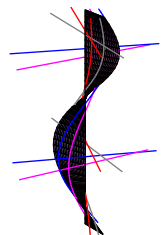
Figure 1: B-dependent scattering length for elastic scattering of two ^{85}Rb atoms in the $|f, m_f\rangle = |2, -2\rangle$ state (part a) and highest part of B-dependent $^{87}Rb_2$ bound-state spectrum for $m_F = m_{f1} + m_{f2} = -4$, together with threshold of $(f_1, m_{f1}, f_2, m_{f2}) = (2, -2, 2, -2)$ channel (part b). Phase values and other parameters are taken from Ref. [8].

numerical simplicity. First, the range where both V_{exch} and V_{hf} need to be neglected can be arbitrarily small. In the extreme case, where it is a single point r_c, it is still possible to solve the uncoupled problem in the region $r < r_c$ in the $S = 0, 1$ basis and beyond r_c in the hf basis. The possibility arises, however, to directly connect the $r < r_c$ and $r > r_c$ solutions, without the intermediate step based on assuming equal local wave numbers: a simple continuity requirement can be imposed at r_c on the total wave function in either basis. The simple model that results resembles the Lane model [5] and also relates to the MQDT [6].

Another way [7] of introducing the above simple pictures starts from the pure $S = 0$ and $S = 1$ eigenstates defined over the full r range without V_{hf}^-. Then taking V_{hf}^- into account mixes these states in a narrow energy band to form perturbed eigenstates near $E = 0$. The mixing matrix elements receive contributions only from large r, where the atoms move slowly, introducing the freedom to shift r_c even to distances where the potential is determined by C_6.

A second element of our description is the assumption that the detailed shape of the triplet and singlet potentials in the inner region is not relevant for the bound state and cold collision properties that are to be calculated. We summarize the history of the atoms in this range by means of the accumulated phases of the rapidly oscillating radial wavefunctions of the uncoupled singlet/triplet channels at the boundary point [7]. To very good approximation these phases vary linearly with E and $l(l + 1)$ over the small E and l ranges to be considered for the cold collisions and bound states of interest. Consistently, they also vary linearly with the V_{hf}^+ spin energies of the triplet states. Introducing a magnetic field does not fundamentally change our foregoing discussion: the Zeeman interaction V_Z is diagonal in the exchange coupling scheme and can therefore be simply considered in combination with $V_{exch} + V_{hf}^+$ for $r < r_c$. On the other hand, since V_Z is a sum of two r-independent single-atom terms, for $r > r_c$ it can also be combined with V_{hf}, thus redefining the threshold energies of the various collision channels. It is of interest to point out that the DIS approximation is an extreme limit of our simplified descriptions: one then even neglects V_{hf} at large r.

The above simple models can be applied to both bound-state and continuum problems. As an example Fig. 1 shows the scattering length for the elastic scattering of two ^{85}Rb atoms in the $|f, m_f\rangle = |2, -2\rangle$ state as a function of the strength of a magnetic field B (part a) and the highest part of the B-dependent ^{85}Rb$_2$ bound-state spectrum (part b). Part a displays the three Feshbach resonances predicted in a recent paper, using interactions extracted from experiment [8]. In part b for simplicity we only show the $m_F = m_{f1} + m_{f2} = -4$ states, associated with the $(f_1, m_{f1}, f_2, m_{f2}) = (2, -2, 2, -2)$ incident channel. The figure also shows the threshold of the continuum in this channel. Note that the Feshbach resonances occur at the intersection points of the bound-state energy curves with threshold, where during a cold collision a transition can occur from the incident channel to a quasi-bound state and back without change of energy.

The scattering length and bound-state spectrum presented in Fig. 1 have rather special features resulting from the approximate equality of the singlet and triplet phases, $\phi_S \approx \phi_T (mod.\pi)$, which explains the phenomenon of the coexisting ^{87}Rb Bose condensates [9, 10]. Moreover, for the actual values of the phases a bound state is very close to threshold in both the singlet and triplet potentials. To test our simple descrip-
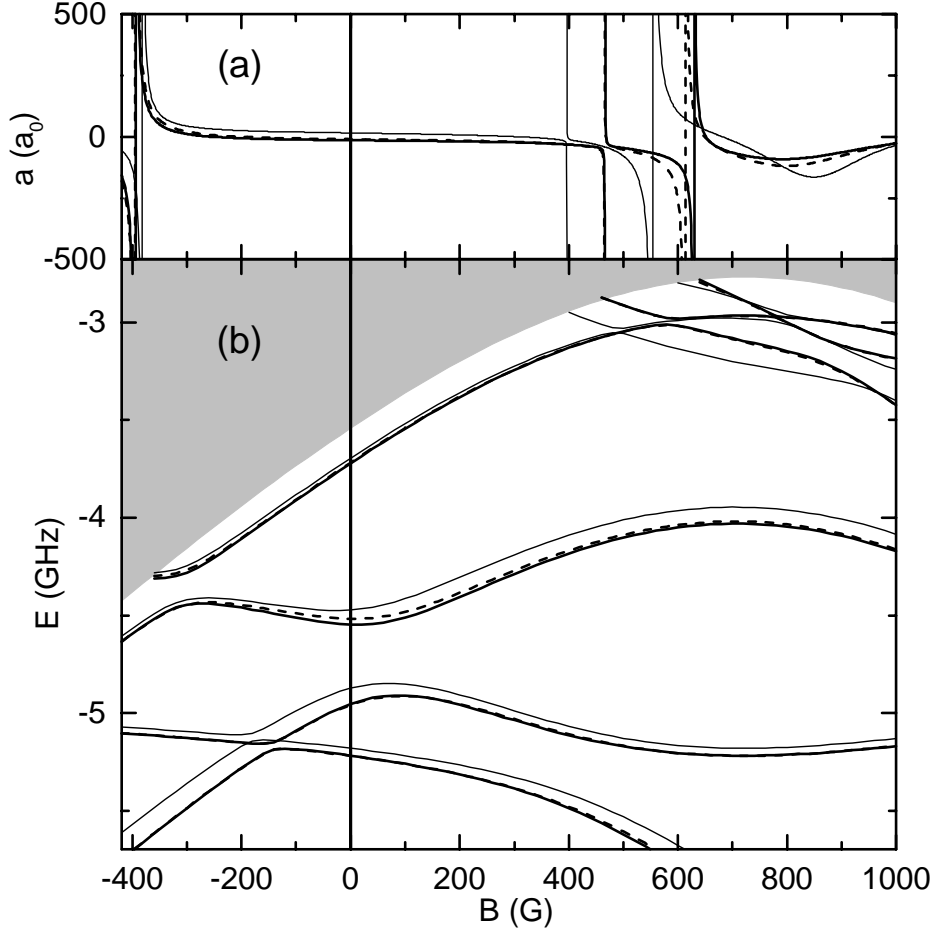
Figure 2: Same as Fig. 1 for more general choice of singlet and triplet phases, corresponding to $v_{DS}(mod.1) = 0.42$, $v_{DT}(mod.1) = 0.20$, where v_D stands for the (generally fractional) s-wave vibrational quantum number at dissociation [12]. Bold solid lines: rigorous coupled-channels calculation. Dashed lines: least simplified description for $r_c = 25\, a_0$. Thin solid lines: simpler diabatic description in which V_{exch}, V_{hf}, and V_Z are left out for $25 < r < 30\, a_0$.

tions more generally, we therefore turn to a less specific choice of phases. For such a choice, Fig. 2 shows a comparison between the rigorously calculated spectrum and scattering length (bold solid lines) and our least simplified description for $r_c = 25\, a_0$ (dashed lines). Clearly, the agreement is excellent. In particular, the model calculation displays the three Feshbach resonances. The resonance field values are reproduced to within 16 G. We repeat that no coupled radial differential equations have to be solved for this description, whereas the full problem for $B \neq 0$ comprises a set of coupled equations for five channels: one singlet and four triplet.
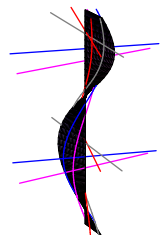
The thin solid lines in Fig. 2 result from the simpler diabatic description in which we leave out V_{exch}, V_{hf}, and V_Z in the range $25 < r < 30\,a_0$. Although less accurate, this diabatic picture apparently still leads to a semi-quantitative description. Clearly, a diabatic assumption can also be introduced over a smaller interval with correspondingly better agreement, but still allowing for the simple description in terms of phases to be presented now.

Neglecting all spin-dependence of the collision problem over a certain interval implies the equality of the local radial wave numbers $k_i(r) = \bar{k}(r)$ for all channels, both in the $S = 0, 1$ basis and in the hf basis. As a consequence, the continuity requirement for the wave function can be formulated in terms of 'interior' and 'exterior' phases that are effectively independent of r over the interval: shifting r by Δr changes all phases by the same amount $\bar{k}\Delta r$, leaving the continuity requirement unchanged since only differences of phases come in. We emphasize, however, that we do not neglect the dependence of the phases on the energy E, nor the differences in kinetic energy further inside among triplet channels: in general there are significant phase differences for the various triplet states, resulting from the diagonalization of $V_{hf}^+ + V_Z$, accumulated over the full interval starting at the repulsive wall at small r [11]. We denote the accumulated phases as $\phi_S, \phi_{T1}, \phi_{T2}, \ldots$. In the extreme case of a single pure triplet channel, which actually occurs for the fully spin-polarized system, the continuity requirement for a bound state to occur at the energy considered can be formulated in terms of an equality of a single interior phase to a single exterior phase resulting from the integration of the Schrödinger equation starting from large r, assuming a wavefunction that goes to zero at infinity. This equality can be imposed equivalently at any point of the interval considered. Due to the spin-independence the same holds for more than one channel. In the general case we therefore introduce new interior phases, independent of the choice for r in the interval, by redefining their values $mod.\pi$ to be 0 in the case that an s-wave bound state is precisely at the singlet or triplet threshold. Correspondingly, we define r-independent exterior phases by assigning the value 0 ($mod.\pi$) to a hf channel i, when the energy E of the system coincides with the threshold $\epsilon_{hf,i}$ where this channel opens:

$$\phi_{hf,i} = \phi_{hf}(E - \epsilon_{hf,i}) \tag{4}$$

with $\phi_{hf}(0) = 0$ by definition. Fig. 3 shows the hf phase $\phi_{hf}(\epsilon)$ as calculated by solving the s-wave Schrödinger equation for $E < \epsilon_{hf,i}$ (solid line). Except for a part very close to threshold where quantum effects are important at the outer turning point, it shows the typical $(-\epsilon)^{\frac{1}{3}}$ behavior, to be expected on the basis of a semiclassical consideration [12] using a pure C_6 potential. For the actual C_6 value the latter behavior is given by the dashed line. The dotted line shows the cubic root expression with a modified C_6 value and a slight shift along the ϕ axis to compensate for an offset caused by the above quantum effects. Clearly, after these adjustments we obtain excellent agreement with the rigorously calculated hf phase. Note that an external magnetic field simply shifts the hf energies by the Zeeman shift. It does not affect the function $\phi_{hf}(\epsilon)$, the interaction $V(r)$ being unchanged. Note also that in our simple descriptions the Zeeman shift of the hf energies is the main mechanism responsible for the Feshbach resonances.

For $E > \epsilon_{hf,i}$, the wavefunction does not need to go to zero at infinity. Instead, it depends on the asymptotic phase shift at large r in the hf channel involved. The treatment with one open channel, which is the most common situation experimentally,
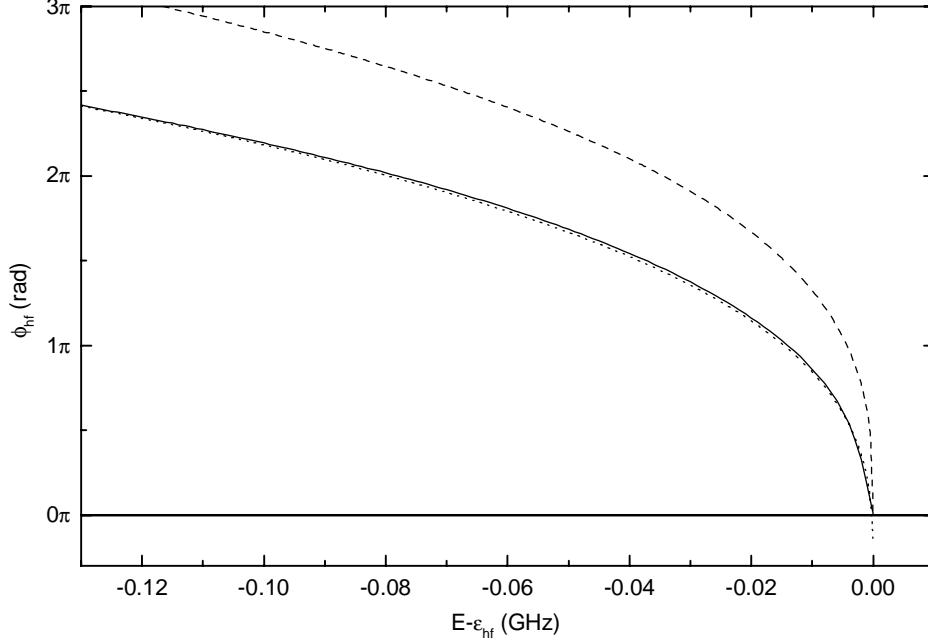
Figure 3: Hyperfine phase $\phi_{hf}(\epsilon)$ calculated by solving s-wave Schrödinger equation for $E < \epsilon_{hf,i}$ (solid line). Dashed line: semiclassical $(-\epsilon)^{\frac{1}{3}}$ behavior for actual value of C_6. Dotted line: cubic root expression with modified C_6 and vertical shift, adjusted to rigorous hf phase for actual potential.

is still relatively simple. In that case we have for the open channel, say $i = 1$:

$$\phi_{hf,1} = \phi_{hf}(E - \epsilon_{hf,1}; \delta), \tag{5}$$

with δ the asymptotic phase-shift. Again, we point out that the DIS approximation is a special case, in which the differences of the hf shifts $\epsilon_{hf,i}$ in Eqs. (4) and (5) are neglected [3].

With the above conventions the continuity requirement for the wave function can be formulated as a set of homogeneous linear equations in the sines and cosines of the phases. For given ϕ_S and ϕ_{Tj} phases, the solution of the coupled bound-state or collision problem can thus be reduced to finding the zeros of the corresponding determinant as a function of E for bound states and as a function of δ for an arbitrary continuum energy for collisions.

Summarizing, we have formulated two simplified approaches that may be used to avoid a cumbersome coupled-channels calculation. In one approach, one neglects the simultaneous spin precessions due to the exchange interaction and due to the incompatible part of the hf interaction, by neglecting one type of precession up to a certain radius r_c and the other type beyond r_c. This approximation has been shown to be very accurate. A second approach is based on the more far-reaching assumption of a radial range where the Hamiltonian is a scalar in spin space, thus leading to a diabatic picture. The
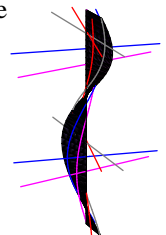
results are not as accurate, but this description is very helpful for physical insight, as it enables a treatment of the continuity requirement in terms of local interior and exterior phases.

References

[1] J.P.H.W. van den Eijnde, Thesis Eindhoven University, 1984 (unpublished).

[2] H.T.C. Stoof, J.M.V.A. Koelman, and B.J. Verhaar, Phys. Rev. B **38**, 4688 (1988).

[3] We point out that the DIS approximation, as introduced in Ref. [2], is not applied to calculate an S-matrix element S_{ij}, but only the part remaining after splitting off threshold factors $k_i^{l_i + \frac{1}{2}}$ and $k_j^{l_j + \frac{1}{2}}$.

[4] E. Tiesinga et al., Phys. Rev. A **43**, 5188 (1991).

[5] A.M. Lane, Nucl. Phys. **35**, 676 (1962).

[6] U. Fano, J. Opt. Soc. Am. **65**, 979 (1975).

[7] B.J. Verhaar, K. Gibble, and S. Chu, Phys. Rev. A **48**, R3429 (1993).

[8] C.C. Tsai et al., Phys. Rev. Lett. **78**, 1245 (1997) (Chapter 3); J.M. Vogels et al., Phys. Rev. A **56**, R1067 (1997) (Chapter 5).

[9] C.J. Myatt et al., Phys. Rev. Lett. **78**, 586 (1997).

[10] S.J.J.M.F. Kokkelmans et al., Phys. Rev. A **55**, R1589 (1997); P.S. Julienne et al., Phys. Rev. Lett. **78**, 1880 (1997); J.P. Burke, Jr. et al., Phys. Rev. A **55**, R2511 (1997).

[11] The papers [10] that explained the coexistence of the ^{87}Rb Bose condensates in terms of approximately equal phases $\phi_S \approx \phi_T$, effectively used an even simpler picture in which the differences of the triplet phases is neglected.

[12] R.J. Le Roy, in *Semiclassical methods in molecular scattering and spectroscopy*, edited by M.S. Child (D. Reidel Publishing Company, London, 1979).

3. Two-color photoassociation spectroscopy of ground state Rb$_2$

C.C. Tsai,[a] R.S.Freeland,[a] J.M. Vogels,[b] H.M.J.M. Boesten,[b] B.J. Verhaar,[b] and D.J. Heinzen[a]

[a] *Dept. of Physics, The University of Texas, Austin, Texas 78712*
[b] *Eindhoven University of Technology, Box 513, 5600MB Eindhoven, The Netherlands*

Abstract

We determine the energies of twelve vibrational levels lying within 20 GHz of the lowest dissociation limit of ^{85}Rb$_2$ with two-color photoassociation spectroscopy of ultracold ^{85}Rb atoms. The levels lie in an energy range for which singlet and triplet states are mixed by the hyperfine interaction. We carry out a coupled channels bound state analysis of the level energies, and derive accurate values for ^{85}Rb$_2$ interaction parameters. The information obtained is sufficient to allow for quantitative calculations of arbitrary Rb ultracold collision properties.

An important reason for the interest in Bose-condensed, magnetically trapped alkali vapors [1, 2, 3] is that it is possible to understand many of their properties from first principles, starting with known atomic interactions. This close contact between theory and experiment requires accurate atomic interaction parameters such as elastic scattering lengths and inelastic collision cross sections. In principle these quantities can be computed from the atomic interaction potentials. Substantial progress has been made, for example, in the determination of Li [4, 5, 6], Na [7, 8, 9], and Rb [10, 11, 12, 13] scattering lengths. Unfortunately, it has still not been possible to calculate many important collision properties because of uncertainties in the potential parameters.

In this paper, we present new results that eliminate most of these uncertainties for Rb. We measure the energies of twelve of the highest bound vibrational levels of ground state ^{85}Rb$_2$ with two-color ultracold atom photoassociation spectroscopy. As illustrated in Fig. 1, ultracold ^{85}Rb atoms collide in the presence of two laser fields of frequency ν_1 and ν_2. Resonances observed at specific values of the frequency difference $\nu_2 - \nu_1$ directly provide the level energies. We analyze the level energies with an inverse perturbation approach with coupled channels bound states, and obtain both singlet and triplet parameters. Two-color photoassociation spectroscopy has previously been used to obtain a single ground state level of Li$_2$ [5], and evidence for ground state levels of Na$_2$ [14]. Our work differs from this in that we obtain a much more complete spectrum, assignment, and analysis.

A unique aspect of our work is that we obtain a molecular spectrum for levels with
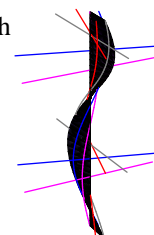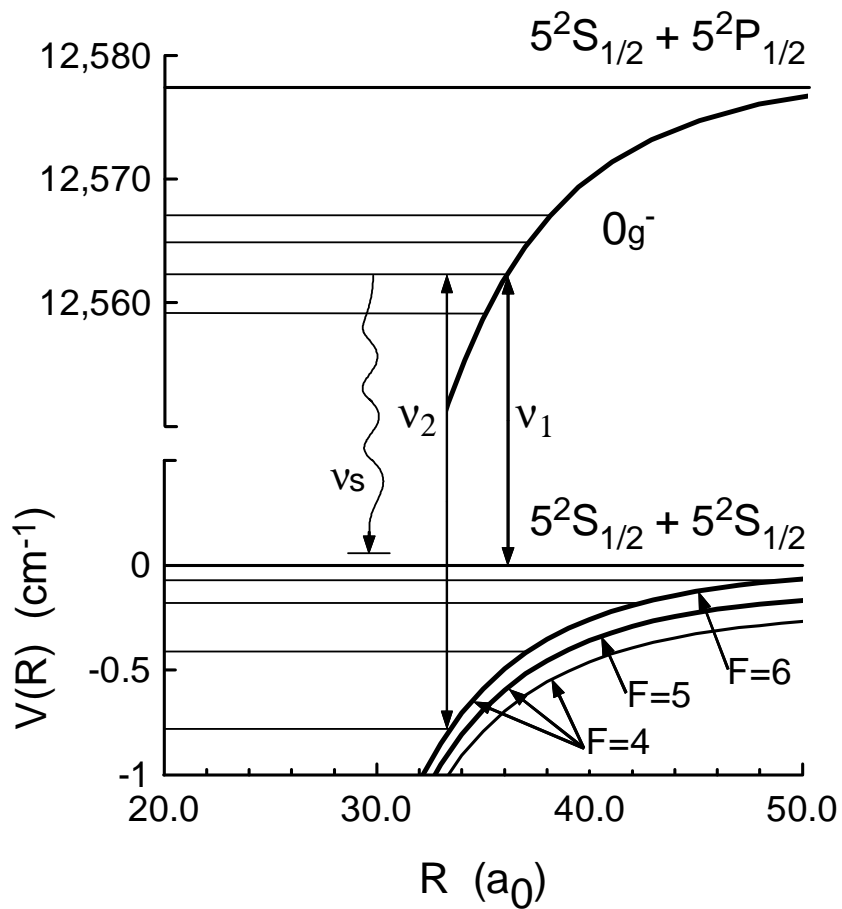
Figure 1: Two-color photoassociation spectroscopy of $^{85}Rb_2$. Colliding, trapped, ultracold ^{85}Rb atoms are irradiated by laser fields of frequency ν_1 and ν_2. Spontaneous emission from the excited level at frequency ν_s leads to loss of the atoms from the trap. Optical double resonance (free-bound-bound) signals occur when the frequency difference $\nu_2 - \nu_1$ coincides with the binding energy of a ground state vibrational level.
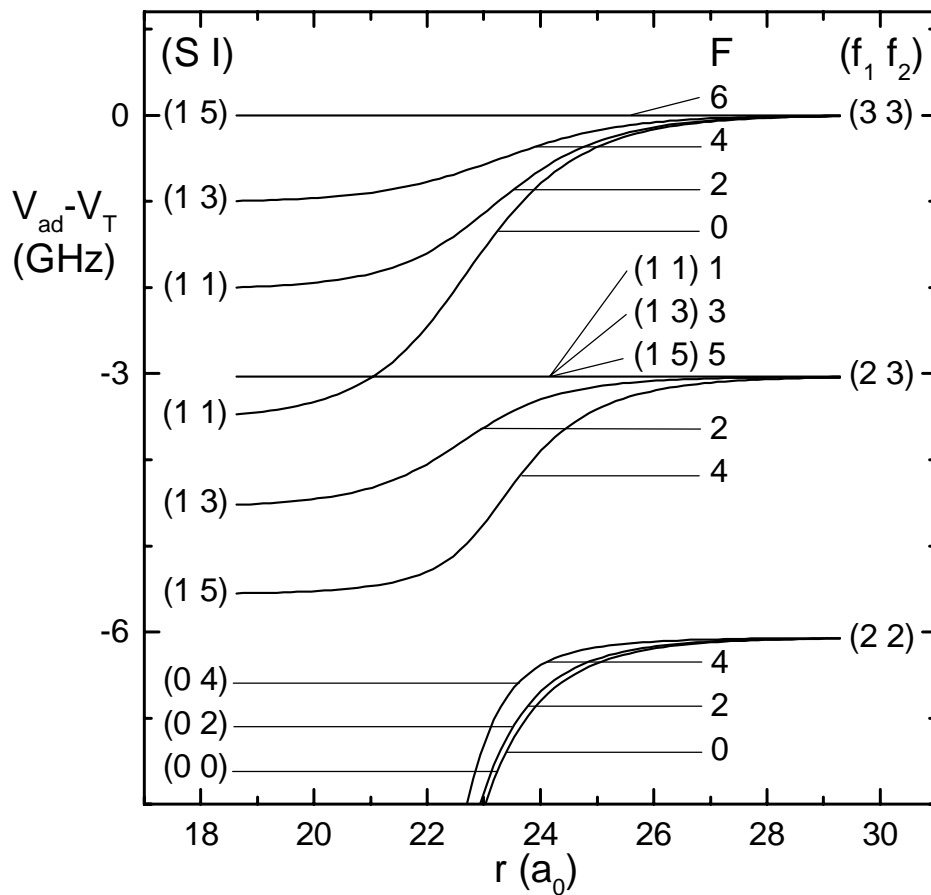
Figure 2: Diagram showing the adiabatic molecular potentials for ground state $^{85}Rb_2$ with the pure triplet, $F = 6$ potential energy subtracted off. The potentials are labeled at short range by their molecular quantum numbers and at long range by their atomic quantum numbers.
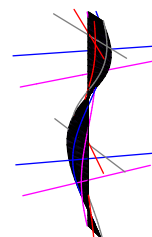
binding energies comparable to the atomic hyperfine splitting. In this range singlet ($S = 0$) and triplet ($S = 1$) states are strongly mixed by the hyperfine interaction $V_{hf} = a(\mathbf{i}_1 \cdot \mathbf{s}_1 + \mathbf{i}_2 \cdot \mathbf{s}_2)$, so that molecular quantum numbers (S, I) are not good. Here $\mathbf{S} = \mathbf{s}_1 + \mathbf{s}_2$, $\mathbf{I} = \mathbf{i}_1 + \mathbf{i}_2$, and $\mathbf{s}_i$ and $\mathbf{i}_i$ are the electronic and nuclear spins of the two atoms ($i = 1, 2$), respectively. Atomic quantum numbers (f_1, f_2, with $\mathbf{f}_i = \mathbf{s}_i + \mathbf{i}_i$) are not good either, since these states are mixed at short range by the exchange interaction. Only the total spin quantum number F, with $\mathbf{F} = \mathbf{f}_1 + \mathbf{f}_2 = \mathbf{S} + \mathbf{I}$, is good at all internuclear distances. Adiabatic molecular potentials for ^{85}Rb$_2$ with the pure triplet ($F = 6$) potential subtracted off are shown in Fig. 2. The change between molecular and atomic (hyperfine) coupling occurs at about 24 a_0. Molecular vibrations on these potentials are are not perfectly adiabatic, so that curves with the same F must be treated with a coupled channels approach.

The experiment is an extension of our previous one-color photoassociation experiments [10, 11, 12]. About 10^4 laser-cooled ^{85}Rb atoms, at a temperature of several hundred microKelvin and a density of about 10^{12} cm^{-3}, are spin-polarized in their $f = 3$, $m_f = 3$ state and held in a far-off resonance optical dipole force trap (FORT) [15]. These atoms are irradiated for 200 ms with two laser fields of frequencies ν_1 and ν_2, which have intensities of 1.6 kW/cm^2, and 30-200 W/cm^2, respectively. These fields are alternated at 200 kHz with the FORT laser. The laser frequency ν_1 is fixed on a photoassociation resonance between the collision state and a $|0_g^-(v, J)\rangle$ excited state near the $5^2S_{1/2} + 5^2P_{1/2}$ dissociation limit, where v is the vibrational quantum number and J the rotational quantum number. This induces substantial trap loss, since the excited states decay mostly to high kinetic energy atoms which escape from the trap. At the end of each 200 ms period, we measure the number of atoms remaining in the trap with laser-induced atomic fluorescence. We produce a two-color spectrum by stepping ν_2 through a succession of values.

A typical two-color photoassociation spectrum is shown in Fig. 3. We observe a decrease in the loss of atoms from the trap whenever ν_2 is tuned to a resonance between the intermediate level and a ground state level. This is due to to power broadening of the excited state, which reduces the absorption rate of photons on the first step and therefore the trap loss. We took spectra with three different values of v in the intermediate state, and with $J = 2$. The positions of the lines depended only on $\nu_2 - \nu_1$, and their widths varied from 0.060 GHz to 0.30 GHz. We observed a total of twelve levels with the energies listed in Table 1. In addition we supplemented the data with the energy of a g-wave shape resonance [12]. We estimated the errors from the differences between the positions of the same level in different spectra. We also took them to be at least $\pm 1/4$ of the linewidths, to allow for possible lineshape effects [16], which we did not attempt to model. The highest level is bound by only 0.16 GHz. To our knowledge, this is the most weakly bound level that has been spectroscopically observed in any molecule.

We assign the spectrum as follows. With a two-photon transition from the initial $M_F = 6$ state, only $F = 4$, 5, or 6 levels should appear in the spectrum. The $F = 6$ and $F = 5$ states are isolated, pure triplet channels, separated from each other by one unit of atomic hyperfine energy (3.036 GHz). (See Fig. 2.) Therefore, we may assign the vibrational progressions converging to the $(f_1, f_2) = (3, 3)$ and $(2, 3)$ limits to the $F = 6$ and $F = 5$ vibrational levels, respectively. The remaining levels must arise from the three coupled, $F = 4$ potentials, and have mixed singlet and triplet character. As

F	l	$E_{exp}(GHz)$	$E_{th}(GHz)$	$[v - v_D]$	(f_1, f_2)
6	4	$+0.015 \pm 0.002$	$+0.013$	-1	(3,3)
6	2	-0.16 ± 0.03	-0.15	-1	(3,3)
5	2		-3.18	-1	(2,3)
4	2	-6.23 ± 0.06	-6.22	-1	(2,2)
6	2	-1.52 ± 0.03	-1.50	-2	(3,3)
5	2	-4.58 ± 0.06	-4.53	-2	(2,3)
4	2	-7.61 ± 0.03	-7.57	-2	(2,2)
6	2	-5.20 ± 0.03	-5.16	-3	(3,3)
5	2		-8.20	-3	(2,3)
4	2	-8.34 ± 0.06	-8.36	-3	(2,3)
4	2	-11.27 ± 0.03	-11.24	-3	(2,2)
6	2	-12.22 ± 0.06	-12.21	-4	(3,3)
4	2		-12.51	-4	(3,3)
5	2	-15.24 ± 0.06	-15.25	-4	(2,3)
4	2	-15.67 ± 0.06	-15.68	-4	(2,3)
4	2	-18.39 ± 0.06	-18.34	-4	(2,2)

Table 1: Experimental energy levels included in analysis and theoretical energy levels calculated with coupled-channel bound-states code, together with (f_1, f_2) progression and integer part of $v - v_D$. The $l = 4$ level included in the table is a shape resonance state observed in Ref. 12.

discussed previously [10], with the $0_g^-(\sim 5^2 S_{1/2} + 5^2 P_{1/2})$ intermediate state, we probe ground rotational states with $l = J = 2$.

To carry out an analysis of these spectra, we have developed an inverse perturbation approach for coupled bound states (coupled IPA). The usual (uncoupled) IPA [17] is a systematic approach to improve an approximate interaction potential $V^0(r)$ on the basis of a comparison of its bound-state energy eigenvalues E_n^0 with experimental values E_n. Changing the potential to $V^0(r) + \Delta V(r)$ changes the energies in first-order perturbation theory by

$$E_n - E_n^0 = \langle \phi_n^0 | \Delta V(r) | \phi_n^0 \rangle, \tag{1}$$

with known unperturbed eigenfunctions ϕ_n^0. Writing the correction $\Delta V(r)$ as a linear combination of suitably chosen basis functions $f_i(r)$,

$$\Delta V(r) = \sum_i c_i f_i(r), \tag{2}$$

turns Eq. (1) into a set of linear equations which allows one to determine optimal expansion coefficients c_i.

Our method differs in two aspects from this approach. First, we incorporate coupled channels bound states, extending the expectation value (1) to a multichannel state. Second, we replace the atomic interaction inside $r = r_0$ with a boundary condition at r_0 on the phases ϕ_S and ϕ_T of the singlet and triplet radial wavefunctions [4]. We choose $r_0 = 20a_0$, small enough that singlet-triplet mixing inside r_0 is negligible, but large enough that the potentials outside r_0 have a simple description involving few parame-
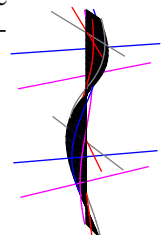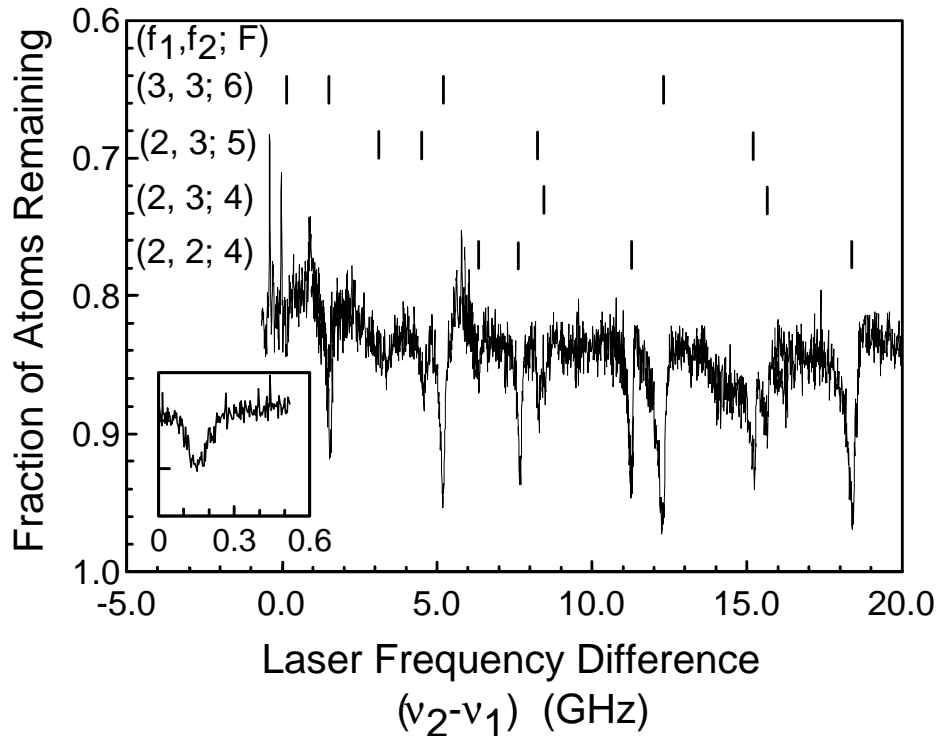
Figure 3: Two-color photoassociation spectrum of $^{85}Rb_2$, with ν_1 tuned into resonance with a level at 12563.1 cm^{-1}. Double resonance signals are observable as a decrease in the trap loss. The positions and quantum numbers of the levels inferred from the analysis are also indicated. The inset at the lower left shows the highest level observed, with a binding energy of only 0.16 GHz.

ters. In our version of IPA, we supplement the equation for the perturbation of the outer solution due to a change ΔV by an equation for the perturbation due to a change in ϕ_S and ϕ_T, making use of boundary perturbation theory [18]. An advantage of our method compared to the conventional IPA is that the set of parameters to be determined is more unique than in Eq. (2), where a subtle choice of basis functions is needed to avoid unrealistic adaptations of the potential. Our method also has the advantage that it treats singlet and triplet states simultaneously. A separate construction of singlet and triplet potentials from measured levels may lead to inconsistencies, as pointed out by Zhao *et al.* [19]. As in conventional IPA we apply our method in an iterative way. In each step we solve the equations for the first-order perturbations to find new parameter values. These then define the new unperturbed solution of Schrödinger's equation for the next step. The perturbation equations are also used to estimate error bars for the parameter values extracted from the coupled IPA analysis.

We write the long-range ($r > r_0$) interaction part of the two-atom Hamiltonian in

the form

$$V = -\frac{C_6}{r^6} - \frac{C_8}{r^8} - \frac{C_{10}}{r^{10}} + V_{exch} + V_{hf}. \tag{3}$$

C_6 is taken to be 4550 ± 100 a.u. [12], the exchange part is from Smirnov and Chibisov [20], and C_8 and C_{10} from Marinescu *et al.* [21]. We neglect the long range spin-dipolar interaction between the atoms, because its contribution to the level energies is small compared to the experimental accuracy. The inner part of the singlet potential has been determined by Amiot [22] by means of a conventional IPA. We adjust the zero of Amiot's energy scale to agree with a new, precise value of the Rb_2 dissociation energy $D_e = 3993.53 \pm 0.06$ cm^{-1} [23]. From this adjusted singlet potential, we calculate $\phi_S(E,)$ for arbitrary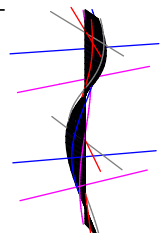 energy E and relative orbital angular momentum l. We treat $\phi_S(0,0)$ as a fit parameter in the analysis, and the calculated variation of $\phi_S(E,l)$ with E and l as boundary conditions for the $r > r_0$ IPA problem. For the triplet state no accurate potential is available, so we treat $\phi_T(0,0)$ and its first derivatives with respect to E and $l(l+1)$ at $E = l = 0$ as variable parameters.

We begin by analyzing the pure triplet ($F = 5, 6$) states. The optimal phase parameters allow us to calculate the $^{85}Rb + {}^{85}Rb$ triplet scattering length to be $a_T({}^{85}Rb) = -440 \pm 140\ a_0$, consistent with the value $-400 \pm 100\ a_0$ from Ref. [12]. Uncertainties of 2% in C_6 and 4% in C_8 and C_{10} are accounted for in the final error limits. The corresponding non-integral s-wave vibrational quantum number at dissociation $v_{DT}(\text{mod}.1)$ has the value 0.95 ± 0.01, where the integer part of v_{DT} is 37 ± 1 [12].

Next we analyze the complete set of levels. Varying $\phi_S(0,0)$ alone, the six measured $F = 4$ levels fall in place within their experimental bounds. All of the theoretical $F \geq 4$, $l = 2$ eigenvalues in the last 20 GHz resulting from the combined optimization are presented in Table 1. We obtain satisfactory agreement with the experimental levels. The triplet scattering length from the combined analysis is identical with the value given above. For the singlet scattering length we find $+4500\ a_0 < a_S({}^{85}Rb) < +\infty$ or $-\infty < a_S({}^{85}Rb) < -1200\ a_0$. The corresponding v_{DS} is 122.994 ± 0.012, where in this case the integer part is quite certain. Our value shows a small discrepancy with the value $123.45(0.20)$ determined by Amiot [22].

A remarkable property of four of the observed $F = 4$ levels is their rather accurate triplet progression asymptotic to the $(f_1, f_2) = (2, 2)$ collision threshold. This results from an approximate equality between singlet and triplet phases for $^{85}Rb_2$ in the coupling region. Because of this, the highest parts of the uncoupled triplet and singlet bound state spectra approximately coincide, and the triplet and singlet interaction potentials are effectively interchangeable. The hyperfine mixing, which takes place almost exclusively at long range where the atoms are almost all of the time, then leads to a spin structure of the coupled states that is almost identical to that in the three asymptotic hyperfine channels. The calculation also shows similar $F = 4$ level progressions asymptotic to the $(f_1, f_2) = (2, 3)$ and $(3, 3)$ thresholds, and some of these levels are observed experimentally. In Table 1 we present for each predicted level the (f_1, f_2) combination characterizing the progression it belongs to and its vibrational quantum number relative to v_D. $F = 4$ levels above the $(f_1, f_2) = (2, 2)$ limit are not given since they are not bound. A very similar phase coincidence has been found to be responsible for the stability of a Bose-condensed mixture of two states of ^{87}Rb [24, 25]. Considering the mass scaling of the wavefunction phases between ^{87}Rb and ^{85}Rb, it turns out that an approx-

imate equality of ϕ_S and ϕ_T (mod.π) in one isotope implies a similar equality in the other.

In combination with other recent results, our measurements have now determined Rb interaction parameters to sufficient accuracy to allow quantitative calculations of Rb cold collision cross sections to be carried out. Calculations based on these parameters [26] are in agreement with all known properties of cold Rb atom scattering [10, 11, 12, 13, 24, 25]. The strong consistency among these measurements provides confirmation for their validity. In addition, it is now possible to precisely calculate other important cold collision properties such as the scattering lengths for arbitrary Rb sublevels, the location of magnetically tunable Feshbach resonances [26], inelastic collision rates, and the collisional frequency shift of a Rb atomic fountain clock [27]. We anticipate that future studies of ultracold Rb collisions will rest on a quantitative footing that is unusual in cold collision physics.

References

[1] M.H. Anderson, J.R. Ensher, M.R. Matthews, C.E. Wieman, and E.A. Cornell, Science **269**, 198 (1995).

[2] K.B. Davis, M.-O. Mewes, M.R. Anderson, N.J. van Druten, D.S. Durfee, D.M. Kurn, and W. Ketterle, Phys. Rev. Lett. **75**, 3969 (1995).

[3] C. C. Bradley, C. A. Sackett, and R. G. Hulet, Phys. Rev. Lett. **78**, 985 (1997).

[4] A.J. Moerdijk, W.C. Stwalley, R.G. Hulet, and B.J. Verhaar, Phys. Rev. Lett. **72**, 40 (1994).

[5] E.R.I. Abraham, W.I. McAlexander, C.A. Sackett, and R.G. Hulet, Phys. Rev. Lett. **74**, 1315 (1995).

[6] E. R. I. Abraham *et al.*, Phys. Rev. A **53**, R3713, (1996).

[7] A.J. Moerdijk and B.J. Verhaar, Phys. Rev. Lett. **73**, 518 (1994).

[8] E. Tiesinga, C. J. Williams, P. S. Julienne, K. M. Jones, P. D. Lett, and W. D. Phillips, J. Res. Natl. Inst. Stand. Technol. **101**, 505 (1996).

[9] K.B. Davis, M.-O. Mewes, M.A. Joffe, M.R. Andrews, and W. Ketterle, Phys. Rev. Lett. **74**, 5202 (1995).

[10] J.R. Gardner, R.A. Cline, J.D. Miller, D.J. Heinzen, H.M.J.M. Boesten, and B.J. Verhaar, Phys. Rev. Lett. **74**, 3764 (1995).

[11] H. M. J. M. Boesten, C. C. Tsai, J. R. Gardner, D. J. Heinzen and B. J. Verhaar, Phys. Rev. A **55**, 636 (1997).

[12] H. M. J. M. Boesten, C. C. Tsai, B. J. Verhaar, and D. J. Heinzen, Phys. Rev. Lett. **77**, 5194 (1996).

[13] N.R. Newbury, C.J. Myatt, and C.E. Wieman, Phys. Rev. A **51**, R2680 (1995).

[14] K. M. Jones, S. Maleki, L. P. Ratliff, and P. D. Lett, J. Phys. B **30**, 289 (1997).

[15] J. D. Miller, R. A. Cline, and D. J. Heinzen, Phys. Rev. A **47**, R4567 (1993).

[16] J. L. Bohn and P. S. Julienne, Phys. Rev. A**54**, R4637 (1996).

[17] C.R. Vidal, Comments At. Mol. Phys. **17**, 173 (1986).

[18] P.M. Morse and H. Feshbach, *Methods of Theoretical Physics* (McGraw-Hill, New York, 1953).

[19] G. Zhao *et al.*, J. Chem. Phys. **105**, 7976 (1996).

[20] B.M. Smirnov and M.I. Chibisov, JETP **21**, 624 (1965).

[21] M. Marinescu, H.R. Sadeghpour, and A. Dalgarno, Phys. Rev. A **49**, 982 (1994).

[22] C. Amiot, J. Chem. Phys. **93**, 8591 (1990).

[23] C.C. Tsai, J.D. Miller, R.A. Cline, and D.J. Heinzen (to be published).

[24] C.J. Myatt, E. A. Burt, R. W. Ghrist, E. A. Cornell, and C. E. Wieman, Phys. Rev. Lett. **78**, 586 (1997).

[25] S.J.J.M.F. Kokkelmans, H.M.J.M. Boesten, and B.J. Verhaar, Phys. Rev. A **55**, R1589 (1997); P.S. Julienne, F. H. Mies, E. Tiesinga, and C.J. Williams, Phys. Rev. Lett. **78**, 1880 (1997); J.P. Burke, Jr., J.L. Bohn, B.D. Esry, and C.H. Greene, Phys. Rev. A **55**, R2511 (1997).

[26] J.M. Vogels, C.C. Tsai, R.S. Freeland, S.J.J.M.F. Kokkelmans, B.J. Verhaar, and D.J. Heinzen, Phys. Rev. A **56**, 2 (1997) (Chapter 5).

[27] S.J.J.M.F. Kokkelmans, B. J. Verhaar, K. Gibble and D.J.Heinzen, Phys. Rev. A. **56**, R4389 (1997).
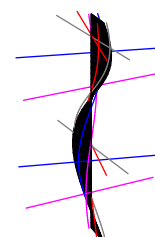
4. Coupled inverse perturbation analysis of two-color cold atom photoassociation spectra

J.M. Vogels[a], R.S. Freeland[b], C.C. Tsai[b], B.J. Verhaar[a], and D.J. Heinzen[b]

[a] *Eindhoven University of Technology, Box 513, 5600 MB Eindhoven, The Netherlands*
[b] *Department of Physics, The University of Texas, Austin, Texas 78712*

Abstract

We describe a new inverse perturbation method that is well suited to the analysis of the bound states of the alkali dimers near their dissociation limit. The method combines inverse perturbation theory, coupled channels bound state theory, and an accumulated phase method to treat the short range part of the molecular potentials. We apply this method to analyze the bound-state energies measured in a two-color photoassociation experiment in an ultracold ^{85}Rb gas. This analysis yields information on the interactions between ultracold ^{85}Rb atoms that is important to the understanding of ultracold Rb collisions and Bose-Einstein condensation.

4.1 Introduction

The techniques of laser cooling and evaporative cooling have opened the new field of ultracold atom physics for alkali atoms, with spectacular research subjects such as Bose-Einstein condensation, laser-cooled atomic clocks, and atom lasers. It is generally realized that atom interaction processes play a key role in many of these experiments. It is therefore important to obtain a complete, consistent picture of these interactions. In this paper we describe and apply a new theoretical method to obtain information on the interactions between cold atoms, making use of measured energies of bound diatomic states close to the dissociation threshold. The method is an extension of Inverse Perturbation Analysis (IPA) [1], previously used to obtain a single adiabatic Born-Oppenheimer interaction potential curve from bound-state energies of that potential. The coupled inverse perturbation analysis (CIPA) that we propose generalizes this method to cases where different electronic states are strongly coupled, so that the Born-Oppenheimer approximation breaks down. We apply this method to the analysis of the highest bound states of ^{85}Rb$_2$, which have recently been measured with two-color photoassociation spectroscopy [2]. In this case the molecular singlet and triplet states are strongly coupled
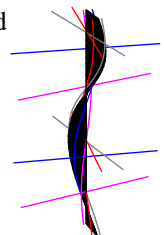
by the hyperfine interaction. We also use the information obtained from this analysis to determine interaction parameters that are important to the physics of collisions of ultra-cold [85]Rb atoms. A brief report of this work has been given previously [2]; in this paper we give a more extensive description of the experimental and theoretical method and of the results.

In the case of ground-state alkali atoms there are two short range adiabatic Born-Oppenheimer potentials, corresponding to total spin $S = 0$ (singlet potential) or $S = 1$ (triplet potential). Along the lines of our previous work, at small interatomic distances we do not describe the singlet and triplet potentials in detail, but summarize that information in the form of the phases accumulated [3] by the associated rapidly oscillating $S = 0$ and $S = 1$ radial wavefunctions up to a radius r_0, which is chosen between 16 and 20 a_0 depending on the alkali atom considered. It is well-known that both cold collision properties and the precise positions of the highest molecular bound states are extremely sensitive to very small changes of the $r < r_0$ potentials. Except for the lighest alkali species, potentials in this range are not known with sufficient accuracy to allow for reliable application to cold collisions. Fortunately, it is possible to avoid this difficulty using boundary conditions at r_0 in the form of accumulated singlet and triplet phases that summarize the short-range collisional information. In our coupled IPA we search for optimal values of the interaction parameters in the range $r > r_0$ and of the accumulated phases.

The main advantage of our generalized approach is that it can cope with bound states close to the continuum, which often show strong singlet-triplet mixing by the hyperfine interaction. In contrast, the conventional IPA can be used only for analyzing pure triplet and singlet bound diatomic states. Clearly, the higher mixed states can be expected to bear a greater resemblance to the nearby states in the continuum and can therefore more profitably be used for obtaining information on cold collisions by extrapolation through the dissociation threshold. Even for analyzing lower states without significant mixing, however, our approach has a definite advantage in that it naturally allows for a simultaneous analysis of singlet and triplet levels. This is important in view of the fact that the singlet and triplet potentials have certain parameters in common, such as the position of the dissociation threshold and the dispersion coefficients. A separate analysis may therefore lead to inconsistencies, such as a crossing of the singlet and triplet potentials at long range [4]. A further advantage of our method is that the potential variations searched for extend over longer radial intervals. This applies to both the interactions in the range $r < r_0$, since they are effectively described via accumulated phases, and for the $r > r_0$ interactions which are described by analytic expressions for dispersion and exchange contributions. In this way one does not run into the pitfalls associated with applications of the conventional IPA where non-physical fluctuations in the local potentials over short distances, of the order of the distance between outer turning points of successive ro-vibrational levels, are difficult to avoid in the search for improved potentials.

One-color cold atom photoassociation experiments have yielded a great deal of information on the interactions between alkali atoms [5, 6]. In these experiments, a tunable laser excites transitions between the intially free state of a pair of colliding, laser-cooled ground state atoms and excited bound molecular levels of those atoms. These experiments directly yield the level structure of the electronically excited states. The line-
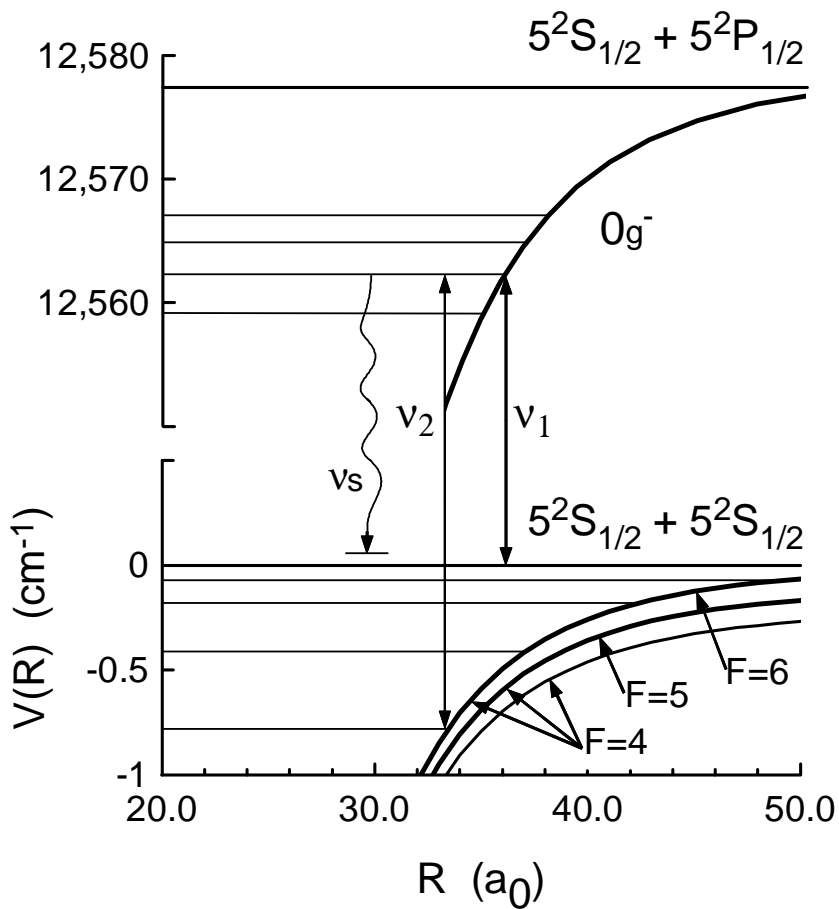
Figure 1: Two-color photoassociation spectroscopy of $^{85}Rb_2$. Colliding, trapped, ultracold ^{85}Rb atoms are irradiated by laser fields of frequency ν_1 and ν_2. Spontaneous emission from the excited level at frequency ν_s leads to loss of the atoms from the trap. Optical double resonance (free-bound-bound) signals occur when the frequency difference $\nu_2 - \nu_1$ coincides with the binding energy of a ground state vibrational level.
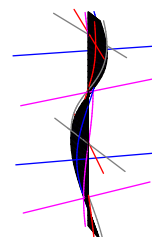
shapes and strengths of one-color photoassociation spectra have also provided information on the properties of the collisional ground state for ultracold Rb [7, 8, 9, 10, 11], Na [12], and Li [13]. More direct information on ground state cold collision properties can be obtained through the direct measurement and analysis of the highest bound levels of the electronic ground state. This can be accomplished through two-color photoassociation spectroscopy, as shown in Fig. 1. A laser at a fixed frequency ν_1 excites transitions from the collisional ground state to a particular excited level. A second tunable laser of frequency ν_2 couples this excited level back to the vibrational levels of the electronic ground state. This yields a spectrum of these high lying bound levels. Experiments of this kind have been completed for Rb [2], Na [14], and Li [15].

In our Rb two-color photoassociation experiments, we select a specific intial two-atom spin state by carrying out the experiment on a doubly-polarized gas sample, i.e. with maximum projections of electronic and nuclear spins of an atom along a quantization direction z. The atoms occupy the highest hyperfine state of the ^{85}Rb atomic Breit-Rabi diagram (see Fig. 2). As the excited electronic state we select the 0_g^- state asymptotically connected to the $5\,^2S_{1/2} + 5\,^2P_{1/2}$ dissociation limit [16]. In this way we avoid a complex hyperfine 'spaghetti' of excited states [17], since the nuclear spins in this $\Omega = 0$ state are decoupled in very good approximation from the remaining molecular degrees of freedom. Moreover, the $0_g^- (S + P_{1/2})$ electronic state has the advantage that the two $1/2$ angular momenta of the $S_{1/2}$ and $P_{1/2}$ atomic states turn out to be coupled to give a vanishing two-atom electronic angular momentum $j = 0$. The total molecular angular momentum $\mathbf{J}$ in the exited state (excluding the nuclear spins) thus equals the orbital angular momentum $\mathbf{l}$ of the collision. The resulting $J = l$ selection rule has been of considerable help in the past to simplify the analysis of our previous one-color photoassociation experiments [7, 8, 9]. We note that this is not a general property of $\Omega = 0$ states. For example, for the 0_g^- "pure long range state" connecting to the $5\,^2S_{1/2} + 5\,^2P_{3/2}$ limit [16, 18], the atomic angular momenta $1/2$ and $3/2$ do not couple to $j = 0$. Selecting the $0_g^- (S + P_{1/2})$ state, we do not only define the partial wave channel $l = J$ from which the excitation occurs, but also the rotational l value of the final Rb$_2$ bound states formed.

Even with this simplification the observed bound state spectrum should be expected to be rather complex. In particular, the complexity arises from the fact that the total spins f_1 and f_2 ($= 2$ or 3, see Fig. 2) of the separated atoms are not conserved during a collision. These quantum numbers are only good at long range. At smaller distances the exchange interaction mixes the (f_1, f_2) quantum numbers. At short range where it dominates, the molecular quantum numbers (S, I) with $\mathbf{S} = \mathbf{s}_1 + \mathbf{s}_2$ the total electron spin and $\mathbf{I} = \mathbf{i}_1 + \mathbf{i}_2$ the total nuclear spin, are good quantum numbers. For not too strong B fields the total angular momentum $\mathbf{F} = \mathbf{f}_1 + \mathbf{f}_2$ is conserved at all distances. Figure 2 of Ref. [2] shows adiabatic molecular potentials for ^{85}Rb$_2$ with the pure triplet $F = 6$ potential subtracted off. The change between molecular and atomic (hyperfine) coupling occurs between 19 and 26 a_0 for the ^{85}Rb + ^{85}Rb system. The above-mentioned radius r_0 is chosen at the left-hand boundary of this range, because we want S to be a good quantum number up to this point. Starting from r_0, the radial motion on the potentials is not perfectly adiabatic, so that curves with the same F must be treated as a coupled channels problem. Often, an r independent diabatic basis of pure (S, I) or pure (f_1, f_2) states is the most convenient choice for coupled channels calculations. By selecting an
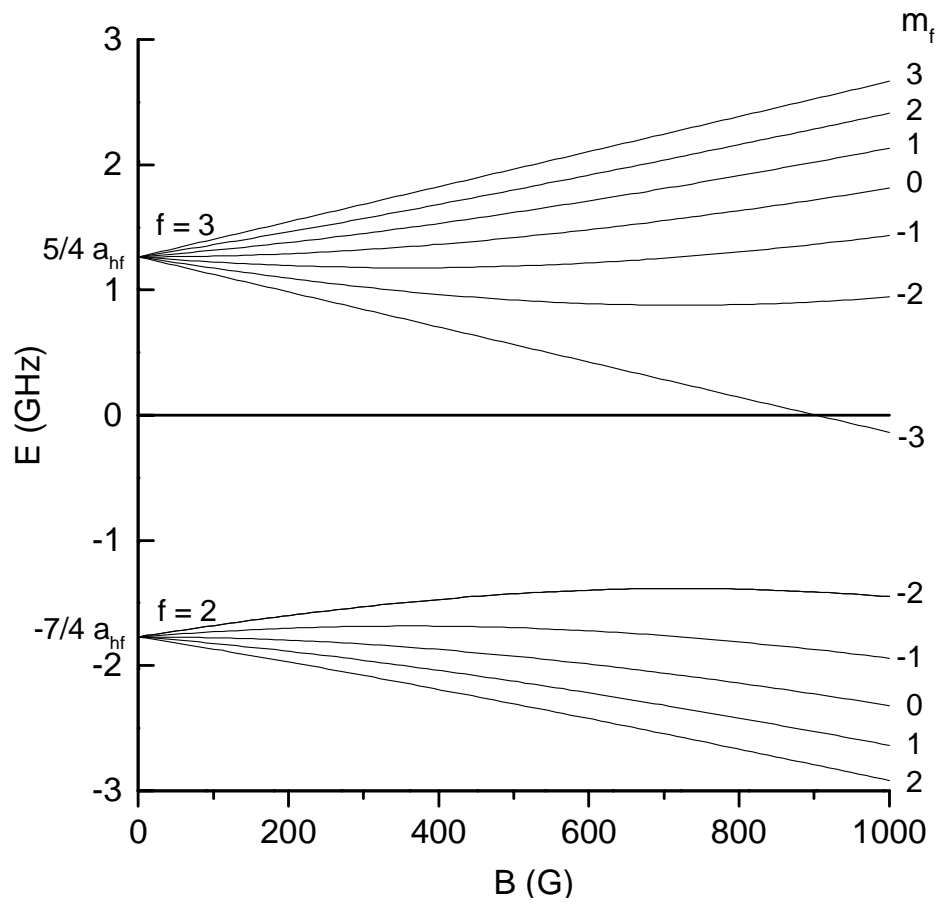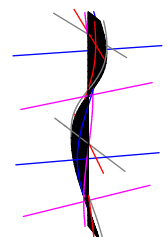
Figure 2: Breit-Rabi diagram of ^{85}Rb atomic ground state.

initial $|F, m_F\rangle = |6, +6\rangle$ two-atom state with the two electronic and the two nuclear spins fully oriented, only $F = 4$, 5, or 6 bound levels should appear in the spectrum, the change in F being at most 1 in each of the optical transitions. Together, the above choices for the initial and intermediate states lead to a considerable reduction of the complexity of the observed bound state spectrum.

This paper is organized as follows. In Section 4.2 we describe our coupled IPA method, starting from the conventional IPA and including internal degrees of freedom and accumulated phases. Section 4.3 describes the two-color photoassociation experiment. Section 4.4 is devoted to the application of our method of analysis to this experiment. In Section 4.5 we formulate some conclusions.

4.2 Coupled Inverse Perturbation Approach (Coupled IPA)

We extract optimal values for the interaction parameters from the bound-state data by an extension of the existing Inverse Perturbation Approach (IPA) [1] to a situation of coupled channels. The conventional IPA is a method to improve a potential, in such a way that the corresponding Schrödinger equation reproduces as well as possible a set of experimental bound-state energies E_n:

$$\left[-\frac{\hbar^2}{2\mu} \Delta + V(r) \right] \psi_n = E_n \psi_n, \tag{1}$$

with μ the reduced mass, equal to half the atomic mass in the present application. One makes a comparison with theoretical eigenvalues E_n^0 associated with an approximate potential $V^0(r)$ and its eigenfunctions ψ_n^0:

$$\left[-\frac{\hbar^2}{2\mu} \Delta + V^0(r) \right] \psi_n^0 = E_n^0 \psi_n^0. \tag{2}$$

Using first-order perturbation theory and an expansion of the difference potential $\Delta V = V - V^0$ in a set of suitable basis functions $g_i(r)$, the energy differences are expressed as

$$\Delta E_n \equiv E_n - E_n^0 = \langle \psi_n^0 | \Delta V | \psi_n^0 \rangle = \sum_i c_i \langle \psi_n^0 | g_i(r) | \psi_n^0 \rangle. \tag{3}$$

This set of linear equations for the unknown expansion coefficients c_i is solved generally as a least-squares problem to construct a new theoretical potential $V^0(r) + \Delta V(r)$ and the whole procedure is restarted until one reaches convergence.

The conventional IPA can only be applied to singlet and triplet potentials separately, since it assumes the absence of coupling. It therefore needs unmixed experimental singlet and triplet states as input. To formulate our coupled IPA, both Eq. (1) and (2) are considered as coupled equations in the singlet-triplet or hyperfine basis, or any other basis. The IPA equation (3) can be carried over to the multi-channel case essentially without change, ψ_n^0 now standing for a coupled state:

$$\Delta E_n = \langle \psi_n^0 | \Delta V | \psi_n^0 \rangle = \sum_i \left[c_{iS} \langle \psi_n^0 | P_S g_{iS}(r) | \psi_n^0 \rangle + c_{iT} \langle \psi_n^0 | P_T g_{iT}(r) | \psi_n^0 \rangle \right], \tag{4}$$

with ΔV an operator in spin space,

$$\Delta V = P_S \Delta V_S(r) + P_T \Delta V_T(r), \tag{5}$$

and P_S and P_T projection operators on the singlet and triplet spin subspaces, respectively.

The extension of the IPA to include coupling requires the complex task of introducing a coupled-channels matrix structure into the previous equations. This is not the only modification we introduce. As pointed out in Section 4.1 a further ingredient of our approach is the replacement of the short-range parts $r < r_0$ of the potentials $V_S(r)$ and $V_T(r)$ by a boundary condition at r_0, the largest interatomic distance where the radial motion with S as a good quantum number is still adiabatic. This takes the form of an accumulated phase $\phi_{S/T}$ of the corresponding rapidly oscillating radial wave functions $\psi_{S/T}(r)$ in each of the adiabatic channels, defined by the WKB expression

$$\psi(r_0) = A \frac{\sin\left(\int^{r_0} k(r)dr\right)}{k^{\frac{1}{2}}(r_0)} \equiv A \frac{\sin\phi(r_0)}{k^{\frac{1}{2}}(r_0)}, \tag{6}$$

$k(r)$ being the local radial wave number:

$$k^2(r) = \frac{2\mu}{\hbar^2}\left[E - V(r) - \frac{\hbar^2 l(l+1)}{mr^2}\right]. \tag{7}$$

In these equations we have omitted the subscript S or T for simplicity. Differentiating Eq. (6) we find that ϕ is related to the local logarithmic derivative by

$$k\cot\phi = \frac{\psi'}{\psi} + \frac{k'}{2k}. \tag{8}$$

The validity of the WKB approximation is not a prerequisite for this approach: we could have specified the boundary condition by means of a logarithmic derivative of the radial wave function. We come back to this later in this section. The accumulated phase may be considered as a convenient parametrization of the logarithmic derivative. Its convenience stems from its accurate linearity,

$$\phi = \phi^0 + E\phi^E + l(l+1)\phi^l, \tag{9}$$

over the relatively small E and l ranges near $E = l = 0$, relevant for cold collisions, making it possible to fit experimental data with three parameters: ϕ^0, ϕ^E, ϕ^l. In contrast, the logarithmic derivative shows the typical tangent-shaped excursions through infinity each time a radial node passes the point $r = r_0$. Figure 3 shows ϕ_S and ϕ_T as a function of E for $l = 0$ (part a) and as a function of $l(l+1)$ for $E = 0$ (part b), in both cases over ranges much larger than needed for the analysis in Section 4.4. The E and $l(l+1)$ ranges covered by the actual measurement are indicated by the double-sided arrows in the graphs. Over this range the E dependence is linear to within $\Delta\phi_S = \pm 6.10^{-5}$ and $\Delta\phi_T = \pm 11.10^{-5}$, and the $l(l+1)$ dependence even to within $\Delta\phi_S = \pm 1.10^{-6}$ and $\Delta\phi_T = \pm 3.10^{-6}$. The graph for ϕ_S was calculated using Amiot's IPA singlet potential [19], that for ϕ_T using the Krauss and Stevens triplet potential [20]. In some of our previous analyses we also included higher-order derivative terms to extend the E and l ranges. Note that

$$\tau = 2\hbar\frac{d\phi}{dE} \equiv 2\hbar\phi^E \tag{10}$$
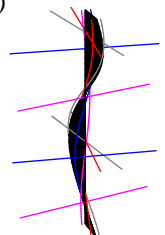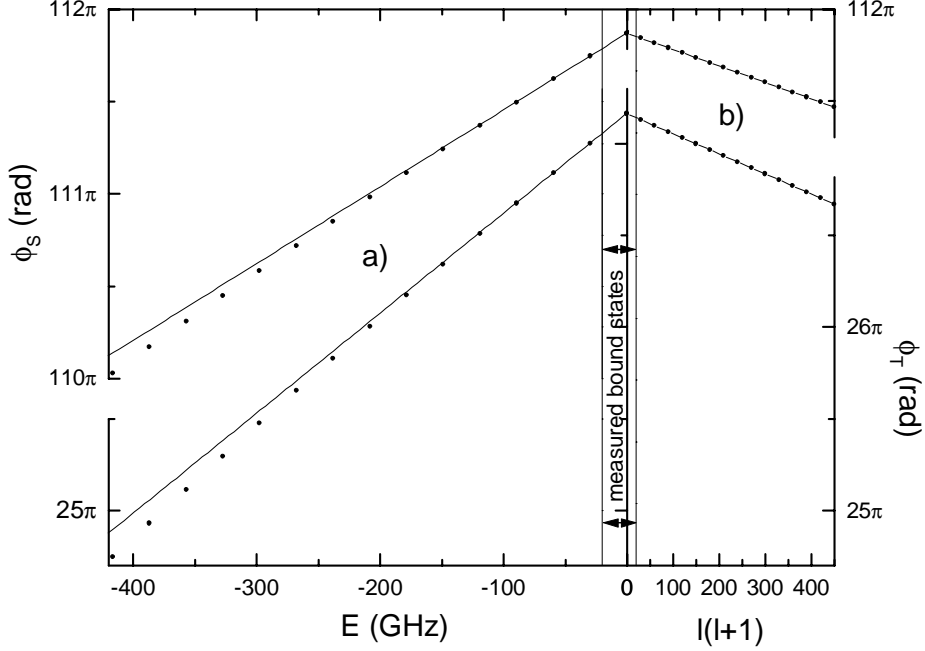
Figure 3: (a) Accumulated phases $\phi_S(E, l = 0)$ and $\phi_T(E, l = 0)$ vs. E for IPA singlet and ab-initio triplet potentials. (b) Accumulated phases $\phi_S(E = 0, l)$ and $\phi_T(E = 0, l)$ vs. $l(l + 1)$ for same potentials.

is the classical time interval needed for the atoms to move from r_0 inward and back to r_0. Indeed, for the shallower triplet potential the phase is seen to be a steeper function of energy. Furthermore, the second derivative of $\phi_{S/T}(E)$ with respect to E is seen to be negative, in agreement with the decreasing sojourn time left of r_0 for increasing energy.

A refinement that we introduce to increase the accuracy of our approach, is to subtract not only $V(r)$ and the angular kinetic energy $\hbar^2 l(l + 1)/mr^2$ from the total energy E to obtain the radial wave number (7) in the range $r < r_0$, but also the spin Zeeman energy V_Z and the part $V_{hf}^+ = \frac{1}{2} a_{hf}/\hbar^2 \mathbf{S} \cdot \mathbf{I}$ of the total two-atom hyperfine interaction operator $V_{hf} = a_{hf}/\hbar^2 (\mathbf{s}_1 \cdot \mathbf{i}_1 + \mathbf{s}_2 \cdot \mathbf{i}_2)$, which is diagonal in S.

The fact that we generally include a search for the above phase parameters in our coupled IPA implies that Eq. (4) has to be modified, since we want to derive a different set of parameters characterizing the modifications of the potentials, from the discrepancies ΔE_n between theoretical and experimental eigenvalues. To include potential corrections in the interior region $r < r_0$ via changes of the accumulated phases, we have to find a solution for the following complications:

1) The normalization of the state ψ_n^0 is tacitly assumed in the perturbation theory expression (4), although the phase description for the $r < r_0$ dynamics implies that the

part of ψ_n^0 in the interior region is not explicitly dealt with. Rewriting Eq. (4) as

$$\Delta E_n \langle \psi_n^0 | \psi_n^0 \rangle = \langle \psi_n^0 | \Delta V | \psi_n^0 \rangle, \tag{11}$$

we need to deal with the part $\langle \psi_n^0 | \psi_n^0 \rangle_{r < r_0}$ of the normalization integral. This difficulty plays a role independent of whether a potential correction extends over $r < r_0$, over $r > r_0$, or over both.

2) $V_S(r)$ and $V_T(r)$ are continuous functions of r. When a potential correction in the exterior region extends up to r_0, this has consequences for the inner potentials, i.e. for the phase parameters.

Complication 1) is easily solved starting from the WKB expression (6) for the accumulated phase in one particular adiabatic channel to be denoted by the abbreviated notation α (α includes in particular the quantum number S). Differentiating with respect to E we have

$$\frac{\partial \phi_\alpha}{\partial E} = \frac{2\mu}{\hbar^2} \int^{r_0} \frac{1}{2k_\alpha} dr \approx \frac{2\mu}{\hbar^2} \int^{r_0} \frac{\sin^2 \phi_\alpha(r)}{k_\alpha} dr = \frac{2\mu}{\hbar^2 A_\alpha^2} \langle \psi_n^0 | \psi_n^0 \rangle_{\alpha, r < r_0}. \tag{12}$$

Writing ψ near r_0 in the form (6), we find A_α. Eq. (12) then allows us to express the part $\langle \psi_n^0 | \psi_n^0 \rangle_{r < r_0}$ of the normalization integral in terms of the derivatives $\frac{\partial \phi_\alpha}{\partial E}$. In connection with complication 2) we also need to express the part $\langle \psi_n^0 | \Delta V | \psi_n^0 \rangle_{r < r_0}$ in changes of the phase parameters. We use the WKB expression

$$\Delta \phi_\alpha = -\frac{2\mu}{\hbar^2} \int_0^r \frac{1}{2k_\alpha} \Delta V_\alpha dr \approx$$

$$-\frac{2\mu}{\hbar^2} \int_0^r \frac{\sin^2 \phi_\alpha(r)}{k_\alpha} \Delta V_\alpha dr = -\frac{2\mu}{\hbar^2 A_\alpha^2} \langle \psi_n^0 | \Delta V_\alpha | \psi_n^0 \rangle_{\alpha, r < r_0}. \tag{13}$$

With these relations, the main equation of our coupled IPA method is found to be

$$\Delta E_n \left[\langle \psi_n^0 | \psi_n^0 \rangle_{r > r_0} + \frac{\hbar^2}{2\mu} \sum_\alpha A_\alpha^2 \frac{\partial \phi_\alpha}{\partial E} \right] =$$

$$\sum_i \left[c_{iS} \langle \psi_n^0 | P_S g_{iS}(r) | \psi_n^0 \rangle + c_{iT} \langle \psi_n^0 | P_T g_{iT}(r) | \psi_n^0 \rangle_{r > r_0} \right] - \frac{\hbar^2}{2\mu} A_\alpha^2 \Delta \phi_\alpha, \tag{14}$$

where $\Delta \phi_\alpha$ is written in the form

$$\Delta \phi_\alpha = \Delta \phi_\alpha^0 + E_n^0 \Delta \phi_\alpha^E + \phi_\alpha^E \Delta E_n + l(l+1) \Delta \phi_\alpha^l, \tag{15}$$

following from Eq. (9). Like the IPA equations (4) we started from, (14) is a set of linear equations for the unknown parameters (in this case c_{iS}, c_{iT}, $\Delta \phi_\alpha^0$, $\Delta \phi_\alpha^E$, $\Delta \phi_\alpha^l$) in terms of the energy differences ΔE_n. Again, we solve it as a least-squares problem. Clearly, in case some of the parameters are already known with sufficient accuracy from other sources, the corresponding terms in Eqs. (14) and (15) are replaced by 0.

At this point we emphasize again that our CIPA method avoids the intricate instability and convergence problems of the IPA by replacing the non-unique 'mathematical' basis functions $g_i(r)$ (or $g_{iS}(r)$ and $g_{iT}(r)$) by accumulated phases and by long-range interaction terms. Two further remarks are in place. The first relates to the channels α. The label α distinguishes the various spin eigenstates of $V_Z + V_{hf}^+$, so that the dynamical problem is diagonal in α for $r < r_0$. For a vanishing or weak magnetic field, α
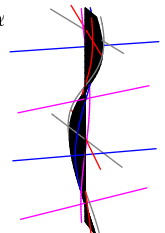
corresponds to the combination of quantum numbers S, I, F, m_F. For a strong B field each α contains a combination S, I, m_F, but a mixture of F values. The second remark relates to the use of the WKB approximation in the foregoing formulation. Our approach is most easily explained using the WKB approximation. We note, however, that the WKB approximation is not essential for the validity of the coupled IPA. To see this we start from an equation for the Wronskian of the unperturbed and perturbed states $|\psi_n^0\rangle$ and $|\psi_n\rangle$:

$$
\frac{\partial}{\partial r} \sum_\alpha (\psi_{n\alpha}^0 \frac{\partial}{\partial r} \psi_{n\alpha} - \psi_{n\alpha} \frac{\partial}{\partial r} \psi_{n\alpha}^0) =
$$
$$
2\mu/\hbar^2 \sum_{\alpha'\alpha} \psi_{n\alpha'}^0 (\Delta V_{\alpha'\alpha} - \Delta E_n \delta_{\alpha'\alpha}) \psi_{n\alpha}, \tag{16}
$$

following from the time-independent Schrödinger equations for $|\psi_n^0\rangle$ and $|\psi_n\rangle$. Here, the channel components $\psi_{n\alpha}(r)$ and $\psi_{n\alpha}^0(r)$ are chosen to be real. Integrating over r from r_0 to ∞, we find to first order in the modifications ΔV and ΔE_n:

$$
\sum_\alpha \left[\psi_{n\alpha}^0(r_0) \right]^2 \Delta\Lambda_\alpha = 2\mu/\hbar^2 \sum_{\alpha'\alpha} \int_{r_0}^\infty \psi_{n\alpha'}^0 (\Delta V_{\alpha'\alpha} - \Delta E_n \delta_{\alpha'\alpha}) \psi_{n\alpha}^0 dr, \tag{17}
$$

with Λ_α the logarithmic derivative of the radial wave function in channel α at r_0. This equation enables us to formulate the coupled IPA in terms of logarithmic derivatives. As pointed out above, however, the convenient properties of accumulated phases lead us to reformulate the approach by parametrizing the logarithmic derivative for each of the channels α via

$$
\Lambda = \frac{k(r_0)}{tan\phi} - \frac{k'(r_0)}{2k(r_0)}. \tag{18}
$$

This definition of the accumulated phase has been used in all our previous work [3, 7, 8, 9, 2]. It corresponds to the integral $\int^{r_0} k(r) dr$ when the WKB approximation applies. Starting from equation (17), equations similar to Eq. (14) can be derived by expressing the differentials $\Delta\Lambda_\alpha$ in the variations $\Delta\phi_\alpha$ and ΔE_n. In Section 4.4 we describe the application of our coupled IPA method to the measured $^{85}Rb_2$ bound-state spectrum making use of the foregoing formalism.

4.3   Two-color photoassociation experiment

We have measured the energies of the highest bound states of $^{85}Rb_2$ with two-color photoassociation spectroscopy [2]. The experiment is very similar to our previous one-color photoassociation experiments [7, 8, 9, 18]. About 10^4 ^{85}Rb atoms are transferred from a magneto-optic trap (MOT) to a far off resonance optical dipole force trap (FORT) [21]. The atomic density is about 10^{12} cm^{-3} and the temperature is a few hundred microKelvin. The FORT is created from a 1.7 W, linearly polarized laser detuned 35 nm from the rubidium D_2 line, focused to a 10 μm gaussian waist. This creates a trap with 12 mK depth. The atoms are doubly spin polarized in the $f = 3, m_f = 3$ state by a repumper beam tuned to the ^{85}Rb $5^2S_{1/2}(f = 2)$ to $5^2P_{3/2}(f = 3)$ transition and an optical pumping beam tuned to the ^{85}Rb $5^2S_{1/2}(f = 3)$ to $5^2P_{3/2}(f = 3)$ transition. The optical pumping beam is circularly polarized with an intensity of 100 μW/cm^2. A 3

G magnetic field is applied parallel to the FORT and optical pumping beam propagation direction.

Once the FORT has been loaded, the FORT laser beam is alternated with two photoassociation laser beams and the optical pumping and repumper beams in 5 μs cycles for a total of 200 ms. This is done to avoid the effect of the AC Stark shift of the trap laser on the photoassociation spectra and the optical pumping process. At the start of each cycle, only the FORT beam is applied for 2.5 μs. After this, the FORT beam is turned off, and only the optical pumping and repumper beams irradiate the atoms for 0.5 μs. For the last stage of each cycle, only the photoassociation beams are applied for 2.0 μs. Photoassociation laser beam 1, at frequency ν_1, is ordinarily kept at a constant frequency that excites transitions to a $|0_g^-(v,J)\rangle$ state near the $5^2S_{1/2} + 5^2P_{1/2}$ dissociation limit. Photoassociation laser beam 2, at frequency ν_2, is tuned to the blue of ν_1 (Fig. 1). Both photoassociation laser beams are colinear with the FORT beam, and are focused to a waist of 20 μm. Photoassociation beam 1 is supplied by a temperature and current tuned SDL-5401-G1 diode laser with an intensity of 1.6 kW/cm^{-2} and a linewidth of less than 20 MHz. Photoassociation beam 2 is supplied by a Ti:Sapphire ring laser with an intensity of 30-200 W/cm^{-2} and linewidth less than 2 MHz. After the 200 ms cycling process is complete, the number of atoms in the trap is measured with laser-induced fluorescence. This process is repeated for a succession of laser frequencies ν_2.

As in the one-color experiments, the photoassociation beam 1 promotes trap loss when resonant with a free-bound transition. A pair of free atoms absorbs a photon from beam 1 to create a short-lived excited molecular state, which then spontaneously decays to a pair of free atoms with a kinetic energy high enough to escape from the trap. Figure 4 shows the one-color photoassociation spectrum obtained by scanning only one of the photoassociation beams across a single vibrational level at 12573.1 cm^{-1}. The upward going peaks are associated with the trap loss induced by this laser. The $J = 0$, 2 and 4 rotational levels are visible in this spectrum. For the two color spectra, photoassociation beam 1 is tuned to the maximum of the $J = 2$ peak, and induces a constant loss of about 20 % of the atoms in the absence of the second laser.

Figures 5a and 5b show the two-color photoassociation spectra with ν_1 tuned to the $J = 2$ rotational levels of two different vibrational levels at 12563.1 cm^{-1} and 12573.1 cm^{-1}, respectively. As ν_2 becomes resonant with a bound-bound transition between the excited state and a ground molecular state, the trap loss decreases. The positions of the ground state vibrational levels are thus visible as downward going peaks in the two-color spectra. This occurs because the excited state is power broadened by photoassociation laser 2. This reduces the efficiency of excitation of the colliding atoms by photoassociation laser 1, and therefore reduces the trap loss. A theory of these two-color trap loss lineshapes has been given by Bohn and Julienne [22]. Figure 6 shows a magnified view of the two-color photoassociation spectrum for very small positive and negative frequency differences $\nu_1 - \nu_2$. For zero and negative frequency differences, upward going peaks are observed which are due to one-color trap loss induced by photoassociation laser 2 by transitions to $J = 0$, 1, and 2. (For this spectrum $J = 1$ is visible because the atoms were not polarized.) For a positive frequency difference of about 160 MHz, the spectrum shows a downward going peak associated with the highest bound level observed in this experiment.
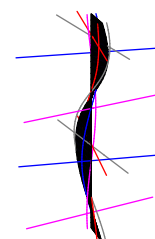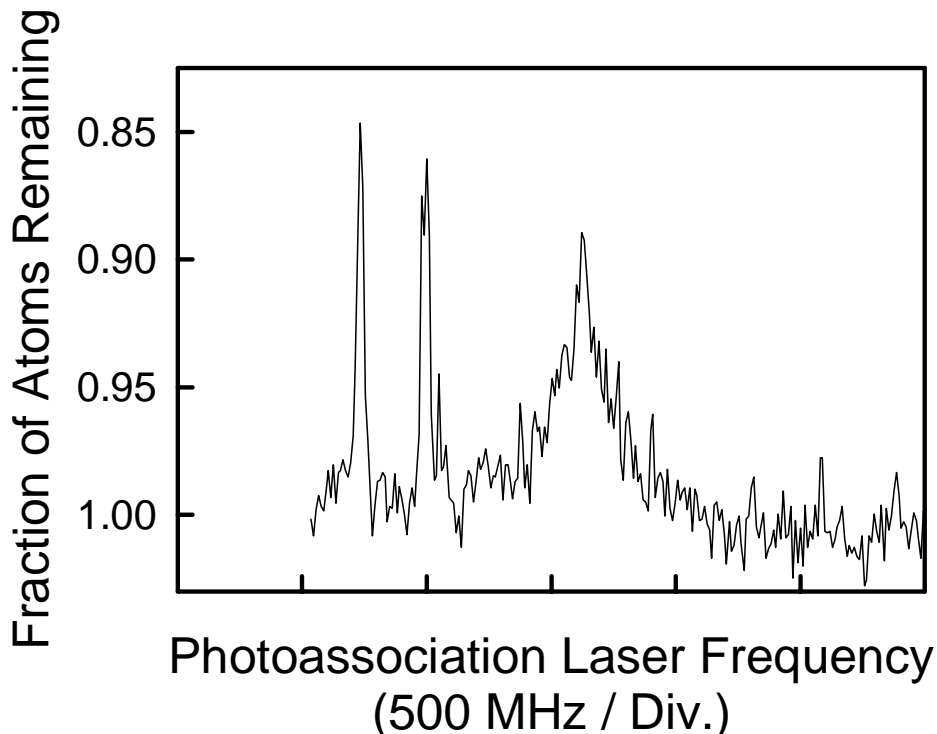
Figure 4: One-color photoassociation spectrum of $^{85}Rb_2$. A single vibrational level near 12573.1 cm^{-1} is shown, with J =0, 2, and 4 rotational levels visible.

We investigated the first 20 GHz below the $5^2S_{1/2}(f = 3) + 5^2S_{1/2}(f = 3)$ dissociation limit. The intermediate state at 12563.1 cm^{-1} resulted in a spectrum showing more ground molecular states than the state at 12573.1 cm^{-1}. We also observed a few of these same levels with an intermediate state at 12561.8 cm^{-1}. From these photoassociation spectra, the binding energies of 12 ground state levels were measured, as shown in Table 1. We searched for but did not find molecular states with binding energies greater than 20 GHz, presumably due to small Franck Condon factors.

The frequency scan of photoassociation laser 2 was calibrated to an accuracy of ± 20 MHz with a scanning Michelson interferometer wavemeter and a 300 MHz free spectral range etalon. The zero of the frequency difference $\nu_1 - \nu_2$ was determined by the point at which the second laser induced one-color trap loss on the $0_g^-(J = 2)$ line, as in Fig. 7. Photoassociation laser 1 was passively stabilized and demonstrated drift below 20 MHz over the course of a scan.

The widths of the observed lines varied from about 60 MHz to about 300 MHz. The widths of the broadest lines were probably dominated by power broadening, whereas for the narrowest lines the thermal width of the initial continuum state plays a significant role. To our knowledge there are no explicit calculations for thermally averaged two-color photoassociation lineshapes in the literature. However, one-color thermally averaged photoassociation lineshapes have been calculated previously [7, 8, 9, 23]. These
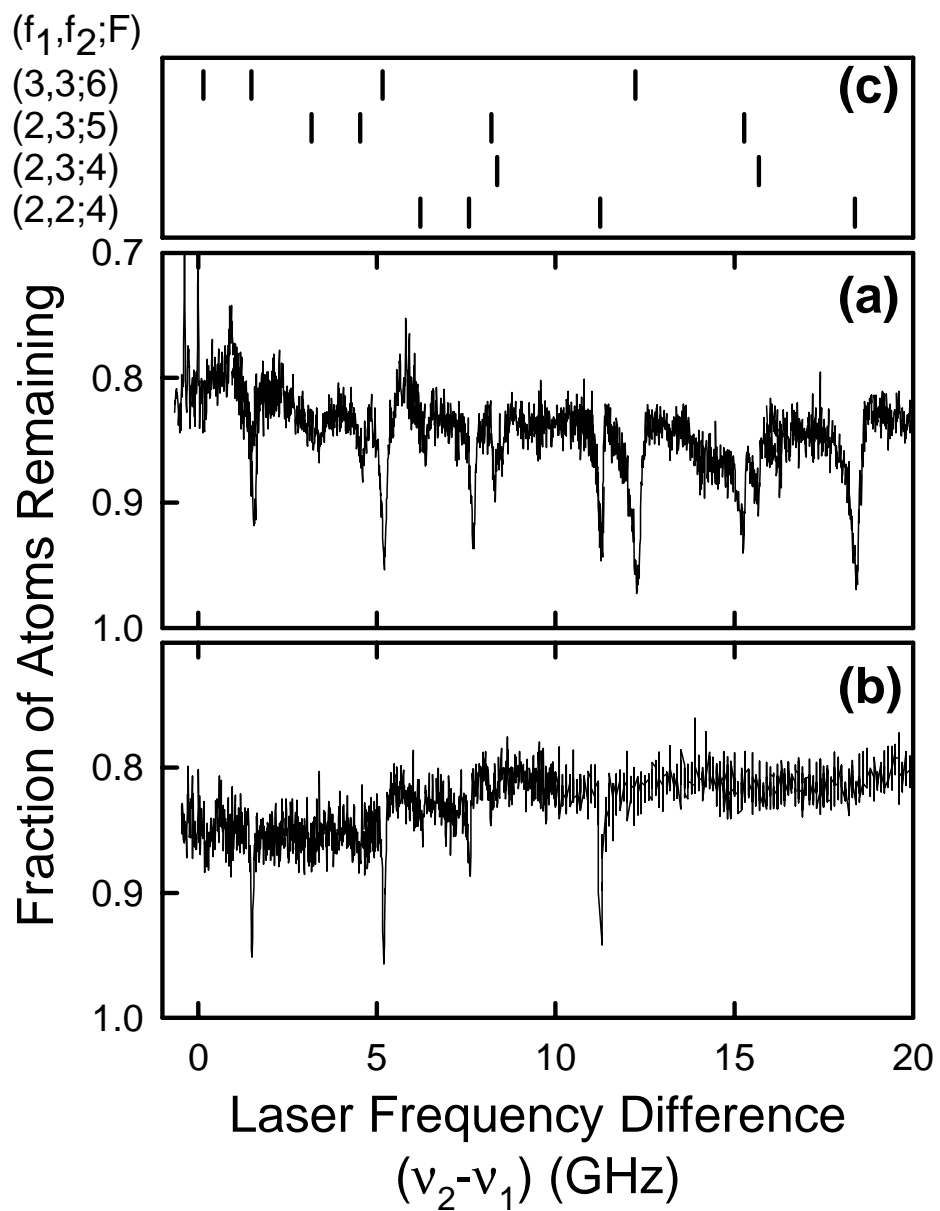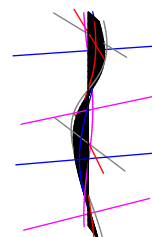
Figure 5: Two-color photoassociation spectra with ν_1 tuned to intermediate vibrational levels states near 12563.1 cm^{-1}(a) and 12573.1 cm^{-1}(b). The two-color spectrum is obtained by setting ν_1 to the intermediate state $J = 2$ rotational level, and scanning ν_2 to the blue of ν_1. (c) Assignments of the observed levels.
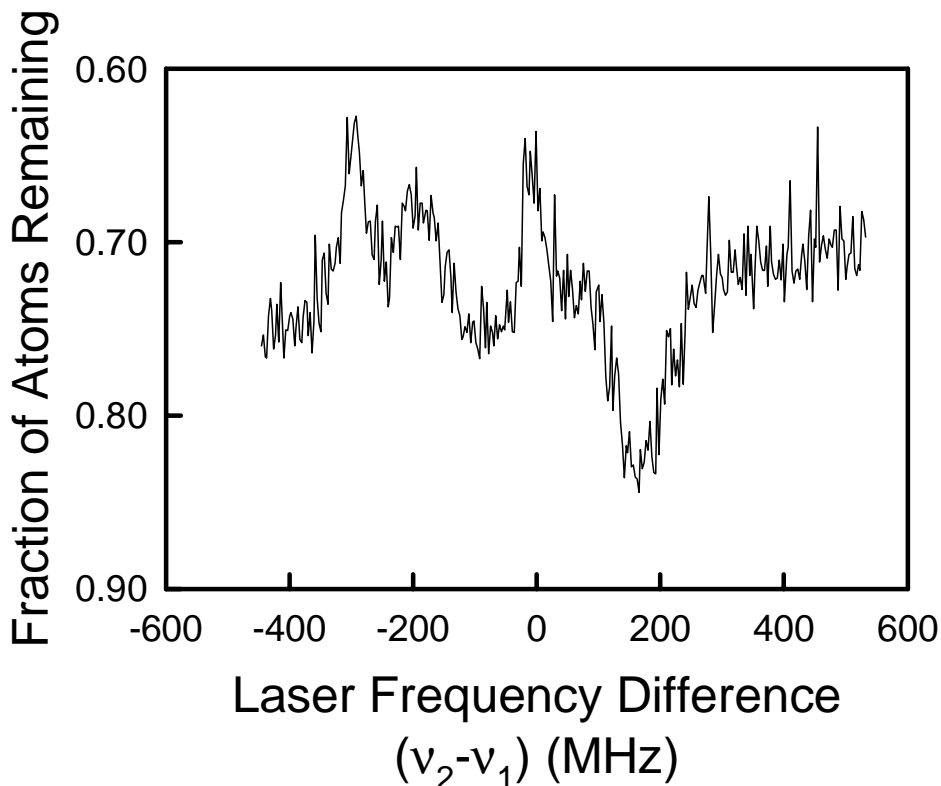
Figure 6: High resolution two-color photoassociation spectra for very small laser frequency difference $(\nu_2 - \nu_1)$. ν_1 is tuned to the $J = 2$ intermediate state near 12563.1 cm^{-1}. The data shows three upward going peaks indicating further one-color trap loss as $|0_g^-(v, J = 0, 1, 2)\rangle$ states are excited. The downward going peak shows the most weakly bound ground molecular state observed in this experiment, with a binding energy of 160 MHz.

calculations show that the photoassociation peaks can easily be shifted by 1-2 $k_B T$ relative to the peak position in the absence of thermal broadening effects, where T is the temperature of the gas and k_B is Boltzmann's constant. For our conditions this shift would be in the range from about 6 to 20 MHz. Similar shifts should occur for our two-color spectra, and they should occur in both the calibration spectrum (as in Fig. 7), which determines the zero of the laser difference frequency, as well as in the observed lines. In addition, line pulling due to drifts in the frequency of laser 1 and AC Stark shifts could also play a role in the position of these lines. These shifts are difficult to evaluate accurately since the tuning of laser 1 and the gas temperature are not accurately known, and since we did not attempt to model the lineshapes. However, in our judgement these shifts could easily amount to 30 MHz for all lines and perhaps be as large as 100 MHz for the broadest lines. These lineshape effects are the dominant error in our experiment, and we also note that they are a systematic error; i.e. all levels may dis-

| F	l	$E_{exp}(GHz)$	$E_{th,1}(GHz)$	$E_{th,2}(GHz)$	$[v - v_D]$	(f_1, f_2)
6	4	$+0.015 \pm 0.002$	+0.014	+0.015	-1	(3,3)
6	2	-0.16 ± 0.06	-0.14	-0.14	-1	(3,3)
5	2		-3.18	-3.18	-1	(2,3)
4	2	-6.23 ± 0.06	-6.22	-6.22	-1	(2,2)
6	2	-1.52 ± 0.06	-1.48	-1.46	-2	(3,3)
5	2	-4.58 ± 0.06	-4.51	-4.50	-2	(2,3)
4	2	-7.61 ± 0.06	-7.56	-7.54	-2	(2,2)
6	2	-5.20 ± 0.06	-5.13	-5.09	-3	(3,3)
5	2		-8.17	-8.12	-3	(2,3)
4	2	-8.34 ± 0.06	-8.35	-8.33	-3	(2,3)
4	2	-11.27 ± 0.06	-11.23	-11.18	-3	(2,2)
6	2	-12.22 ± 0.06	-12.24	-12.14	-4	(3,3)
4	2		-12.50	-12.43	-4	(3,3)
5	2	-15.24 ± 0.06	-15.28	-15.18	-4	(2,3)
4	2	-15.67 ± 0.06	-15.67	-15.61	-4	(2,3)
4	2	-18.39 ± 0.06	-18.38	-18.29	-4	(2,2)

Table 1: Spectrum of $^{85}Rb_2$ $l = 2, F = 4, 5, 6$ levels observed experimentally, including assignments of (f_1, f_2) progressions and integer parts of the v quantum number relative to the dissociation limit v_D for the progression involved. Theoretically predicted levels without $(E_{th,1})$ and with $(E_{th,2})$ Feshbach resonance data taken into account. The $l = 4, F = 6$ g-wave shape resonance state observed by one-color spectroscopy is also included.

play a shift in a common direction. In our first report on these results [2] we quoted an overall error of ± 30 MHz to ± 60 MHz on the level energies, depending on the narrowest linewidth observed for each level. In the present paper we prefer to quote a more conservative error limit of ± 60 MHz for all experimental energies.

4.4   Application of Coupled IPA to two-color photoassociation experiment

We assign the quantum numbers of the observed bound states as follows. As pointed out earlier, due to the above-mentioned selection rule $l = J$, which is valid also in the downward transition, we produce $l = 2$ bound ground-state Rb$_2$ levels only, since a $J = 2$ rotational level of the lower 0_g^- electronic state is excited as an intermediate state. Also, with a two-photon transition from the initial $|F, m_F\rangle = |6, +6\rangle$ state of two doubly-polarized atoms, only $F = 4, 5,$ or 6 levels can be formed with $m_F \geq 4$. Note furthermore that for all B, f_1 and f_2 are good quantum numbers if $F = 5$ or 6. In addition, for $l =$ even Bose symmetry excludes $F = 5$ for $(f_1, f_2) = (3, 3)$. We should therefore expect to see two mutually shifted pure triplet vibrational progressions converging to the $(f_1, f_2) = (3, 3)$ hyperfine threshold for $F = 6$ and to the $(2, 3)$ hyperfine threshold for $F = 5$, respectively. These are the two sequences indicated
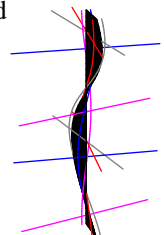
as (3,3;6) and (2,3;5) above the spectrum in Fig. 5c. The energy differences between pairs of corresponding levels in the progressions indeed correspond to the single-atom hyperfine splitting 3.04 GHz. The remaining levels must be assigned $F = 4$ and have mixed singlet-triplet character. In view of this one would expect these levels to display a less regular pattern than the $F = 5$ and 6 levels. Anticipating our further analysis we note, however, that f_1 and f_2 continue to be approximately good quantum numbers [24] for the mixed singlet-triplet states because of an approximate equality of singlet and triplet phases for ^{85}Rb. (see also Tsai et al. [2]). This equality is similar to that which has been discovered for ^{87}Rb [25, 26, 27], and in fact follows from it by mass scaling of the wavefunction phases. We note that this scaling of small phase differences is not expected in general, but just happens to occur for the particular case of Rb. As a consequence, the $F = 4$ states display a pattern almost as regular as the $F = 5$ and 6 states. Table 1 shows the spectrum of $l = 2, F = 4, 5, 6$ levels observed in our experiment, including the assignments of the (f_1, f_2) progressions and the integer parts of the differences $v - v_D$, with v the vibrational quantum number and v_D its generally non-integral value at the dissociation limit for the progression involved. We also include the $l = 4, F = 6$ g-wave shape resonance state observed by one-color spectroscopy [9], which will also be used in the following analysis.

We analyze the energy spectrum as follows. Referring to Section 4.2, we characterize the singlet potential in the interval $0 < r < 19 \, a_0$ by the singlet accumulated phase ϕ_S^0, which we take as a fit parameter, and by its derivatives ϕ_S^E and ϕ_S^l, calculated on the basis of the above-mentioned IPA potential of Amiot [19]. In the same interval the triplet interaction is characterized by three similar parameters: ϕ_T^0 is taken as a fit parameter, whereas ϕ_T^E and ϕ_T^l are taken from the Krauss and Stevens ab-initio triplet potential [20]. For $r > 19 \, a_0$ we write the interaction operator as

$$V(r) = -\frac{C_6}{r^6} - \frac{C_8}{r^8} - \frac{C_{10}}{r^{10}} + V_{exch} + V_{hf}. \tag{19}$$

For C_6 we consider values in a range that includes at the lower end the interval 4550 $\pm$ 100 a.u., determined in a previous one-color photoassociation experiment [9], and at the higher end the interval 4700 $\pm$ 50 a.u. from the analysis in Ref. [28]. Values for C_8 and C_{10} are taken from Marinescu et al. [29]. The exchange interaction is taken from G. Hadinger and G. Hadinger [30].

The actual application of our coupled IPA consists of a number of iterations, in each of which Eq. (17) is solved as a least-squares problem. At the beginning of an iteration step, eigenfunctions ψ_i^0 and eigenvalues E_i^0 ($i = 1....M$) are calculated for certain phase and potential parameters x_j ($j = 1....N$, $N < M$). This gives us a vector $\underline{\Delta E}$ having the set of differences with the experimental energies ΔE_i as components, from which the vector $\underline{\Delta x}$ with the changes Δx_j as components is to be determined. Writing Eq. (17) in the form

$$\underline{\Delta E} = \underline{\underline{M}} \, \underline{\Delta x}, \tag{20}$$

we use the same wavefunctions ψ_i^0 to calculate the $M \times N$ matrix $\underline{\underline{M}}$. To take into account the experimental error bars we divide the components ΔE_i and M_{ij} by the ith error bar without changing our notation. The least-squares solution is found by solving Eq. (20) for the parameter changes $\underline{\Delta x}$ using the pseudo-inverse of $\underline{\underline{M}}$ (see Ref. [31]):

$$\underline{\Delta x} = \underline{\underline{M}}^{-1} \underline{\Delta E}. \tag{21}$$

This iteration step is repeated until convergence has been reached. It turns out that highly accurate values of the elements of $\underline{M}$ are needed for correct and rapid convergence. This is especially true for directions in parameter space for which the least-squares sum varies slowly. We have paid special attention to this aspect by studying the $M = N = 1$ case. In our coupled IPA procedure the g-wave shape resonance is included as a quasi-bound state, by assuming its wave function to vanish at a radius far inside the centrifugal barrier. Generally, the CIPA method converges after 3 to 4 iterations.

Parenthetically, we note that our method is easily extended to cases where (part of) the measured data consist of energy *differences* between states without information on absolute positions with respect to the dissociation threshold, for instance. In such cases the differences between elements of $\underline{\Delta E}$ and between elements of $\underline{M}$ are used in equations (20) and (21) instead of the elements themselves.

Since we have normalized the components of $\underline{\Delta E}$ to the measured energy uncertainty intervals, the covariance matrix for the finally obtained parameter values is given by

$$\frac{\chi^2}{M - N}(\underline{\underline{M}}^T \underline{\underline{M}})^{-1}, \tag{22}$$
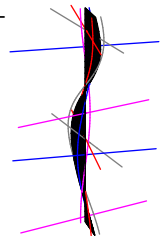
the diagonal elements of which give the square of the final parameter errors. In this expression χ^2 is the least-squares sum.

In view of the large discrepancy of the results of our previous paper [2] with the later results obtained by Roberts et al. [28], we here repeat the analysis of Ref. [2] but now without a restriction on C_6. Also, as noted above, we keep ϕ_T^E fixed to the ab-initio value. We thus treat C_6, ϕ_S^0, and ϕ_T^0 as parameters in a fit to the two-photon data in combination with the energy position of the g-wave shape resonance. While the triplet parameters are primarily determined by the $F = 5$ and 6 levels including the g-wave shape resonance, the singlet phase parameter ϕ_S^0 is mostly determined by the mixed singlet-triplet $F = 4$ states, in particular those with $(f_1, f_2) = (2, 3)$. We find $C_6 = 4650 \pm 50$ a.u., a range with a considerable overlap with the interval 4700 ± 50 a.u. from Ref. [28]. Considering the C_6 range 4550 ± 100 a.u. found by Boesten et al. [9], which is based on independent information, i.e. a Franck-Condon oscillation in the photoassociation spectrum, one would conclude that our central value $C_6 = 4650$ a.u. may be considered as the optimal overall result, if the Franck-Condon oscillation is taken into account. The theoretical level energies that follow from this analysis are given in the fourth column ($E_{th,1}$) of Table 1. For varying C_6 near the above central value $\overline{C}_6$ we subsequently derive optimal values of ϕ_S^0 and ϕ_T^0. The corresponding vibrational quantum numbers at dissociation $v_{DS}(\text{mod.}1)$ and $v_{DT}(\text{mod.}1)$ are

$$
\begin{aligned}
v_{DS} &= +0.0050 + 1.8(10^{-4})(C_6 - \overline{C}_6) \pm 0.0095, \\
v_{DT} &= -0.0518 + 1.0(10^{-4})(C_6 - \overline{C}_6) \pm 0.0032, \tag{23}
\end{aligned}
$$

with the C_6 values in a.u.

The analysis of Ref. [28] included the parameters of a magnetic-field induced Feshbach resonance that has been observed in the ^{85}Rb + ^{85}Rb elastic scattering channel by two groups [10, 28] since the experimental two-color photoassociation work that we analyzed above. As a following step therefore we supplement the foregoing analysis by including the extremely accurate values of the resonance field $B_{peak} = 155.2 \pm 0.4$ G and the resonance 'width' $\Delta = 11.6 \pm 0.5$ G, measured by the JILA group [28] as addi-

tional experimental data in our parameter search with corresponding coupled-channels $\underline{M}$ matrix elements. We thus find a χ^2 minimum at $C_6 = 4700 \pm 50$ a.u., in agreement with Ref. [28] and consistent with the above $C_6 = 4650$ a.u. value. The set of theoretical energy levels obtained in the overall fit are included in Table 1 (fifth column: $E_{th,2}$).

We also give the optimal v_{DS}, v_{DT} values for varying C_6 near the central value 4700 a.u. of the latter fit:

$$v_{DS} = +0.0090 + 0.8\,(10^{-4})(C_6 - \overline{C}_6) \pm 0.0009\,,$$
$$v_{DT} = -0.0568 + 1.4\,(10^{-4})(C_6 - \overline{C}_6) \pm 0.0011. \tag{24}$$

The corresponding scattering lengths are (in a.u.):

$$a_S = +2650 - 12.93\,(C_6 - \overline{C}_6) \pm 250\,,$$
$$a_T = -361 - 1.17\,(C_6 - \overline{C}_6) \pm 10. \tag{25}$$

The agreement between the experimental and theoretical energies is quite good. Relative to the theoretical energies $E_{th,1}$, the measured level energies show a small systematic difference of -20 MHz, and a random scatter of about ± 30 MHz, within our measurement error. For the set of theoretical energies $E_{th,2}$, the systematic difference increases to -63 MHz, and the scatter remains about ± 30 MHz. The systematic difference is probably due to lineshape effects, as discussed in the experimental section 4.3. For completeness we point out that the above analysis following Eq. (23), including only the bound state data, yields the values $B_{peak} = 148 \pm 10$ G, $\Delta = 9 \pm 4$ G.

The analysis of the two-color photoassociation experiment presented in this section illustrates how our coupled IPA method is applied in practice. We believe that the method will be useful also for further work on the extraction of interactions between cold atoms from highly excited bound diatomic states.

Parenthetically, we note that the sensitivity of v_{DS} and v_{DT} to C_6, described by the second terms on the right-hand side of Eqs. (23), can be determined either by completing the coupled IPA iteration successively for various choices of C_6 or, more easily, by making use of our coupled IPA method. The formalism presented in Section 4.2 allows us to consider C_6 or other parameters formally as parameters x_j and to translate their variations $\underline{\Delta x}$ into variations $\underline{\Delta E}$ by means of the corresponding $\underline{M}$ matrix elements calculated in our coupled IPA method. The latter in turn can be translated into variations of v_{DS} and v_{DT} or any other parameters determined in the coupled IPA search, using the inverse equation (21). This procedure is applicable generally in the case of parameters for which one wants to indicate the dependence of the final results explicitly as in equations (23) instead of including them in the parameter search.

4.5   Conclusions

We have described a coupled inverse perturbation approach for extracting information on interactions between cold atoms from energies of bound diatomic states. It is a generalization of the conventional IPA to situations where external and internal (spin) degrees of freedom of the two bound atoms are coupled. Basically the approach has the purpose to extrapolate interaction properties from just below the dissociation threshold to just above, i.e. the cold-collision regime. Although the method is applied here to

bound states of two identical ground state alkali atoms, it is applicable to any pair of cold atoms where the short-range interactions are taken into account in terms of a boundary condition on the radial wavefunctions at a certain interatomic distance r_0. In our case of two alkali atoms the boundary condition takes the form of an accumulated phase for the wavefunction in the singlet and triplet spin channels. The latter description derives its usefulness from the fact that cold collisions together with the considered highest part of the bound state spectrum comprise an energy range small compared to the typical relative kinetic energies of the two atoms in the distance range $r < r_0$. We have made clear that the validity of the WKB approximation for $r < r_0$ is not essential.

We illustrated the coupled IPA by an application to the bound $^{85}Rb_2$ states measured in a two-color photoassociation experiment and a g-wave shape resonance observed in a one-color photoassociation experiment. We also performed a combined parameter search by including the measured resonance field and resonance width of a recently observed Feshbach resonance.

References

[1] C.R. Vidal and H. Scheingruber, J. Mol. Spectrosc. **65**, 46 (1977).

[2] C.C. Tsai, R.S. Freeland, J.M. Vogels, H.M.J.M. Boesten, B.J. Verhaar, and D.J. Heinzen, Phys. Rev. Lett. **78**, 1245 (1997) (Chapter 3).

[3] B.J. Verhaar, K. Gibble, and S. Chu, Phys. Rev. A **48**, R3429 (1993).

[4] L. Li, A.M. Lyra, W.T. Luh, and W.C. Stwalley, J. Chem. Phys. **93**, 8452 (1990); G. Zhao, W.T. Zemke, J.T. Kim, B. Ji, H. Wang, J.T. Bahns, W.C. Stwalley, L. Li, A.M. Lyyra, and C. Amiot, J. Chem. Phys. **105**, 7976 (1996).

[5] P. D. Lett, P. S. Julienne, and W. D. Phillips, Ann. Rev. Phys. Chem. **46**, 423 (1995).

[6] D. J. Heinzen, in *Atomic Physics 14*, eds. D. J. Wineland, C. E. Wieman, and S. J. Smith (AIP Press, New York, 1995) pp. 369-388; D. J. Heinzen, Int. J. Mod. Phys. B **11**, 3297 (1997).

[7] J. R. Gardner, R. A. Cline, J. D. Miller, D. J. Heinzen, H. M. J. M. Boesten, and B. J. Verhaar, Phys. Rev. Lett. **74**, 3764 (1995).

[8] H. M. J. M. Boesten, C. C. Tsai, B. J. Verhaar, and D. J. Heinzen, Phys. Rev. Lett. **77**, 5194 (1996).

[9] H. M. J. M. Boesten, C. C. Tsai, J. R. Gardner, D. J. Heinzen, and B. J. Verhaar, Phys. Rev. A. **55**, 636 (1997)

[10] Ph. Courteille, R. S. Freeland, D. J. Heinzen, F. A. van Abeelen, and B. J. Verhaar, Phys. Rev. Lett. **81**, 69 (1998).

[11] H. M. J. M. Boesten, C. C. Tsai, D. J. Heinzen, A. J. Moonen, and B. J. Verhaar,
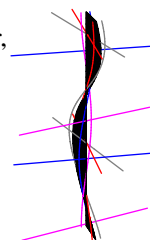
J. Phys. B. **32**, 287 (1997)

[12] E. Tiesinga, C. J. Williams, P. S. Julienne, K. M. Jones, P. D. Lett, and W. D. Phillips, J. Res. Nat. Inst. Stand. Technol. **101**, 505 (1996).

[13] E. R. I. Abraham, W. I. McAlexander, J. M. Gerton, R. G. Hulet, R. Côté, and A. Dalgarno, Phys. Rev. A **53**, R3713 (1996).

[14] K.M. Jones, S. Maleki, L.P. Ratliff, and P.D. Lett, J. Phys. B **30**, 289 (1997).

[15] E.R.I. Abraham, W.I. McAlexander, C.A. Sackett, and R.G. Hulet, Phys. Rev. Lett. **74**, 1315 (1995); E. R. I. Abraham, W. I. McAlexander, J. M. Gerton, R. G. Hulet, R. Côté, and A. Dalgarno, Phys. Rev. A **55**, R3299 (1997).

[16] M. Movre and G. Pichler, J. Phys. B **13**, 2631 (1977).

[17] C.J. Williams and P.S. Julienne, J. Chem. Phys. **101**, 2634 (1994).

[18] R. A. Cline, J. D. Miller, and D. J. Heinzen, Phys. Rev. Lett. **73**, 632 (1994); and erratum, Phys. Rev. Lett. **73**, 2636 (1994).

[19] C. Amiot, J. Chem. Phys. **93**, 8591 (1990).

[20] M. Krauss and W.J. Stevens, J. Chem. Phys. **93**, 4236 (1990).

[21] J.D. Miller, R.A. Cline, and D.J. Heinzen, Phys. Rev. A **47**, R4567 (1993).

[22] J.L. Bohn and P.S. Julienne, Phys. Rev. A **54**, R4637 (1996).

[23] R. Napolitano, J. Weiner, C. J. Williams, and P. S. Julienne, Phys. Rev. Lett. **73**, 1352 (1994).

[24] J.M. Vogels, B.J. Verhaar, and R.H. Blok, Phys. Rev. A **57**, 4049 (1998) (Chapter 2).

[25] S.J.J.M.F. Kokkelmans, H.M.J.M. Boesten, and B.J. Verhaar, Phys. Rev. A **55**, R1589 (1997).

[26] P.S. Julienne, F.H. Mies, E. Tiesinga, and C.J. Williams, Phys. Rev. Lett. **78**, 1880 (1997).

[27] J.P. Burke, Jr., J.L. Bohn, B.D. Esry, and C.H. Greene, Phys. Rev. A **55**, R2511 (1997).

[28] J.L. Roberts, N.R. Claussen, J.P. Burke, Jr., C.H. Greene, E.A. Cornell, and C.E. Wieman, Phys. Rev. Lett. **81**, 5109 (1998).

[29] M. Marinescu, H.R. Sadeghpour, and A. Dalgarno, Phys. Rev. A **49**, 982 (1994).

[30] G. Hadinger and G. Hadinger, J. Mol. Spectr. **175**, 441 (1996).

[31] R. Penrose, Proc. Cambr. Phil. Soc. **51**, 406 (1955).

5. Prediction of Feshbach resonances in collisions of ultracold rubidium atoms

J.M. Vogels[a], C.C. Tsai[b], R.S. Freeland[b], S.J.J.M.F. Kokkelmans[a], B.J. Verhaar[a], and D. J. Heinzen[b]

[a] *Eindhoven University of Technology, P.O. Box 513, 5600MB Eindhoven, The Netherlands*
[b] *University of Texas, Austin, Texas 78712*

Abstract

On the basis of recently measured Rb_2 bound-state energies and continuum properties, we predict magnetically-induced Feshbach resonances in collisions of ultracold rubidium atoms. The resonances make it possible to control the sign and magnitude of the effective particle-particle interaction in a Rb Bose condensate by tuning a bias magnetic field.

For the case of [85]Rb they occur at field values in the range where these atoms can be magnetostatically trapped. For [87]Rb they are predicted to occur at negative field values. The observation of Bose Einstein condensation (BEC) in dilute ultracold gas samples of rubidium [1], lithium [2] and sodium atoms [3] has made it possible for the first time to study this macroscopic quantum phenomenon in its pure form without complicated modifications due to strong interactions. A variety of new experiments has been proposed or already carried out, fascinating examples being the observation of collective shape oscillations and the observation of the relative phase of two Bose condensates [4, 5]. A rich variety of other experiments would come into reach if one could alter arbitrarily, possibly even in real time, the sign and magnitude of the atom-atom scattering length a. The scattering length occurs as the coefficient of the condensate self-interaction term in the condensate wave equation and has a profound effect on the stability and other properties of the condensate. An opportunity to change this parameter would arise if it were possible to tune the scattering length by means of external fields, i.e. either a static magnetic field [6] or a time-dependent optical [7] or rf field [8].

A situation where a can be changed between positive and negative values either through 0 or $\pm\infty$ by tuning a dc magnetic field is that of a Feshbach-type resonance between the initial two-atom continuum state and a quasibound molecular state at a common value of the energy [9]. Due to their different spin structures these states have different g-factors, so that the continuum and bound state energies can be tuned into
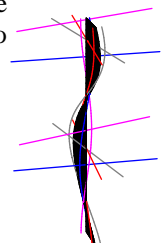
resonance at specific values of B. If we can find a resonance at a field value for which the atoms can be magnetostatically trapped, the above situation of a tunable scattering length should be readily achievable experimentally. In particular, changing the sign of a from positive to negative would turn a stable condensate into a collapsing unstable one, of which the time-development can be studied. A variety of other experiments would become possible too. For instance, a could be changed on the time scale of the resonance lifetime or the particle interaction could be made repulsive in one part of space and attractive in an other.

Rubidium atoms were the first atomic species for which BEC has been realized. The purpose of this paper is to point out that they may also be the atomic species for which B-field tuning of the scattering length is first achieved. For rubidium atoms the information available on the atom-atom interaction has long been insufficient for a prediction of the kind we envisage. This situation has drastically changed by the observation of two coexisting ^{87}Rb condensates [10] and by the results of a two-color photoassociation (PA) experiment on a cold ^{85}Rb gas sample [11]. In the latter experiment the last 20 GHz of bound levels in the lowest molecular singlet and triplet states was measured, allowing us to precisely determine a complete set of Rb$_2$ interaction parameters.

Before these developments, important information on the low-energy triplet ($S = 1$) collisional wavefunction had been obtained from cold-atom photoassociation work in our two groups on rubidium atoms, leading to the observation of its node structure [12] and the observation of shape resonances [13, 14]. Due to the hyperfine interaction pure singlet incident collision channels do not exist. As a consequence, information on the singlet interaction properties can only be obtained by studying mixed singlet-triplet collision channels. Very useful, but still insufficient, information of this kind came available [15] via a measurement of the absolute value of the scattering length $a_{1,-1}$ for elastic collisions of cold ^{87}Rb atoms in the $|f, m_f\rangle = |1, -1\rangle$ hyperfine state (see Fig. 1 for the ground-state hyperfine diagrams of ^{87}Rb and ^{85}Rb). As pointed out above, very important additional information came from the recent observation of overlapping $|2, 2\rangle$ and $|1, -1\rangle$ Bose condensates [10]. Three groups have independently pointed out that the extremely small rate constant $G_{(2,2)+(1,-1)}$ for decay due to collisions between atoms in the two different states, implied by the stability of the double Bose condensates, should be a strongly constraining factor in the determination of the remaining cold collision properties [16, 17, 18]. In the following we will show that this and all other available ^{85}Rb + ^{85}Rb and ^{87}Rb + ^{87}Rb cold-collision observations fit into a consistent picture, which can be derived from the bound states of the two-color PA experiment [11]. This allows us to make a reliable and accurate prediction of Feshbach resonances.

In order to calculate bound or continuum state wavefunctions, we write the Rb$_2$ long-range interaction potentials in the form

$$V_S(r) = -\frac{C_6}{r^6} - \frac{C_8}{r^8} - \frac{C_{10}}{r^{10}} + V_{exch}, \tag{1}$$

with the exchange part taken from Smirnov and Chibisov [19], the dispersion coefficients C_8 and C_{10} from a calculation by Marinescu et al. [20], and C_6 from previous photoassociation work [14]. We do not need the full information on the short-range singlet ($S = 0$) and triplet ($S = 1$) interaction potentials. Rather, this information is summarized in a boundary condition on the $S = 0$ and $S = 1$ radial wave functions at the interatomic distance $r = r_0 = 20$ a$_0$, on the basis of which Schrödinger's equa-
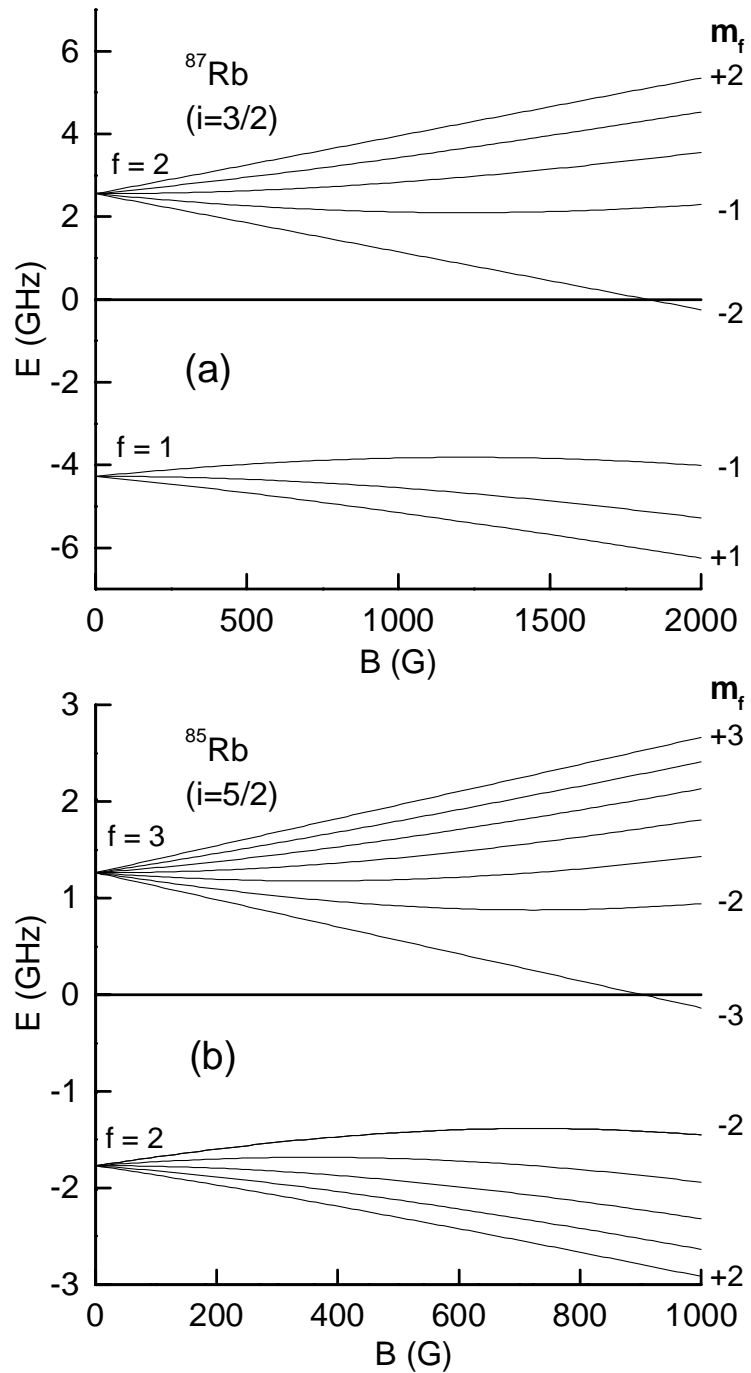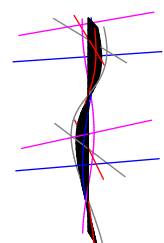
Figure 1: Hyperfine diagrams for electronic ground state of a) ^{87}Rb, b) ^{85}Rb.
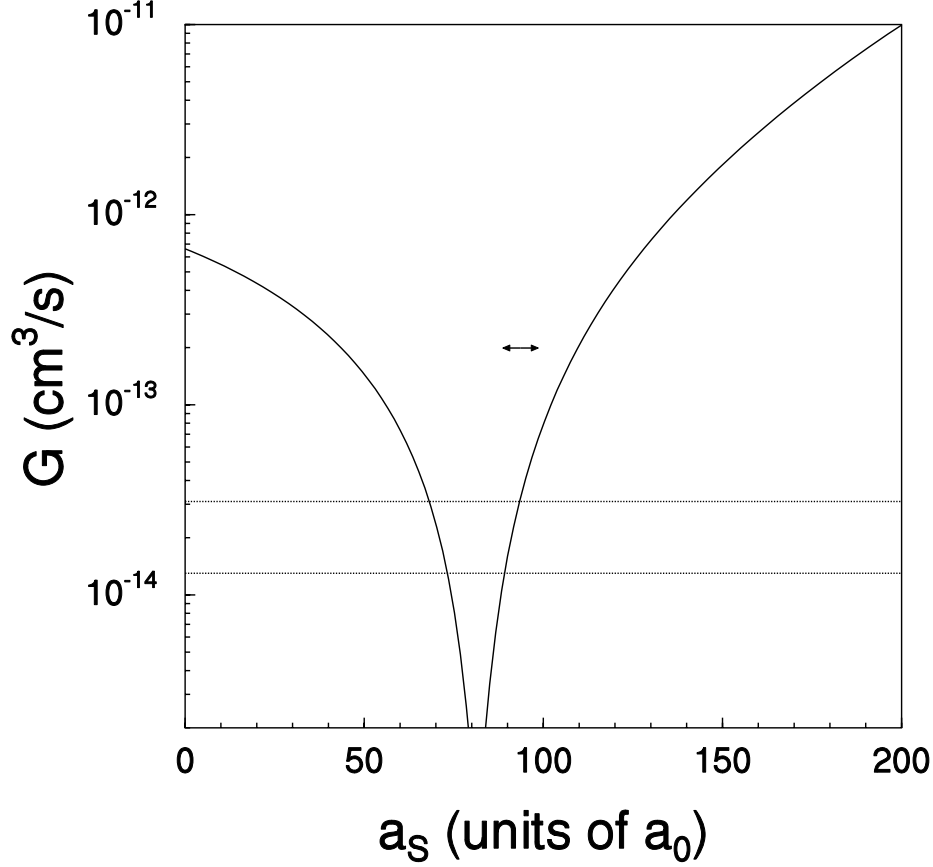
Figure 2: Rate constant $G_{(2,2)+(1,-1)}$ for decay due to collisions between ^{87}Rb atoms in different hyperfine states as a function of the singlet scattering length. The horizontal lines indicate the experimental range. The two-sided arrow indicates the a_S range following from the two-color PA experiment.

tion is solved for $r > r_0$. The boundary condition takes the form of a specific choice of the phases ϕ_S, ϕ_T of the oscillating singlet and triplet radial wavefunctions in a small region of energy E and interatomic angular momentum l near $E = l = 0$ [21]. This phase information was extracted from an analysis of the energies of the highest ^{85}Rb$_2$ bound states [11], and of the g-wave shape resonance observed in Ref. [14]. We also used available information on the total number of Rb$_2$ singlet and triplet bound states in this analysis [22, 23, 14].

With the parameters thus determined we can calculate the continuum quantities of interest. For the ^{85}Rb + ^{85}Rb triplet and singlet scattering lengths, we find [11] $a_T(^{85}\text{Rb}) = -440 \pm 140 \, a_0$ (corresponding fractional s-wave vibrational quantum number v_D at dissociation (modulo 1) $= 0.95 \pm 0.01$) and $+4500 \, a_0 < a_S(^{85}\text{Rb}) < +\infty$ or $-\infty < a_S(^{85}\text{Rb}) < -1200 \, a_0$ ($v_D = 122.994 \pm 0.012$). A coupled-channel calcula-

tion allows us to predict a value for the scattering length of a pair of ^{85}Rb atoms in the $|2, -2\rangle$ state. We find $a_{2,-2} = -450 \pm 140 \, a_0$. Mass-scaling the phases to ^{87}Rb enables us to predict bound-state and ultracold scattering properties for this isotope too, in particular the mixed hyperfine decay rate constant $G_{(2,2)+(1,-1)}$. In this mass-scaling transformation we correct for the different local de Broglie wavelengths, multiplying $\phi_{S/T}(E, l)$ by a square root of the atomic mass ratio and taking into account the total phase change from the inner turning point to r_0. We find excellent agreement between the bound-state and continuum properties. As an illustration Fig. 2 shows the calculated $G_{(2,2)+(1,-1)}$ as a function of the ^{87}Rb singlet scattering length, which corresponds directly with the singlet phase. The two-sided arrow indicates the maximum a_S range ± 5 a_0 obtained from the two-color PA bound-state energies, including the uncertainty in the dispersion coefficients. The position of the G-curve along the a_S axis is uncertain by $\pm 6 \, a_0$, with the error bar $\pm 3 \, a_0$ due to the uncertainty in the number of bound triplet states (38 ± 1 for ^{85}Rb$_2$ [14]) as an important contribution. Clearly, there is a preference for the a_S interval along the right-hand slope of the G-minimum. Good agreement is obtained between the calculated and measured rate constant (horizontal lines) with the *same* set of parameters determined above.

On the basis of this consistency we are now able to predict the field-dependent scattering lengths for a further comparison with experiment and to search for Feshbach resonances. Figure 3 shows the calculated B-dependence of $a_{1,-1}$ for ^{87}Rb in the range $-B_0 < B < B_0$, where B_0 is the maximum field for which an atom in the $|f = i - \frac{1}{2}, m_f = -(i - \frac{1}{2})\rangle$ hyperfine state, with i the nuclear spin, is weak-field seeking and thus trappable. The figure is extrapolated to negative fields to include collisions of ultracold $|1, +1\rangle$ atoms [24]. Note that reversing the field direction for constant m_f is equivalent to reversing m_f for a fixed field. Four Feshbach resonances are found at negative field values (383, 643, 850, 1018 G) and none at positive fields smaller than 1250 G. The latter as well as the flat B-dependence in this range is consistent with the results of Newbury et al. [15], in particular with the absence of Feshbach resonances with magnetic field width ≥ 2 G over the field range 15-540 G. Also, the calculated $a_{1,-1}$ value $106 \pm 6 \, a_0$ in this range agrees with the measured absolute magnitude 87 ± 21 a_0. We find $a_{1,-1}$ to be positive, in agreement with the apparent stability of a large condensate of ^{87}Rb $|1, -1\rangle$ atoms [10, 15]. The occurrence of Feshbach resonances at negative fields is also consistent with the field dependence of the highest ^{87}Rb$_2$ s-wave bound-state energies, calculated by means of our coupled channels method. The threshold of the elastic $|1, -1\rangle + |1, -1\rangle$ collision channel intersects with bound-state energy curves at four negative B values, which agree with the four values given above.

Figure 4 shows similar results for ^{85}Rb. This time we find two broad Feshbach resonances at positive fields 142 G and 524 G, and a very narrow one at 198 G, all three in the weak-field seeking B range. From the shape of the excursions through $\pm\infty$ it appears that the resonances are due to molecular states crossing the threshold of the incoming channel from above with increasing B. Again this is consistent with a calculation of coupled-channels bound-state energies. An interesting phenomenon in both Fig. 3 and 4 is the occurrence of a very narrow resonance. It arises from a molecular state with the electronic spins and the nuclear spins adding up to the maximum possible F value at $B = 0$. Their narrow width is due to the selection rule $\Delta F = 0$, by which the transition from the incoming channel with F lower by 2 can only take place via the
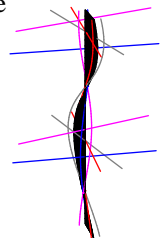
Figure 3: Predicted field-dependent scattering length for collisions of ^{87}Rb atoms in $|1,-1\rangle$ state. Three broad Feshbach resonances occur for negative fields at 383, 643, and 1018 G. A narrow resonance occurs at 850 G.
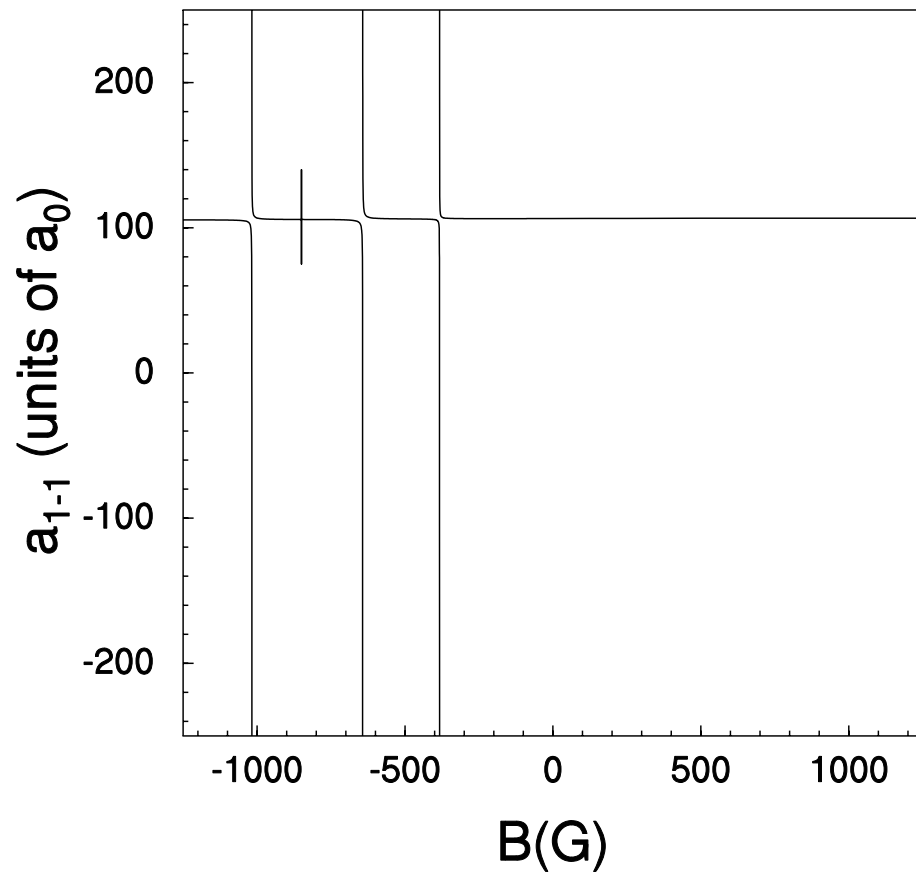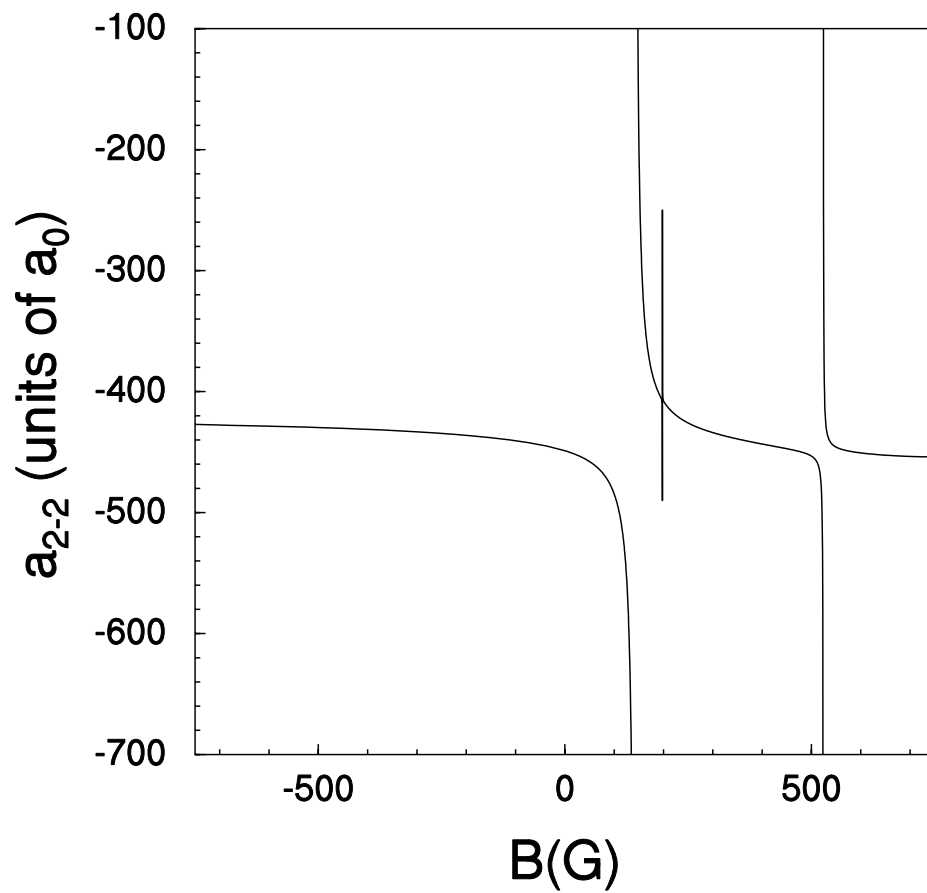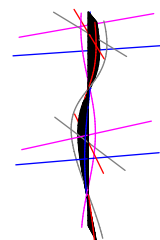
Figure 4: Predicted field-dependent scattering length for collisions of ^{85}Rb atoms in $|2, -2\rangle$ state. Two broad Feshbach resonances occur in the weak-field seeking range at 142 and 524 G, and a narrow one at 198 G.
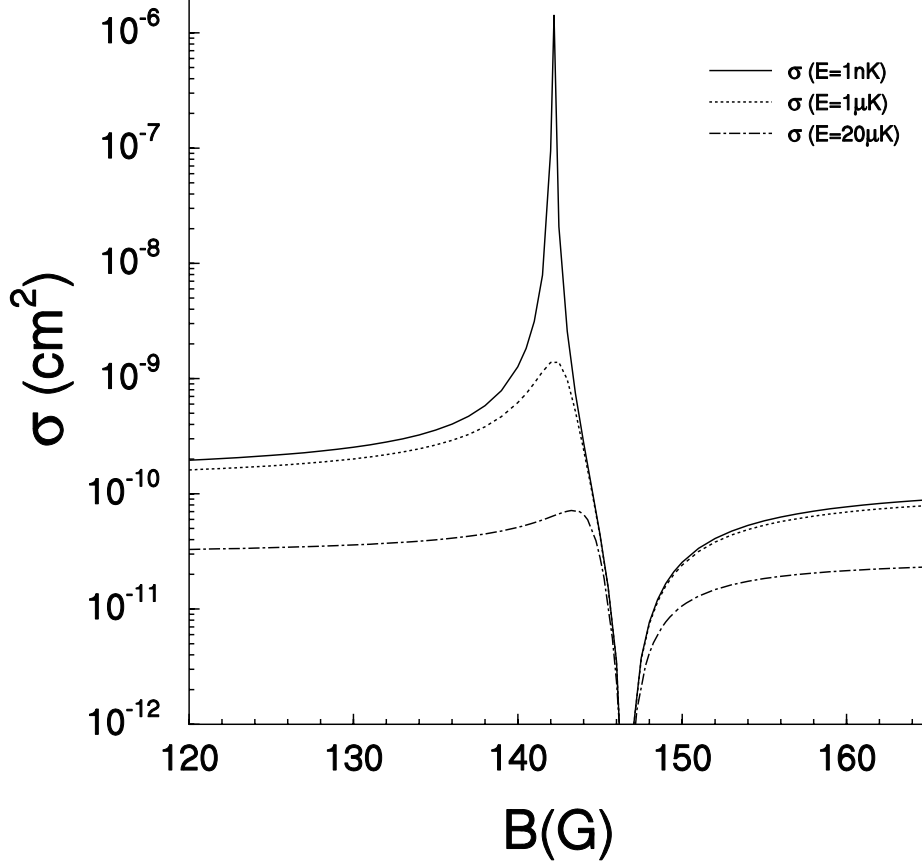
Figure 5: Resonance structure of elastic cross section in ^{85}Rb $|2,-2\rangle + |2,-2\rangle$ channel as a function of B for three collision energies. For each energy σ increases from a background value to the quantum limit $8\pi/k^2$, then decreases to 0 and finally returns to background value.

Zeeman interaction in second order.

We finally give the values of the singlet/triplet scattering lengths deduced in the analysis, including error bars on the various experimental and theoretical input parameters. We find: $a_T(^{87}Rb) = 102 \pm 6$ a_0 and $a_S(^{87}Rb) = 93 \pm 5$ a_0. We also find that the predicted field positions of the Feshbach resonances are reliable to within about 10 G for ^{85}Rb and 40 G for ^{87}Rb. To give an impression of the resonance behavior to be expected for ^{85}Rb + ^{85}Rb scattering, Fig. 5 shows the elastic cross section for three collision energies as a function of B in the range of the first resonance at 142 G. For the lowest energies the background value is almost equal to $8\pi a_{2,-2}^2$. For each energy σ increases to the quantum limit $8\pi/k^2$ close to the resonance field value and subsequently decreases to 0 before returning to the background value. Apparently, although the maximum gradually disappears with increasing energy, the resonance shape is sufficiently pronounced to be observable in an experiment similar to that of Ref. [15].

An important conclusion of our work is that we can account for all presently known properties of Rb_2 bound and continuum states with a single set of parameters. These include the triplet scattering lengths from earlier experiments [13, 14], the highest bound $^{85}Rb_2$ states measured in the two-color PA experiment [11], the double condensate stability [10], the measured scattering length $a_{1,-1}(^{87}Rb)$ and the absence of resonances in that quantity wider than 2 G in the range 15-540 G [15]. This enables us to deduce scattering lengths and positions of Feshbach resonances. The prediction of such resonances in an interesting field range should be readily verifiable experimentally. If confirmed, they will give rise to a variety of fascinating new possibilities for studying Bose condensates.

References

[1] M.H. Anderson, J.R. Ensher, M.R. Matthews, C.E. Wieman, and E.A. Cornell, Science **269**, 198 (1995).

[2] C.C. Bradley, C.A. Sackett, and R.G. Hulet, Phys. Rev. Lett. **78**, 985 (1997).

[3] K.B. Davis, M-O Mewes, M.R. Anderson, N.J. van Druten, D.S. Durfee, D.M. Kurn, and W. Ketterle, Phys. Rev. Lett. **75**, 3969 (1995).

[4] D.S. Jin, J.R. Ensher, M.R. Matthews, C.E. Wieman, and E.A. Cornell, Phys. Rev. Lett. **77**, 420 (1996).

[5] M.R. Andrews, C.G. Townsend, H.-J. Miesner, D.S. Durfee, D.M. Kurn, and W. Ketterle, Science **275**, 637 (1997).

[6] E. Tiesinga, A.J. Moerdijk, B.J. Verhaar, and H.T.C. Stoof, Phys. Rev. A **46**, R1167 (1992); E.Tiesinga, B.J. Verhaar, and H.T.C. Stoof, Phys. Rev. A **47**, 4114 (1993).

[7] P.O. Fedichev, Yu. Kagan, G.V. Shlyapnikov, and J.T.M. Walraven, Phys. Rev. Lett. **77**, 2913 (1996).

[8] A.J. Moerdijk, B.J. Verhaar, and T.M. Nagtegaal, Phys. Rev. A **53**, 4343 (1996).

[9] B.J. Verhaar in *Atomic Physics* **14**, C.E. Wieman, D.J. Wineland, and S.J. Smith (Ed.), AIP, New York, 1995, pp. 211-218.

[10] C.J. Myatt, E.A. Burt, R.W. Ghrist, E.A. Cornell, and C.E. Wieman, Phys. Rev. Lett. **78**, 586 (1997).

[11] C.C. Tsai, R.S. Freeland, J.M. Vogels, H.M.J.M. Boesten, D.J. Heinzen, and B.J. Verhaar, Phys Rev Lett **79**, 7 (1997) (Chapter 2).

[12] J.R. Gardner, R.A. Cline, J.D. Miller, D.J. Heinzen, H.M.J.M. Boesten, and B.J. Verhaar, Phys. Rev. Lett. **74**, 3764 (1995).

[13] H.M.J.M. Boesten, C.C. Tsai, J.R. Gardner, D.J. Heinzen and B.J. Verhaar, Phys.
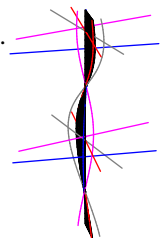
Rev. A **55**, 636 (1997).

[14] H.M.J.M. Boesten, C.C. Tsai, D.J. Heinzen and B.J. Verhaar, Phys. Rev. Lett. **77**, 5194 (1997).

[15] N. Newbury, C. Myatt, and C. Wieman, Phys. Rev. A **51**, R2680 (1995).

[16] S.J.M.M.F. Kokkelmans, H.M.J.M. Boesten, and B.J. Verhaar, Phys. Rev. A **55**, R1589 (1997).

[17] P.S. Julienne, F.H. Mies, E. Tiesinga, and C.J. Williams, Phys. Rev. Lett. **78**, 1880 (1997).

[18] J.P. Burke, J.L. Bohn, B.D. Esry, and C.H. Greene, Phys. Rev. A **55**, R2511 (1997).

[19] B.M. Smirnov and M.I. Chibisov, JETP **21**, 624 (1965).

[20] M. Marinescu, H.R. Sadeghpour, and A. Dalgarno, Phys. Rev. A **49**, 982 (1994).

[21] A.J. Moerdijk, W.C. Stwalley, R.G. Hulet, and B.J. Verhaar, Phys. Rev. Lett. **72**, 40 (1994).

[22] C. Amiot, J. Chem. Phys. **93**, 8591 (1990).

[23] C.F. Tsai, J.D. Miller, R.A. Cline, and D.J. Heinzen (to be published).

[24] We thank Eric Cornell for pointing to the interest of such collisions.

6. Rigorous description of three-body collisions between ultracold alkali atoms, I. Method

J.M. Vogels, F.A. van Abeelen, and B.J. Verhaar

*Eindhoven University of Technology, Box 513, 5600 MB Eindhoven, The Netherlands*

Abstract

We formulate a rigorous method to calculate the stationary scattering wave function for a three-body collision between three ultracold doubly-polarized ground-state alkali atoms, based on the Faddeev formalism. The circumstances of the collision correspond to the conditions prevailing in Bose-Einstein condensed and other ultracold gas samples. The method combines a pair-correlated hyperspherical expansion in 6D with the accumulated phase approach for the pair interactions. It enables us to calculate the complex 6D elastic scattering length and the three-body recombination constant.

The realization of Bose-Einstein condensation [1, 2, 3, 4] in ultracold dilute atomic hydrogen and alkali gases has been the starting point for a great variety of experimental and theoretical studies. An attractive aspect of these systems is the ability to perform rigorous calculations of properties of these systems. At the low densities of the ultracold atomic samples used in most of the experimental studies single-atom and two-atom processes dominate the properties, and these can generally be calculated rigorously. In a subset of experiments at higher densities, however, three-body collisions are important, both in atomic hydrogen [5] and in atomic alkali [6] gas clouds, as they give rise to recombination losses (dimerization). Understandably, with the exception of a publication on atomic hydrogen [7], all existing theoretical treatments of three-body collisions of ultracold atoms are based on (possibly crude) approximations.

A first category of such calculations applies to resonance recombination. This process proceeds in two sequential stages. First, two atoms collide and are trapped into a long-lived quasi-bound state. Subsequently, this quasi-molecule is stabilized in a collision with a third atom in which it undergoes a transition into a bound state. The importance of such a process was recognized in 1976 by Stwalley in connection with the stability of spin-polarized atomic hydrogen [8]. Reynolds et al. presented a theoretical treatment for the case of cold atomic hydrogen [9], based on an earlier treatment for thermal atoms [10]. Recently, a similar mechanism was studied [11] for three-body
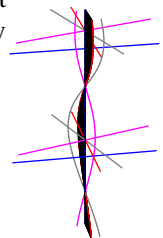
(Feshbach) resonance recombination losses in a sodium optical trap [12].

Studies of non-resonant (or direct) recombination processes were made by Greben et al. [13] and by Kagan et al. [14] using various approximations. Three-body recombination calculations for alkali atoms were carried out on the basis of a Jastrow approximation by Moerdijk et al. [15] and, using a different approximation, by Fedichev et al. [16].

A rigorous calculation describing a three-body collision for doubly polarized H atoms has been carried out in 1986 by de Goey et al. [7]. This was a calculation in the momentum representation based on the Faddeev formalism [17]. Until now, an extension to other spin states for H atoms or to alkali atoms for even the simplest, doubly polarized, spin state has proven to be difficult, primarily due to the strongly attractive pair interactions, i.e., the large number of bound states in the two-body subsystems.

In this paper we propose a method that should make it possible to cope with this last problem. The method combines aspects of several previous approaches. Like the 1986 calculation for doubly polarized H atoms, it is based on the Faddeev scheme, but in contrast it is a coordinate space approach. The motivation for turning to coordinate space is the great advantage of using accumulated phases [18] to 'summarize' the net effect of the, often insufficiently known, short range potentials in the two-atom subsystems. To implement these, a division in short range and long range problems in coordinate space is essential. Also, our approach bears some analogy with the earlier approximate Jastrow approach of Moerdijk et al. [15]. Our three-body wave function contains similarly a product of three zero-energy s-wave two-body pair scattering wave functions (subject to a modification discussed below), inspired by the approximate Jastrow form of the rigorous H + H + H wave function in Ref. [7]. In our case, however, the Jastrow product is turned into a rigorous expression by multiplying it by a series of hyperspherical harmonic terms in the 6D relative coordinate space $\mathcal{R}^6$ resulting from splitting off the trivial total center of mass motion of the three atom system. Building in the radial node structure of the pair wave functions from the outset is a rather essential ingredient of any successful approach. Any attempt to account for the complicated node structure - the number of nodes in the Cs-Cs triplet s-wave radial wave function is more than 50 within an interatomic distance of $r = 20\,a_0$ - via a hyperspherical expansion alone, is deemed to fail because of slow convergence. The idea of combining a Jastrow ansatz with a hyperspherical expansion in a 'pair-correlated hyperspherical harmonic' basis has been investigated previously for the three-nucleon problem by Kievsky et al. [19, 20]. In that problem the pair-correlated hyperspherical basis has a definite advantage relative to a pure hyperspherical harmonic expansion in that the strongly repulsive short range core of the nucleon-nucleon interaction is automatically taken care of by the Jastrow functions. Atom-atom interactions have this feature in common with nucleon-nucleon potentials. In the context of cold atoms an even stronger motivation for splitting off a Jastrow part from the hyperspherical harmonic expansion is to be found in the fact that it appears to be the only way to implement the accumulated phase approach in a three-body theory. In the spirit of the accumulated phase method each of the Jastrow factors coincides with the pair scattering wave function only up to a certain interatomic distance. Beyond that distance the atom pair becomes increasingly susceptible to perturbations by the third atom so that it becomes less meaningful to incorporate the structure of the wave function of the unperturbed pair. We therefore define the Jastrow function
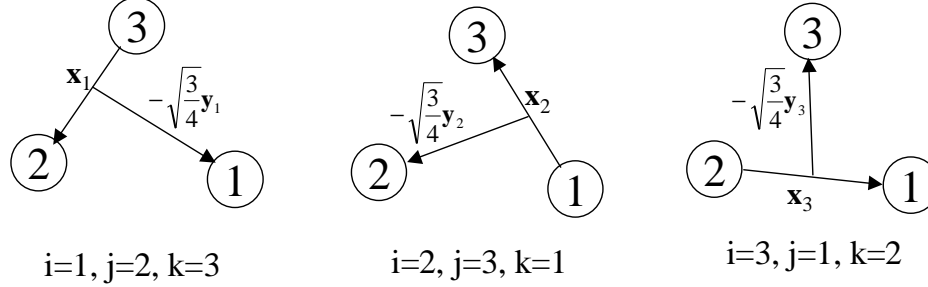
i=1, j=2, k=3   i=2, j=3, k=1   i=3, j=1, k=2

Figure 1: The three sets of Jacobi coordinates.

to tend smoothly to a constant value of unity in an r interval of roughly 10 to 30 a_0 beyond the last but one node of the zero-energy scattering wave function.

Since we expect the finite (see Ref. [21]) $T \to 0$ limit of the three-body recombination constant to apply at the relevant low temperatures of the BEC experiments, we consider an initial state with three atoms approaching one another with zero energy in relative s-waves. The magnetic dipolar interaction playing a negligible role, we have to consider a central pure-triplet atom-pair interaction and a total angular momentum $L = M_L = 0$ for the three-body state. As the total spin state has a well-defined totally polarized character $S = M_S = \frac{3}{2}, I = m_I = 3i$, with i the nuclear spin, we leave out the spin part of the total wave function, so that the three-body wave function Ψ only describes the geometry of the triangle defined by the atom positions, the orientation of the triangle in $\mathcal{R}^3$ space being isotropic. In $\mathcal{R}^6$ we describe the triangular geometry by the 6D radius ρ, corresponding to the linear dimensions of the triangle, supplemented with two angles varying on the hypersphere of constant ρ and characterizing the shape of the triangle. For $L \neq 0$ the total wave function would also depend on three other (Euler) angles on the hypersphere, characterizing the orientation of the triangle. The former two angles are usually chosen in one of three different ways depending on the choice $i = 1, 2, 3$ of the Jacobi coordinates $\vec{x}_i, \vec{y}_i$ (see Ref. [22] and Fig. 1). For instance, $\vec{x}_1$ is the radius vector from atom 3 to atom 2, while $\vec{y}_1$ is $-(\frac{4}{3})^{\frac{1}{2}}$ times the radius vector from the center-of-mass of the pair (23) to atom 1. One of the above angles, ϕ_i, characterizes the relative magnitude of $\vec{x}_i$ and $\vec{y}_i$: $x_i = \rho \cos \phi_i, y_i = \rho \sin \phi_i, \phi_i \in [0, \frac{\pi}{2}]$. The other angle, θ_i, is the angle between $\vec{x}_i$ and $\vec{y}_i$. A surface element of the hypersphere with radius ρ is then given by

$$\rho^5 d\Omega = 8\pi^2 \rho^5 \sin \theta_i d\theta_i \sin^2 \phi_i \cos^2 \phi_i d\phi_i. \tag{1}$$

We write the total collisional wave function as a sum of three Faddeev components, $\Psi = \psi(\vec{x}_1, \vec{y}_1) + \psi(\vec{x}_2, \vec{y}_2) + \psi(\vec{x}_3, \vec{y}_3)$, with a hyperspherical part of the form

$$\Psi^{HS} = f(r_{12})f(r_{23})f(r_{31}) \sum_{i=1}^{3} \sum_{K,l} U_{Kl}(\rho)|(K,l)_i\rangle. \tag{2}$$

The superscript HS serves to distinguish the hyperspherical part (2) of the total wave function from an additional, asymptotic contribution Ψ^A to be considered below. For
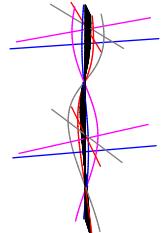
each i the states

$$|(K,l)_i\rangle = N_{Kl}P_l(\cos\theta_i)P_{K,l}(\phi_i). \tag{3}$$

form an orthonormal set of eigenstates of the 6D 'angular momentum' operator $\underline{K}^2$ on the hypersphere with eigenvalues $K(K+4)$. The coefficient N_{Kl} is a normalization constant, P_l is a Legendre polynomial of $\cos\theta_i = \hat{x}_i.\hat{y}_i$ and $P_{K,l}(\phi_i)$ is proportional to a Jacobi polynomial [23]. The expressions (2) and (3) are special cases of more complicated expressions valid without the $T \to 0$ limit: the angular momentum quantum numbers l and λ associated with the degrees of freedom $\hat{x}_i$ and $\hat{y}_i$, respectively, are in our case coupled to $(L, M_L) = (0,0)$ and therefore equal. We have $K = 2(n+l)$ with $n = 0, 1, 2, ...$

The expression (2) alone would in principle suffice to describe a zero-energy three-atom collision. With one or more atom + di-atom decay channels open at that energy, however, it would also have to describe the outgoing wave states in these channels with a large separation between a single atom and an atom pair, i.e., $|\vec{y}_i| \gg |\vec{x}_i|$. Such contributions are concentrated in an increasingly smaller part of the hypersphere surface close to $\phi_i = \frac{\pi}{2}$, requiring increasingly large K values in the hyperspherical part ψ^{HS}. It is therefore advantageous to include in the total wave function explicit terms describing outgoing wave states Ω_{vlm_l} for the open decay channels v, l, m_l in the asymptotic region of space:

$$\Psi = \Psi^{HS} + \Psi^A,$$
$$\Psi^A = -\sum_{i=1}^{3}\sum_{vlm_l} A_{vlm_l}\Omega_{vlm_l}(\vec{x}_i, \vec{y}_i). \tag{4}$$

Here, v, l, m_l denote the vibrational and rotational quantum numbers of a rovibrational di-atom state, while A_{vlm_l} is the amplitude for the transition from the free three-body channel 0 to the atom + di-atom decay channel v, l, m_l.

The function Ω_{vlm_l} is defined by

$$\Omega_{vlm_l}(\vec{x}_i, \vec{y}_i) = \chi_{vl}(x_i)Y_{lm_l}(\hat{x}_i)y_i^{-1}O_l(k_{vl}y_i)Y^*_{lm_l}(\hat{y}_i)f(x_j)f(x_k)C(y_i). \tag{5}$$

In this equation χ denotes a rovibrational pair wave function and (ijk) is a cyclic permutation of (123). Furthermore, O_l is an outgoing wave solution for the relative motion of the atom + di-atom system including a long-range atom + di-atom van der Waals potential with twice the atom-atom C_6 dispersion coefficient. For large y_i, O_l tends to the Riccati-Hankel function $\hat{h}_l^+(k_{vl}y_i) \to \exp(ik_{vl}y_i)$. Here, k_{vl} is related to the total initial 6D kinetic energy E by energy conservation:

$$E \equiv \frac{\hbar^2}{2\mu}\underline{\kappa}^2 = E_{vl} + \frac{\hbar^2}{2\mu}k_{vl}^2, \tag{6}$$

with $\mu = \frac{1}{2}m$, $E_{vl} (< 0)$ the di-atom internal energy, and $\underline{\kappa}$ the initial 6D wave vector. Finally, $C(y_i)$ is a smooth damping function equal to 1 for large y_i and 0 for small y_i with a transition region between roughly 40 and 60 a_0. With this factor included, Ψ^A contributes only for large atom + di-atom distances.

For reasons of symmetry $A_{vlm_l} (\equiv A_{vl})$ is independent of m_l, so that the sum over m_l in Eq. (4) is an $L = 0$ state, i.e., invariant under 3D rotations via the combination of spherical harmonics in Eq. (5). The recombination amplitude A_{vl} is proportional to the S-matrix element $S_{vlm_l,0} (\equiv S_{vl,0})$, connecting the initial free three-atom channel

with the v, l, m_l recombination channel: when Ψ^{HS} is normalized such that its free three-atom part equals $\exp(i\underline{\kappa}.\underline{\rho}) \approx 1$ in the $E \to 0$ limit, A_{vl} is given by [24]

$$A_{vl} = \frac{2^3 \pi}{6^{\frac{1}{2}}} k_{vl}^{\frac{1}{2}} \frac{S_{vl,0}(E)}{\kappa^2}. \tag{7}$$

The matrix element $S_{vl,0}$ is related to the elastic $K = 0 \to K = 0$ (free $\to$ free) S-matrix element $S_{0,0}$ by unitarity:

$$|S_{0,0}|^2 + \sum_{vl}(2l+1)|S_{vl,0}|^2 = 1. \tag{8}$$

Furthermore, $S_{0,0}$ can be expressed [25] in the complex 6D elastic scattering phase shift $\delta_{0,0}$ and, for $E \to 0$, the complex 6D elastic scattering length a:

$$S_{0,0} = e^{2i\delta_{0,0}},$$
$$\cot \delta_{0,0} \approx -\frac{32}{\pi(\kappa a)^4} + O(\frac{1}{\kappa^2}). \tag{9}$$

In terms of A_{vl} the $E \to 0$ recombination rate constant L is given by

$$L = \sum_{vl}(2l+1)L_{vl}, \qquad L_{vl} = \frac{3^{\frac{5}{2}}}{4m}\hbar k_{vl}|A_{vl}|^2, \tag{10}$$

which describes the decrease in the number N_0 of condensate atoms:

$$\frac{dN_0}{dt} = -\frac{1}{6}3Ln_0^2 N_0, \tag{11}$$

where n_0 is the density of condensate atoms. The factor 3 arises from the disappearance of all three atoms from the condensate, the factor $\frac{1}{6}$ is due to the fact that the atoms are condensed and not thermal. This convention for L is similar to the convention being used for two-body decay. Finally, for large enough ρ the 6D isotropic part of the total Ψ is given by

$$\Psi(K=0) = \left(\frac{2}{\kappa\rho}\right)^2 [H_2^*(\kappa\rho) + S_{0,0}H_2(\kappa\rho)] \approx 1 - (\frac{a}{\rho})^4 \quad (E \to 0), \tag{12}$$

where H_2 is an outgoing and H_2^* an ingoing Hankel function [26].

In view of different conventions used in the literature, it is of interest to specify the definition of L on which the above equation (10) is based. We define L as an intrinsic recombination event rate via the loss rate equation

$$\frac{dn}{dt} = -3Ln^3 \tag{13}$$

for an uncondensed gas sample, with the factor 3 denoting the number of atoms lost in a three-body recombination event. (The corresponding rate equation for a condensed gas contains an additional factor 1/6 on the right-hand side). This definition is in line with the usual convention for two-body decays where the rate coefficients are also defined via event rates. It has the advantage that the number of atoms lost in a single event occurs as an explicit factor in the equation, while the remaining coefficient has a meaning independent of the experimental circumstances. Often, the analysis of experimental data is based on an effective rate equation:

$$\frac{dn}{dt} = -L_{eff}n^3. \tag{14}$$
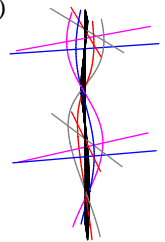
In fact, Moerdijk et al. [15] calculate a coeffcient $L_{eff} = 3L$ for an uncondensed gas and Dalibard et al. [27] report an experimental value $L_{eff} = \frac{1}{6} \cdot 3L$ for a condensed gas.

Our approach to determine the total wave function is based on a Kohn variational principle [28]. We consider the functional

$$S_{0,0}[\tilde{\Psi}] = \tilde{S}_{0,0} - \frac{\kappa^4}{64\pi^2} i \langle \tilde{\Psi}^* | \mathcal{L} | \tilde{\Psi} \rangle. \tag{15}$$

Here, $\mathcal{L} = \frac{2\mu}{\hbar^2}(E - H)$ and $\tilde{\Psi}$ is defined by equations similar to (2), (4), and (12), with trial quantities $\tilde{S}_{0,0}$, $\tilde{A}_{vl}$, $\tilde{U}$ replacing the analogous quantities in Ψ. We impose the requirement that the functional be stationary under variations of the trial quantities. Under square-integrable variations of the hyperradial wave functions $\tilde{U}$ and variations of $\tilde{S}_{0,0}$ this requirement leads to the following set of coupled equations:

$$\left[\underline{\underline{A}}(\rho)\frac{d^2}{d\rho^2} + \underline{\underline{B}}(\rho)\frac{d}{d\rho} + \underline{\underline{C}}(\rho) + \frac{2\mu}{\hbar^2}E\underline{\underline{N}}(\rho) \right] \underline{U}(\rho) = \sum_{vl} A_{vl}\underline{D}_{vl}(\rho), \tag{16}$$

in which $\underline{U}$ is a column vector with components $U_{K'l'}$, while $\underline{\underline{A}}$, $\underline{\underline{B}}$, $\underline{\underline{C}}$, and $\underline{\underline{N}}$ are matrices with rows Kl and columns $K'l'$ [19, 23]. The $(Kl, K'l')$ element of the total matrix between the square brackets is defined as an Ω integral:

$$[\quad]_{Kl,K'l'} = \langle f(r_{12})f(r_{23})f(r_{31}) \sum_{i=1}^{3} (K,l)_i | \mathcal{L} | f(r_{12})f(r_{23})f(r_{31}) \sum_{i'=1}^{3} (K',l')_{i'} \rangle_\Omega. \tag{17}$$

Each column vector $\underline{D}_{vl}$ has components

$$(\underline{D}_{vl})_{Kl} = \sum_{i,i'=1}^{3} \langle f(r_{12})f(r_{23})f(r_{31})(K,l)_i | \mathcal{L} | \Omega_{vl}(\vec{x}_{i'}, \vec{y}_{i'}) \rangle_\Omega, \tag{18}$$

in which

$$\Omega_{vl}(\vec{x}_{i'}, \vec{y}_{i'}) = \sum_{m_l} \Omega_{vlm_l}(\vec{x}_{i'}, \vec{y}_{i'}). \tag{19}$$

Numerically, in the $T = 0$ limit we determine a homogeneous solution $\underline{U}^{hom}(\rho)$ of Eq. (16), regular for small ρ and satisfying boundary conditions

$$U_{Kl}^{hom}(\rho) \underset{\rho\to\infty}{\sim} \quad 1 + O\left(\frac{1}{\rho^4}\right) \quad (Kl) = (00),$$

$$U_{Kl}^{hom}(\rho) \underset{\rho\to\infty}{\sim} O\left(\frac{1}{\rho^4}\right) \quad (Kl) \neq (00), \tag{20}$$

for large ρ. For each separate combination v, l on the right-hand side of Eq. (16) we also determine the (unique) solution $\underline{U}^{vl}(\rho)$ of the inhomogeneous equation with only $-\underline{D}_{vl}$ on the right-hand side, that is regular for small ρ and obeys boundary conditions

$$U_{Kl}^{vl}(\rho) \underset{\rho\to\infty}{\sim} O\left(\frac{1}{\rho^4}\right) \tag{21}$$

for all (Kl), including (00). Note that only the homogeneous part for $(K, l) = (0, 0)$ contains an incoming wave, corresponding to the term 1 in Eq. (20). In terms of the

above solutions we would thus dispose of the total hyperspherical part Ψ^{HS} in Eq. (4):

$$\Psi^{HS} = \Psi^{HS,hom} - \sum_{v,l} A_{vl} \Psi^{HS,vl},\tag{22}$$

with

$$\Psi^{HS,hom} = f(r_{12})f(r_{23})f(r_{31})\sum_i \sum_{Kl} U_{Kl}^{hom}(\rho)|(K,l)_i\rangle,$$

$$\Psi^{HS,vl} = f(r_{12})f(r_{23})f(r_{31})\sum_i \sum_{Kl} U_{Kl}^{vl}(\rho)|(K,l)_i\rangle,\tag{23}$$

if the decay amplitudes A_{vl} were known.

We determine the latter by considering variations of the trial decay amplitudes $\tilde{A}_{vl}$ in the above functional, leading to

$$\langle \sum_i \Omega_{vl}^*(\vec{x}_i,\vec{y}_i)|\mathcal{L}|\Psi^{HS} - \sum_{i'}\sum_{v'l'} A_{v'l'}\Omega_{v'l'}(\vec{x}_{i'},\vec{y}_{i'})\rangle = 0.\tag{24}$$

Equation (24) has the form of a set of algebraic equations

$$\sum_{vl'} X_{vl,v'l'} A_{v'l'} = Y_{vl},\tag{25}$$

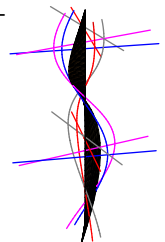with the X and Y coefficients defined by

$$X_{vl,v'l'} = \langle \sum_i \Omega_{vl}^*(\vec{x}_i,\vec{y}_i)|\mathcal{L}|\Psi^{HS,v'l'}\rangle + \langle \sum_i \Omega_{vl}^*(\vec{x}_i,\vec{y}_i)|\mathcal{L}|\sum_{i'}\Omega_{v'l'}(\vec{x}_{i'},\vec{y}_{i'})\rangle,$$

$$Y_{vl} = \langle \sum_i \Omega_{vl}^*(\vec{x}_i,\vec{y}_i)|\mathcal{L}|\Psi^{HS,hom}\rangle.\tag{26}$$

In summary, a calculation along the lines of the above method might run as follows. Assuming cut-off values K_{max}, l_{max}, ρ_{max} for K, l, ρ, and confining oneself to a restricted set of two-body bound states v, l as final states close to the dissociation limit, elements of the matrices $\underline{A}$, $\underline{B}$, $\underline{C}$, $\underline{N}$, and of the column vectors $\underline{D}_{vl}$ are calculated in a grid of ρ values. Then Eq. (16) is solved for homogeneous and inhomogeneous solutions $\underline{U}^{hom}(\rho)$ and $\underline{U}^{vl}(\rho)$. This defines Ψ^{HS} via Eqs. (22) and (23), and therefore the X and Y coefficients in the algebraic equations (25) via Eqs. (26). Solving Eqs. (25) finally gives the decay amplitudes. The calculation is repeated for increasing values of K_{max}, l_{max}, and ρ_{max}, until convergence is obtained.

We believe that a rigorous calculation using the above method is practically feasible with present-day computer facilities. In practice, most of the computer time is needed for the accurate calculation of the integrals over Ω involved in calculating $\underline{A}$, $\underline{B}$, $\underline{C}$, $\underline{N}$, $\underline{D}_{vl}$ as well as $\underline{X}$ and $\underline{Y}$. To calculate these an adaptive integration scheme is chosen which guarantees that from integration point to integration point the step in each inter-atomic distance is restricted within a certain range near 0 depending on r. On a modern processor, this results in a total calculation time of about two days. This calculation time can be reduced dramatically on a parallel processing system because the calculation of the matrices/vectors can be carried out independently for each value of ρ. The temporary storage used in the integration algorithm over Ω raises the memory requirements from 100 MB on a single processor to 50 MB per processor on a massively parallel machine.

Calculations along these lines should be very important for understanding the ex-

perimental data concerning three-body recombination which are becoming available. Additionaly, they should be able to provide guidance in judging the feasibility of further experiments.

References

[1] M.H. Anderson et al., Science **269**, 193 (1995).

[2] K. Davis et al., Phys. Rev. Lett. **75**, 3969 (1995).

[3] C.C. Bradley et al., Phys. Rev. Lett. **78**, 985 (1997).

[4] D.G. Fried, T.C. Killian,L. Willmann, D. Landhuis, S.C. Moss, D. Kleppner, and T.J. Greytak, Phys. Rev. Lett. **81**, 3811 (1998).

[5] I.F. Silvera and J.T.M. Walraven, in *Progr. in Low. Temp. Phys.*, edited by D.F. Brewer (Elsevier, New York, 1986) Vol. X, p. 147.

[6] See for instance, D.M. Stamper-Kurn, M.R. Andrews, A.P. Chikkatur, S. Inouye, H.-J. Miesner, J. Stenger, and W. Ketterle, Phys. Rev. Lett. **80**, 2027 (1998).

[7] L.P.H. de Goey, T.H.M. van den Berg, N. Mulders, H.T.C. Stoof, B.J. Verhaar, and W. Glöckle, Phys. Rev. B **34**, 6183 (1986).

[8] W.C. Stwalley, Phys. Rev. Lett. **37**, 1628 (1976).

[9] M.W. Reynolds, I. Shinkoda, R.W. Cline, and W.N. Hardy, Phys. Rev. B **34**, 4912 (1986).

[10] R.E. Roberts, R.B. Bernstein, and C.F. Curtiss, J. Chem. Phys. **50**, 5163 (1969).

[11] E. Timmermans, P. Tommasini, R. Côté, M. Hussein, and A. Kerman, cond-mat/9805323.

[12] J. Stenger, S. Inouye, M.R. Andrews, H.-J. Miesner, D.M. Stamper-Kurn, and W. Ketterle, Phys. Rev. Lett. **82**, 2422 (1999).

[13] J.M. Greben, A.W. Thomas, and A.J. Berlinsky, Can. J. Phys. **59**,945 (1981).

[14] Yu. Kagan, I.A. Vartanyantz, and G.V. Shlyapnikov, Sov. Phys.-JETP **54**, 590 (1981).

[15] A.J. Moerdijk, H.M.J.M. Boesten, and B.J. Verhaar, Phys. Rev. A **53**, 916 (1996).

[16] P.O. Fedichev, M.W. Reynolds, and G.V. Shlyapnikov, Phys. Rev. Lett. **77**, 2921 (1996).

[17] L.D. Faddeev, Sov. Phys.-JETP **12**,1014 (1961).

[18] B.J. Verhaar, K. Gibble, and S. Chu, Phys. Rev. A **48**, R3429 (1993); A.J. Moerdijk and B.J. Verhaar, Phys. Rev. Lett. **73**, 518 (1994); A.J. Moerdijk, W.C. Stwalley, R.G. Hulet, and B.J. Verhaar, Phys. Rev. Lett. **72**, 40 (1994).

[19] A. Kievsky, M. Viviani, and S. Rosati, Nucl. Phys. A **551**, 241 (1993); ibid. **577**, 511 (1994).

[20] A. Kievsky, M. Viviani, and S. Rosati, Phys. Rev. C **56**, 2987 (1997).

[21] A.J. Moerdijk and B.J. Verhaar, Phys. Rev. A **53**, 19 (1996).

[22] W. Glöckle, *The quantum mechanical few-body problem* (Springer, Berlin, 1983).

[23] F. Koppens, F.A. van Abeelen, and B.J. Verhaar, Internal Report Eindhoven University of Technology, 1997 (unpublished).

[24] J.P.J. Driessen, L.P.H. de Goey, and B.J. Verhaar, Internal Report Eindhoven University of Technology, 1984 (unpublished).

[25] B.J. Verhaar, L.P.H. de Goey, J.P.H.W. van den Eijnde, and E.J.D. Vredenbregt, Phys. Rev. A **32**, 1424 (1985); B.J. Verhaar, L.P.H. de Goey, E.J.D. Vredenbregt, and J.P.H.W. van den Eijnde, Phys. Lett. A **110**, 371 (1985).

[26] P.M. Morse and H. Feshbach, *Methods of theoretical physics* (McGraw-Hill, New York, 1953) p. 1322.

[27] J. Söding, D. Guéry-Odelin, P. Desbiolles, F. Chevy, H. Inamori, and J. Dalibard, cond-mat/9811339.

[28] See related derivation in Ref. [20] and in L.M. Delves, *Advances in nuclear physics*, edited by M. Baranger and E. Vogt, Vol. 5 (Plenum Press, New York, 1972), p. 128.
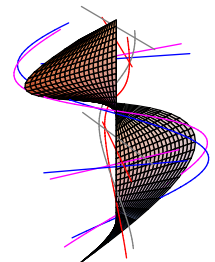
Summary

The achievement of the critical phase density in a gas of alkali atoms has stimulated a breakthrough in the research field of Bose-Einstein condensation. The most important interaction in such a gas is the s-wave scattering of two colliding atoms: The sign of the scattering length determines whether the atoms effectively repel or attract each other. This results in a mutual mean-field effect of the atoms, which expresses itself for instance in frequency shifts of atomic clocks based on cold atoms. In a condensate the effects of the mean field are very diverse. When the scattering length is negative, only a small metastable condensate can be formed: A larger condensate collapses under the attractive interactions. When the atoms repel each other the mean field energy generally dominates the kinetic energy, and the condensate is in the Thomas-Fermi regime.

It is therefore interesting that collisions, and thus also the scattering length, can be controlled by the magnetic field in which collisions take place. This results from resonance behavior arising from the coupling of the collision channel with other hyperfine channels in which a (quasi-)bound state occurs. These so-called Feshbach resonances are the main subject of this thesis.

After an introduction in chapter 1, a simple model is presented in chapter 2 by which the structure and the properties of bound states and collision states of pairs of identical alkali atoms in the electronic ground state can be understood. The states involved are the very weakly bound states on the one hand and the ultracold collisions on the other hand, both very close to the dissociation limit. As a consequence the two types of states are closely related. Essentially, the simple picture comes down to dividing the total interatomic distance range in two regions, in each of which a part of the total Hamiltonian is neglected. In the separation point the total multichannel wave function is subjected to a requirement of continuity. The model accounts for a whole range of features present in the system. In particular it gives a description of the coupling mechanism between hyperfine states which causes the Feshbach resonances, as well as the approximate positions and the widths of the resonances.

In chapter 3 we discuss an experiment that has led to a prediction of Feshbach resonances for ^{85}Rb en ^{87}Rb (see chapter 5). This two-color photoassociation experiment has been analyzed by an approach developed in this thesis work. The energies of multichannel bound states of ^{85}Rb$_2$ molecules are measured in an optical trap by coupling these states to an electronically excited ^{85}Rb$_2$ state with a laser. Using a second laser, the latter state is coupled to a low-temperature collisional state of two trapped ground state atoms. Via the latter coupling atoms can escape from the trap: an atom pair in the electronically excited state can spontaneously emit a photon as a result of which the atoms leave each other with large speed. When the frequency of the first laser corresponds to the energy difference of the excited state and the ground state which is to be measured, the above-mentioned coupling suppresses the spontaneous decay by decreasing the population of the excited state. This influences the measured loss of atoms from the trap. From the energies determined in this way parameters have been extracted that characterize the atom-atom interactions.

To analyze the levels obtained in the experiment in chapter 3, a new method has

been developed in chapter 4. These levels are strongly coupled and very close to the collision threshold. The method is based on Inverse Perturbation Analysis (IPA) which enables to use observed bound states in a potential to derive properties of that potential. Our Coupled Inverse Perturbation Analysis (CIPA) is a generalization which allows to analyze levels in which coupling occurs between internal states of different electronic and nuclear spin. Secondly, we can combine this approach with a description of the short-range interaction in terms of accumulated phases. Even when the short-range behavior is not yet sufficiently known, this enables the use of levels close to threshold.

In chapter 5 the results of the CIPA analysis lead to predictions of three Feshbach resonances in ultracold ^{85}Rb + ^{85}Rb collisions and four resonances in ^{87}Rb + ^{87}Rb collisions. These ^{85}Rb resonances are the first that were predicted to occur at fields at which the atoms can be trapped in a static magnetic field. One of the ^{85}Rb resonances has in the meantime been observed by the group of Heinzen and also in the groups of Cornell and Wieman. The observation of the resonance by the groups of Cornell and Wieman in Boulder has subsequently made it possible to pin down in very great precision the interaction parameters for cold Rb atoms (chapter 4). Currently, these groups are trying to use this resonance to make an ^{85}Rb condensate in a magnetic trap: Away from resonances the scattering length is negative for ^{85}Rb, so that a large condensate cannot be made. A three body decay process seems to hamper this, however.

In chapter 6 we treat a rigorous method to reconstruct the stationary collision state of a three-body collision between three ultracold, double-polarized ground-state alkali atoms. The method is based on the Faddeev formalism. The circumstances of the collision correspond to Bose-Einstein condensed and other ultracold gases. The method combines a pair-correlated expansion in hyperspherical harmonics in 6D with the accumulated phase for the pair interactions. It allows us to calculate the complex 6D elastic scattering length and the three-particle recombination rate.
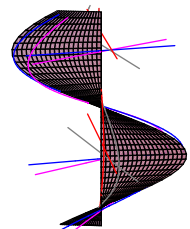
Samenvatting

Het bereiken van de kritische fase-dichtheid in een gas van alkali-atomen heeft een stroomversnelling teweeggebracht in het onderzoek naar Bose-Einstein condensatie. Het belangrijkste wisselwerkingsproces in zo'n gas is de s-golf verstrooiing van twee botsende atomen: het teken van de verstrooiingslengte bepaalt of de atomen elkaar effectief afstoten dan wel aantrekken. Dit resulteert in een mean-field effect van de atomen op elkaar, wat zich bijvoorbeeld uit in frequentieverschuivingen van atomaire klokken gebaseerd op koude atomen. In een condensaat zijn de effecten van het mean field zeer divers. Indien de verstrooiingslengte negatief is, kan er slechts een klein metastabiel condensaat gevormd worden. Een te groot condensaat valt in elkaar onder de aantrekkende interacties. Indien de atomen elkaar afstoten gaat de mean-field energie al snel overheersen ten opzichte van de bewegingsenergie, en het condensaat bevindt zich in het Thomas-Fermi regiem.

Interessant is daarom dat de botsingen, en derhalve de verstrooiingslengte, gestuurd kunnen worden door het magneetveld waar de botsingen zich in afspelen. Dit is een gevolg van resonantiegedrag, dat ontstaat door koppeling van het botsingskanaal met andere hyperfijnkanalen waarin zich een (quasi-)gebonden toestand bevindt. Deze zgn. Feshbach-resonanties vormen het hoofdonderwerp van het proefschrift.

Na een inleiding in hoofdstuk 1 is in hoofdstuk 2 een simpel model gepresenteerd waarmee de structuur en de eigenschappen kunnen worden begrepen van gebonden toestanden en botsingstoestanden van paren identieke alkali-atomen in de electronische grondtoestand. Het betreft de zeer zwak gebonden toestanden enerzijds en de ultrakoude botsingen anderzijds, beide zeer dicht bij de dissociatie limiet. Daardoor zijn die twee onderling nauw gerelateerd. In essentie komt het eenvoudige beeld neer op het verdelen van de totale range van interatomaire afstanden in twee gebieden, in elk waarvan een deel van de totale Hamiltoniaan verwaarloosd wordt. In het scheidingspunt wordt continuïteit opgelegd aan de multikanaals-golffunctie. Het model verklaart een spectrum aan eigenschappen in het systeem. In het bijzonder geeft het een beschrijving van het koppelingsmechanisme tussen de hyperfijntoestanden dat de resonantie veroorzaakt, als ook de globale posities en de breedten van de resonanties.

In hoofdstuk 3 komt een experiment aan de orde dat geleid heeft tot een voorspelling van Feshbach resonanties voor ^{85}Rb en ^{87}Rb (zie hoofdstuk 5). Dit twee-kleuren fotoassociatie experiment is geanalyseerd met een in dit promotiewerk ontwikkelde aanpak. De bindingsenergieën van multikanaals gebonden toestanden van ^{85}Rb$_2$ molekulen worden gemeten in een optische val door deze toestanden met een laser te koppelen aan een electronisch aangeslagen ^{85}Rb$_2$ toestand. Met een tweede laser wordt deze laatste toestand gekoppeld aan lage-temperatuurs botsingstoestanden van grondtoestand atomen in de optische val. Via deze laatste koppeling kunnen atomen uit de val ontsnappen: een atoompaar in een elektronisch aangeslagen toestand kan spontaan een foton uitzenden waarbij de atomen elkaar met grote snelheid verlaten. Wanneer de frequentie van de eerste laser overeenkomt met het energieverschil tussen de aangeslagen toestand en de te meten grondtoestand verijdelt de betreffende koppeling dit verval door de populatie van de aangeslagen toestand te verminderen. Dit beïnvloedt het gemeten verlies

van atomen uit de trap. Uit de zo bepaalde energieën worden vervolgens parameters geëxtraheerd die de atoom-atoom interacties karakteriseren.

Om de toestanden verkregen in het experiment in hoofdstuk 3 te analyseren is een nieuwe methode ontwikkeld in hoofdstuk 4. Deze toestanden zijn sterk gekoppeld en liggen erg dicht bij de botsingdrempel. De methode is gebaseerd op Inverse Perturbation Analysis (IPA), welke het mogelijk maakt om gemeten gebonden in een potentiaal te gebruiken om de eigenschappen van die potentiaal af te leiden. Onze gekoppelde Inverse Perturbation Analysis (CIPA) is een generalisatie die het mogelijk maakt toestanden te analyseren waarin zich koppeling afspeelt tussen interne toestanden met verschillende elektronische en nucleaire spin. Ten tweede is het mogelijk de aanpak te combineren met een beschrijving van het korte-afstands gedrag in termen van geaccumuleerde fasen. Zelfs indien het korte-afstands gedrag nog niet voldoende bekend is, maakt dit het mogelijk toestanden dicht bij de drempel te gebruiken.

In hoofdstuk 5 leiden de resultaten van de CIPA analyse tot de voorspelling van drie Feshbach resonanties in ultrakoude ^{85}Rb + ^{85}Rb en vier resonanties in ^{87}Rb + ^{87}Rb botsingen. Deze ^{85}Rb resonanties zijn de eerste resonanties die voorspeld zijn bij velden waarbij de atomen te vangen zijn in een statisch magnetisch veld. Een van de ^{85}Rb resonanties is intussen waargenomen door de groep van Heinzen en ook in de groepen van Cornell en Wieman. De meting van de resonantie door de groepen van Cornell en Wieman in Boulder heeft het vervolgens mogelijk gemaakt om de wisselwerkingsparameters voor koude Rb atomen met zeer grote nauwkeurigheid vast te leggen (hoofdstuk 4). Op dit moment wordt er een poging gedaan in de laatste groepen om deze resonantie te gebruiken om een ^{85}Rb condensaat in een magnetische val te maken: buiten de resonanties is de verstroooiingslengte negatief voor ^{85}Rb, zodat het niet mogelijk is een groot condensaat te maken. Een drie-deeltjes vervals proces lijkt dit te bemoeilijken, zowel in als buiten de resonantie.

In hoofdstuk 6 behandelen we een rigoureuze methode om de stationaire toestand van een drie-deeltjes botsing tussen drie ultrakoude dubbel gepolariseerde grondtoestand alkali atomen te reconstrueren. De methode is gebaseerd op het Faddeev formalisme. De botsingsomstandigheden corresponderen met Bose-Einstein gecondenseerde en andere ultrakoude gassen. De methode combineert een paar-gekorreleerde ontwikkeling in hypersferische harmonischen in 6D met een geaccumuleerde fase voor de paarwisselwerkingen. Dit staat ons toe om de complexe 6D elastische verstrooiingslengte en de drie-deeltjes vervalssnelheid te berekenen.
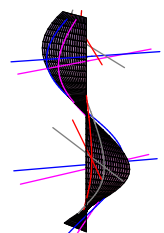
Dankwoord

Ik neem hier de kans om mijn dank uit te spreken aan iedereen die aan dit werk heeft bijgedragen. In de eerste plaats natuurlijk Boudewijn voor zijn enthousiasme en zijn inspirerende begeleiding. Verder zou het werk niet mogelijk en een stuk minder plezierig geweest zijn zonder de vele discussies met Servaas en Frank. Ook de bijdragen van Remco en Frank Koppens mogen hier niet onvernoemd blijven. De introduktie in dit gebied door Hugo en Ard-Jan wordt ook zeer op prijs gesteld.

I am also grateful to Dan Heinzen, Chin-Chun Tsai and Riley Freeland for their beautiful photoassociation spectroscopy and our collaboration. Furthermore many thanks go to the whole MIT group for allowing me to get some taste of fine experimental work and meet some great people.

Tevens wil ik mijn ouders, Marc, Arno en Rianne bedanken.

Curriculum Vitae

1973 :	Geboren te Mariahout
1977-1985 :	Lagere School, Bernadetteschool te Mariahout
1985-1991 :	Atheneum, Lorentz Lyceum te Eindhoven
1991-1996 :	Studie Technische Natuurkunde Technische Universiteit Eindhoven
1996-1999 :	Onderzoeker in Opleiding Werkgemeenschap Atoomfysica en Quantumelectronica Stichting FOM

STELLINGEN

behorende bij het proefschrift

Feshbach resonances in Bose Einstein Condensates

van

Johnny Vogels

Eindhoven, 29 juni 1999

I

Voor velden waarbij ^{85}Rb atomen magnetisch opgesloten kunnen worden zijn er drie (door de exchange wisselwerking geïnduceerde) Feshbachresonanties die de weg naar een instelbaar Bose Einstein condensaat openen.

- Dit proefschrift, hoofdstuk 5

II

Ondanks de positieve uitspraken van Kievsky et al. houdt hun formalisme voor drie-deeltjes verstrooiing geen stand bij hard-core potentialen.

- A. Kievsky, M. Viviani and S. Rosati, Nucl. Phys. A **577**, 511 (1994)

III

De Landau-Zener theorie wordt ver buiten zijn geldigheidsgebied het meest toegepast.

- L. D. Landau, Phys. Z. Sow. **1**, 89 (1932); **2**, 46 (1932)
- C. Zener, Proc. Roy. Soc. A **137**, 696 (1932)
- Dit proefschrift, hoofdstuk 2

IV

Hoe groot de exchange wisselwerking ook is, indien zij dezelfde singlet- en triplet verstrooiingslengte veroorzaakt, koppelt zij geen hyperfijnkanalen.

- Dit proefschrift, Hoofdstuk 2
- S.J.J.M.F. Kokkelmans et al., Phys. Rev. A **55**, R1589 (1997); P.S. Julienne et al., Phys. Rev. Lett. **78**, 1880 (1997); J.P. Burke, Jr. et al., Phys. Rev. A **55**, R2511 (1997)
- C.J. Myatt, E.A. Burt, R.W. Ghrist, E.A. Cornell, and C.E. Wieman, Phys. Rev. Lett. **78**, 586 (1997)

V

Gezien het reversibele karakter van de quantummechanica zou het bestaan van "one-way" berekeningen voor encryptie een illusie kunnen zijn.

- P.W. Shor, Polynomial-Time Algorithms for Prime Factorization and Discrete Logarithms on a Quantum Computer, SIAM Journal on Computing **26**, 1484 (1997)

VI

Met een spinor-condensaat kan men fase-diffusie meten zònder referentiecondensaat.

- C.K. Law, H. Pu, N.P. Bigelow, *Quantum Spin Mixing in Spinor Bose-Einstein Condensates*, Physical Review Letters **81**, 5257 (1998)

VII

Mulders en Engelen hebben zich visueel laten misleiden door de rood-antirood combinatie van quarks "kleur"-neutraal te noemen.

- P.J. Mulders en J. Engelen, Ned. Tijdschrift voor Natuurkunde **65**, 142 (1999)

VIII

De snelle voortgang van de wetenschap vereist dat èn de preprints èn de uiteindelijke versie van publicaties vrij toegankelijk moeten zijn. De kosten van het "referee"-proces kunnen het meest effectief door de auteurs gedragen worden.

- http://publish.aps.org/PRL/disc.html

IX

De huidige zoekmogelijkheden maken het moeilijker om originele stellingen te verzinnen.

X

Ik bel, dus ik ben.

- Vrij naar Descartes